Graduate School ETD Form 9
(Revised 12/07)

PURDUE UNIVERSITY
GRADUATE SCHOOL
Thesis/Dissertation Acceptance

This is to certify that the thesis/dissertation prepared

By Younghun Jung

Entitled
Uncertainty in Flood Inundation Mapping

For the degree of Doctor of Philosophy

Is approved by the final examining committee:

Venkatesh Merwade
Chair

Dennis Lyn

Indrajeet Chaubey

Rao S. Govindaraju

To the best of my knowledge and as understood by the student in the *Research Integrity and Copyright Disclaimer (Graduate School Form 20)*, this thesis/dissertation adheres to the provisions of Purdue University's "Policy on Integrity in Research" and the use of copyrighted material.

Approved by Major Professor(s): Venkatesh Merwade

Approved by: Garrett D. Jeong 09/26/2011
Head of the Graduate Program Date

Graduate School Form 20
(Revised 9/10)

PURDUE UNIVERSITY
GRADUATE SCHOOL

Research Integrity and Copyright Disclaimer

Title of Thesis/Dissertation:

Uncertainty in Flood Inundation Mapping

For the degree of Doctor of Philosophy

I certify that in the preparation of this thesis, I have observed the provisions of *Purdue University Executive Memorandum No. C-22,* September 6, 1991, *Policy on Integrity in Research.**

Further, I certify that this work is free of plagiarism and all materials appearing in this thesis/dissertation have been properly quoted and attributed.

I certify that all copyrighted material incorporated into this thesis/dissertation is in compliance with the United States' copyright law and that I have received written permission from the copyright owners for my use of their work, which is beyond the scope of the law. I agree to indemnify and save harmless Purdue University from any and all claims that may be asserted or that may arise from any copyright violation.

Younghun Jung

Printed Name and Signature of Candidate

09/26/2011

Date (month/day/year)

*Located at http://www.purdue.edu/policies/pages/teach_res_outreach/c_22.html

UNCERTAINTY IN FLOOD INUNDATION MAPPING

A Dissertation

Submitted to the Faculty

of

Purdue University

by

Younghun Jung

In Partial Fulfillment of the

Requirements for the Degree

of

Doctor of Philosophy

December 2011

Purdue University

West Lafayette, Indiana

To my parents

ACKNOWLEDGEMENTS

With a great pleasure and a deep sense of gratitude, I would first like to thank to my major professor, Dr. Venkatesh Merwade, for the opportunity to pursue my academic goals. Also, I greatly appreciate his willingness to provide the resources and moral support during the course of this research. His expertise, guidance and critique have been extremely valuable contributions to my research and greatly enhanced my PhD experience. To my committee members, Dr. Indrajeet Chaubey, Dr. Rao S. Govindaraju, and Dr. Dennis Lyn, I would also like to express my sincere appreciation for their insightful questions and advice on my research.

I am truly grateful to all Hydraulics and Hydrology group members including Dr. Cary Troy and Judith Haan who help in enjoying campus life as well as supporting my research. To Dr. Suresh Rao in Environmental group and Dr. Laura Bowling in Department of Agronomy, I appreciate their encouragement during the course of my doctoral studies. I would also like to thank to Scott Morlock and Moon Kim of the Indiana Water Science Center, and to North Carolina Floodplain Mapping Program for providing data used in this research.

It is also my pleasure to thank to Dr. Myung-Pil Shim and Dr. Hung Soo Kim in Department of Civil Engineering, Inha University, South Korea for always mentoring me in my career choices.

Finally, no words can express my gratitude to my family - parents, sisters, brothers-in-law, nephews, nieces, and other relatives. Without their love, encouragement and understanding, it would not have been possible for me to finish this work and achieve my pursuits.

Thanks to the Almighty Lord for the amazing grace and kindness that he has continuously bestowed on me.

TABLE OF CONTENTS

Page

Page

LIST OF TABLES

Table Page

LIST OF FIGURES

ABSTRACT

Jung, Younghun. Ph.D., Purdue University, December 2011. Uncertainty in Flood Inundation Mapping. Major Professor: Venkatesh M. Merwade.

Flood inundation maps serve as an important tool in decision making related to minimizing losses from flooding. Generally, flood risk management is based on the prediction of flood inundation for the design flood event (e.g., the 100 years). Flood inundation modeling includes hydraulic modeling, hydrologic modeling, and terrain analysis. The accuracy of flood prediction is influenced by various internal and external uncertainties in flood inundation modeling. To address the issue of uncertainty in flood inundation modeling, the objectivities of this study are: 1) to estimate the uncertainty propagation from model variables into flood inundation prediction; 2) to quantify the uncertainty in flood inundation mapping using generalized likelihood uncertainty estimation (GLUE) and sensitivity analysis; and 3) to assess the role of prior and posterior probability distribution functions on the subjectivities in uncertainty quantification using the GLUE methodology. Three variables, namely, discharge, topography, and Manning's *n* are used for uncertainty analysis in this study. The objectives of this study are accomplished by using a 1D HEC-RAS model and data from

study areas including the East Fork White River near Seymour, Indiana (Seymour reach) and the Strouds reach in Orange County, North Carolina (Strouds reach).

Estimation of uncertainty propagation using the FOA method shows that the uncertainty of a single variable is propagated differently to the flood inundation area, depending on the role of other variables in the overall process. In addition, the results from HSY sensitivity analysis show that topography is a major contributor to the uncertainty in the flood inundation area at the Seymour reach, and discharge is the major contributor at the Strouds reach.

Performance of GLUE is assessed by selecting three likelihood functions including the sum of absolute error (SAE) in water surface elevation and inundation width, sum of squared error (SSE) in water surface elevation and inundation width, and a statistic (F-statistic) based on the area of observed and simulated flood inundation map. Results showed that the uncertainty in topography, roughness and flow information created an uncertainty bound in the inundation area that ranged from 1.4 to 4.6% for Seymour reach and 4 to 29% for Strouds reach of the base inundation areas.

The prior and posterior PDFs for model variables are used to investigate the consistency of datasets for behavioral models in the GLUE methodology. The results show that the type of prior probability distribution functions affects the uncertainty bounds for the Seymour reach. The small number of dataset leads to approximate uncertainty bounds, but the use of the effective range provides a reasonable number of datasets to quantify the uncertainty in flood inundation mapping.

CHAPTER 1. INTRODUCTION

1.1.Background

Flood inundation mapping plays a major role in conveying flood risk information to decision makers and the general public for planning purposes and relief operations. In addition to the estimates from the global climate models that predict more frequent floods in the future, recent major floods in many parts of the world show that floods are getting more severe and frequent (e.g., Collins 2009; Hurkmans et al. 2009; Xu et al. 2009). As a result, improvement in our flood prediction capabilities, including flood inundation maps, could prove valuable in efforts to lessen the human and economic losses associated with major flood events.

Flood inundation areas are presently mapped in the following ways: 1) surveying high water marks; 2) extracting the water body from the images obtained by using optical devices or sensors (e.g., aerial photography or satellite image); and 3) flood inundation modeling. The observed flood extent map produced by surveying high water marks is still the fundamental and traditional method used to estimate flood damages. However, the critical weakness of this mapping method is that the water marks can only be measured after the flood waters have receded. In addition, since the high water marks are

intermittent and sparse, describing the inundation area using these sparse points is less accurate. The second method, which uses the geographic information system (GIS) and satellite images, enables a more practical and convenient way to map flood inundation. Many researchers are interested in, and are working on improving the effectiveness of this method because of its high utility value in various fields, including the mapping of flood inundation. However, this method also produces uncertain maps because of the horizontal resolution of the image, type of classification methods, satellite equipment, and image quality.

Typically, flood inundation maps created from high water marks and satellite images are used as observation data to calibrate a hydraulic model. The third method includes hydrologic modeling, hydraulic modeling, and terrain analysis. The accuracy of a flood map obtained from modeling is dependent on several uncertainties related to data and modeling parameters. Incorporating the uncertainties arising from various elements in the overall process is one of the major issues in predicting accurate flood inundation areas. Uncertainty in flood inundation modeling arises from the following: (i) flow estimation from a hydrologic model or a stage-discharge rating curve; (ii) input data, including topography and land use data; (iii) modeling type (1D versus 2D); (iv) model set-up and assumptions (e.g. steady versus unsteady state); (v) model parameters (e.g., Manning's roughness); (vi) lack of model calibration data (e.g., observed flood extent); and (vii) mapping approaches.

Among the several uncertainty sources listed above in relation to flood inundation modeling, topography, flow, and model parameters (Manning's n) have received

significant attention in the literature. In most cases, the model type and topography are dictated by practical considerations, such as experience in using a certain model, industry norms (e.g., 1D HEC-RAS is a norm in creating flood inundation maps); the availability of hydraulic (e.g., hydrograph, water surface elevations, and velocity); and topography data (e.g., cross-sections, bathymetry point measurements). With a predetermined modeling tool and topography data, Manning's n is the only parameter available to calibrate a hydraulic model, which means that the Manning's n value can be changed for a given circumstance, and the variation in Manning's n is transferred to the next process in flood inundation modeling. Typically, Manning's n is often assumed to be different in a main channel and a floodplain. The effect of Manning's n in flood inundation modeling can be changed for other hydrologic conditions including discharge and geometry. Flow conditions that are utilized as input data in hydraulic modeling are usually estimated by hydrologic modeling or statistical methods. Uncertainty in hydrologic model can arise from the various parameters and input data (e.g., precipitation and temperature). Moreover, rating curves that are based on historical discharge can show uncertainty due to the difficulty of mathematical models to perfectly match the relationship between historical discharges and water surface elevations. In addition to the flow conditions, the geometric data used in hydraulic modeling are extracted from the topographic data. Thus, the accuracy of the topography is directly transferred to the bathymetry of the reach.

Several studies have reported the role of uncertainty in flood inundation mapping (Weichel et al 2007; Koivumäki 2010). Uncertainty analysis is usually performed by sensitivity analysis and uncertainty quantification. Sensitivity analysis in flood inundation

modeling has been conducted by Sobol, Kullback–Leibler entropy, Morris regionalized sensitivity analysis, regression and PEST (Pappenberger et al., 2007; Bahremand and Smedt, 2008). Among sensitivity analysis techniques, first-order approximation (FOA) is a regional sensitivity analysis method used to quantify the uncertainty propagation (Bates and Townley, 1988; Melching, 1992). The FOA method normally requires a mathematical equation, but it is complicated to mathematically express the relationship between model variables and flood inundation areas. However, the difficulty in using FOA can be resolved by mathematically describing the relationship between the target variable and the output by statistical methods, such as regression analysis **(**Linton, 1995). The uncertainty propagation rate obtained by FOA method is defined as the ratio of the change in output in relation to the change in the target variable. Thus, FOA method can provide the quantitative information needed to determine the priority of variables that add uncertainty to flood inundation modeling.

Generally, uncertainty propagation analysis is conducted to investigate the sensitivity of model parameters for more accurate model prediction. Unlike a regional FOA method, a global sensitivity analysis such as HSY method can be used to estimate relative sensitivity between model variables. HSY method was first used to assess an environmental model in Western Australia (Hornberger and Spear, 1981) and United Kingdom (Whitehead and Young, 1979). The concept of HSY sensitivity analysis forms the basis for the generalized likelihood uncertainty estimation (GLUE) method developed by Beven and Binley (1992) to estimate uncertainty in wide ranges of environmental applications including flood modeling (Yatheendradas et al., 2008; Hunter et al. 2005;

Heidari et al., 2006). The sensitivity using the HSY method, a basis of the GLUE methodology, is estimated by calculating the maximum difference between two cumulative density functions (CDF) of behavioral and non-behavioral models. A likelihood measure can be defined by several functions including Nash-Sutcliffe efficiency, sum of squared error, and sum of absolute error (Beven, 2009). Among several likelihood functions, the F-statistic is based on spatial extent of flooding, which quantitatively estimates the suitability between an observed and a predicted map (Horritt et al., 2001).

Several techniques have been used to address the issue of uncertainty in flood inundation mapping, including Bayesian forecasting system (Krzysztofowicz, R., 1999, 2002), GLUE (Blazkova and Beven, 2009), parameter estimation (PEST) (Liu et al., 2005), and a methodology based on fuzzy extension principle (Maskey et al., 2004). Among these techniques, the GLUE method proposed by Beven and Binley (1992) is one of the first methods to represent prediction uncertainty in hydrologic and hydraulic modeling. The GLUE method uses Monte Carlo simulations in conjunction with Bayesian theory to produce parameter distributions conditioned on available data and associated uncertainty bounds. The parameter distributions are generated based on parameter sets that can produce acceptable model outputs in comparison with observed data. The criterion for an acceptable model is based on the definition of a user-specified likelihood function.

The GLUE method has found widespread implementation in various studies related to uncertainty analysis in environmental and hydrologic modeling, including flood mapping (Romanowicz and Beven 1998; Pappenberger et al. 2005a, 2006a). While GLUE has

found widespread application in flood inundation mapping because of its simple and flexible conceptual structure, it has been criticized in literature for not being formally Bayesian and statistically coherent (Beven 2009; Vrugt et al. 2005). Specifically, the subjectivity involved in defining the likelihood measure and the criteria for defining acceptable versus unacceptable models have been pointed out as incoherent and inconsistent from a statistical point of view. Even studies that implement formal likelihood measures through sequential data assimilation and multi-model averaging have been reported to have their own weaknesses.

As previously discussed, there is a need to consider uncertainties in the estimation of the rating curve from historic discharge, the variation in Manning's n calibrating parameter, and the extraction of geometric data from topography. Moreover, not only is it necessary to recognize uncertainty propagated from a single variable, but it is also important to be aware of the combined effect of multiple variables and their relative uncertainty in the overall flood inundation mapping process. FOA has been used for sensitivity analysis and can provide quantitative information for the uncertainty propagation rate, which is the ratio of the propagated flood inundation area to change in a target variable. Similarly, GLUE has been widely used in quantifying uncertainty in several fields of hydrology, including hydraulic modeling and flood inundation mapping. However, the effect of the subjectivity issue in the GLUE methodology in quantifying the uncertainty in flood inundation mapping remains to be investigated. Accordingly, the overall goal of this study is to analyze the uncertainty arising from multiple variables in flood inundation mapping using Monte Carlo simulations, GLUE, and FOA.

1.2.Research Objectives

The approach needed to accomplish the goal of analyzing uncertainty in flood inundation mapping involves quantifying uncertainty in flood inundation mapping, estimating uncertainty propagation, and assessing the role of prior and posterior PDFs in uncertainty quantification using the GLUE methodology. Accordingly, the three major topics pursued in this dissertation are:

1) **Estimation of uncertainty propagation in flood inundation mapping.**

   The hypothesis that the uncertainty in one model variable is differently propagated to flood inundation area based on the role of other variables is tested by: (i) estimating the uncertainty propagation rates of individual as well as combined variables in uncertainty propagation by using the FOA method; and (ii) investigating the relative effect of combined model variables in flood inundation mapping through HSY sensitivity analysis.

2) **Uncertainty Quantification in Flood Inundation Mapping using Generalized Likelihood Uncertainty Estimate (GLUE) and Sensitivity Analysis.**

   The topic involves: (i) quantifying and comparing the uncertainty arising from multiple variables in flood inundation mapping using Monte Carlo simulations and GLUE; and (ii) investigating the role of subjective selection of GLUE likelihood measures in quantifying the uncertainty in flood inundation mapping.

3) **Assessment of the role of prior and posterior PDFs in uncertainty quantification using the GLUE methodology.**

This topic involves assessing the effect of prior probability density functions (PDF) on the estimation of the flood inundation area with several likelihood measures.

1.3. Organization of this Dissertation

Chapter 2 includes overall literature reviews on parameterization of model variables including the topography, discharge, and Manning's n, HEC-RAS model, First order approximation (FOA) method, Hornberger-Spear-Young (HSY) method, and Generalized Likelihood Uncertainty Estimation (GLUE) used in this dissertation. Chapter 3 describes study areas and data used in this dissertation. Chapters 4 to 6 describe the three topics of this dissertation in a self contained manner, i.e., each chapter includes introduction, methodology, results, and conclusions.

CHAPTER 2. LITERATURE REVIEW

2.1.Parameterization in flood inundation modeling

2.1.1 The effect of topography

Uncertainties from using topography data arise at two levels in flood inundation mapping. First, topography affects the hydrologic model (e.g., watershed delineation) that is used to derive the flow estimate. Second, topography plays a significant role in the hydraulic modeling that is used to derive water surface elevations corresponding to the design flow. Topography affects the geometry which defines the flow domain, including river cross-sections and bathymetry mesh in a hydraulic model (Marks and Bates, 2000; Werner, 2001; Vazquez et al., 2002). Topography also affects the process of transferring the water surface elevation into flood inundation extent by subtracting the topography from the water surface (Colby et al., 2000; Tate et al., 2002; Bates et al. 2003; Omer et al., 2003; Wang and Zheng, 2005). Although the use of recently available LIDAR (light detection and ranging) data has improved the accuracy of flood inundation mapping, the absence of detailed river bathymetry in LIDAR can lead to flood inundation area errors in the range of 15 – 20% (Cook and Merwade, 2009). The quality of DEMs is determined by the LIDAR device type, filtering, and interpolation methods. Generally, on-line

accessible LiDAR DEMs for USA have vertical uncertainty in the range of 0.05 to 0.25 m root mean squared error (RMSE), but access for the LiDAR DEMs is limited for a few States including Idaho, North Carolina, Ohio, Pennsylvania, and South Carolina. United States Geologic Survey (USGS) also provides national elevation data (NED) at 1/9, 1/3 and 1 arc second resolution which have vertical errors in the range of 0.3-0.5 m, 7 m, and 7-15 m, respectively.

2.1.2 The effect of discharge

Generally, discharge is considered as one of the most uncertain variables in flood inundation mapping (Pappenberger et al. 2006b). Uncertainty in discharge data arises from how the observed discharge data are estimated (stage-discharge rating curve) and from methods used to derive the design flow (e.g., 1% flow or 100-yr return period flow) for a given area. Stage-discharge rating curves that are used to estimate discharge from stage recordings can have standard error ranging from less than 10% for average discharge to up to 40% for flood conditions (e.g., Clarke et al., 1999, 2000; Di Baldassarre and Montanari, 2009). The uncertainty in stage-discharge rating curves gets translated to the discharge input to a hydraulic model, and consequently to water surface elevation estimates and flood extent (Freeman et al., 1996; Herschey 2002; Schmidt, 2002; Parodi and Ferraris, 2004; Bales, 2009; Purvis et al., 2008). When detailed hydrologic modeling is used to derive the design flow, uncertainty arises from precipitation inputs (number of rain gauges, radar rainfall data), model set-up (lumped, semi-distributed and distributed), topography, and model parameters (Hossain et al.,

2004). Use of regression equations to derive design flow is common for ungauged basins (Lara 1987**),** and some of the regression equations have standard errors in the range of 20% to 61%. For example, in a previous study involving Strouds reach in North Carolina, USA, the regression equation from the National Flood Frequency program had a standard error of - 34% to + 57% associated with the design flow estimate (Merwade et al., 2008a). Similarly, the use of flood frequency equations in the United States has a significant level of uncertainty because of the assumptions made in deriving the design flow (Stedinger and Griffis, 2008).

2.1.3 The effect of Manning's n

Manning's n is considered as a "calibrating" parameter that is manipulated to account for all other uncertain variables in the overall hydraulic modeling process (e.g., Nicholas et al. 2005; Horritt 2005; Hunter et al. 2005). Typically, the Manning's n is different at multiple locations, such as in the main channel and floodplain, along the cross-section, but some studies use a single value of Manning's n (e.g., Pappenberger et al. 2005b) for the entire cross-section, thus adding uncertainty. Similarly, many hydraulic models are calibrated for a particular discharge, and this calibrated Manning's n value adds another level of uncertainty in the model because the calibrated Manning's n parameter may yield incorrect solution for other flow conditions.

2.2.HEC-RAS model

The Hydrologic Engineering Center – River Analysis System (HEC-RAS) was developed by the Hydrologic Engineering Center (HEC) of the United States Army Corps of Engineers (USACE 2006). HEC-RAS is one-dimensional (1D) hydraulic model that can simulate steady and unsteady flow conditions in river channels including floodplains. In this study all simulations are conducted by assuming steady state flow condition. The use of 1D HEC-RAS is justified by the assumption that all simulations are performed for 100 year return period flow where the river and its floodplain behave as a single channel; the floodplain only serves as a route to convey the flow parallel to the river centerline, and does not act as storage area. Thus, the cross-sections used in the HEC-RAS model extend across the floodplain. In HEC-RAS, each cross-section is divided into sub-divisions based on the values of roughness coefficients (Manning's n). The basic profile calculation in HEC-RAS is based on the energy equation (Eq. 2.1).

$$Y_2 + Z_2 + \frac{\alpha_2 V_2^2}{2g} = Y_1 + Z_1 + \frac{\alpha_1 V_1^2}{2g} + h_e \qquad (2.1)$$

where, Y_1, Y_2: depth of water at 1 (upstream) and 2 (downstream), V_1, V_2: average velocities, Z_1, Z_2: elevation of channel bottom, α_1, α_2: velocity weighting coefficients, g: gravitational acceleration, h_e: energy head loss.

Total conveyance in HEC-RAS is calculated by summing all incremental conveyances that are calculated for each subdivision by using the continuity and Manning's equation (Eq. 2.2).

$$Q = \frac{1}{n} A R^{\frac{2}{3}} S_f^{\frac{1}{2}} \qquad (2.2)$$

where, n: Manning's roughness coefficient, A: flow area, S_f: friction slope, and R: hydraulic radius.

A high roughness coefficient raises the water surface elevation under the condition of the fixed flow rate and slope based on Manning's equation. Similarly, a change in total conveyance leads to variations in water surface for fixed roughness and slope. The channel bottom elevation has an effect on the water surface elevation (WSE) under the conditions of fixed roughness and flow rate because the elevation is related to the wet area in the Manning's equation, and to the elevation head in the energy equation. HEC-RAS needs geometric data (e.g., channel centerline, cross-section elevations, and spacing) and flow data (input discharge in the main channel including tributaries) and boundary conditions. Typically, geometric data are created using HEC-GeoRAS, which is an ArcGIS tool that allows digitizing cross-sections over a DEM, and exporting this information to HEC-RAS. HEC-GeoRAS also allows importing HEC-RAS output into ArcGIS to create flood inundation map by subtracting topography from water surface, which is created by interpolating water surface elevations at each cross-section.

2.3. First Order Approximation (FOA) method

A first-order approximation (FOA) is a relatively simple technique for estimating the amount of uncertainty transferred by multiple variables in the prediction of a

deterministic model. The basis of FOA method proposed by Benjamin and Cornell (1970) is based on the moment analysis for a function associated with independent random variables. In addition, the FOA method makes it possible to determine the fraction of model output variance (the second moment) contributed by each variable involving uncertainty. Applications using FOA have been performed in various fields including: hydrologic modeling (Garen and Burges 1981; Lei and Schilling 1994); coastal ocean circulation modeling (Blumberg and Georgas 2008); groundwater modeling (Sitar et al. 1987); water quality modeling (Beck 1987; Zhang et al. 2004); and flood risk analysis (Tang et al. 1975; Lee and May 1986; Yen 1989; Johnson and Rinaldi 1998; Liu et al. 2001)

Uncertainty propagation by the FOA method can be derived as follows (Eqs. 2.3-2.8):

Let Y be the model output dependent on a random variable X. The functional relationship can be rewritten by adding an expansion point (x_e).

$$y = f(x) = f\left[x_e + (x - x_e)\right] \tag{2.3}$$

The function can be expanded by using Taylor's theorem about the expansion point,

$$f(x) = f(x_e) + \left.\frac{dy}{dx}\right|_{x=x_e} (x - x_e) + \frac{1}{2!}\left.\frac{d^2y}{dx^2}\right|_{x=x_e} (x - x_e)^2 + \frac{1}{3!}\left.\frac{d^3y}{dx^3}\right|_{x=x_e} (x - x_e)^3 + \dots$$

The mean of the random variable, $\bar{x}$, is typically used as the expansion point in applications to water resources and environmental engineering (Zhao et al. 2011). FOA is based on the analysis of moments for the series expansion of model output truncated after

the first-order term because of an assumption that the second and higher order terms are relatively much smaller than the first two terms.

$$y = f(x) \approx f(\bar{x}) + \left.\frac{dy}{dx}\right|_{x=\bar{x}} (x - \bar{x}) \tag{2.4}$$

As mentioned previously, FOA uses the first and second moments for the first order series of a function, which indicate the mean and variance. In addition, using the properties of the expected value,

$$E[y] = \bar{y} = E\left[f(\bar{x}) + \left.\frac{dy}{dx}\right|_{x=\bar{x}} (x - \bar{x}) \right] = E[f(\bar{x})] + \left.\frac{dy}{dx}\right|_{x=\bar{x}} (E[x] - E[\bar{x}]) = f(\bar{x}) \tag{2.5}$$

By substituting Eq. 2.4 and 2.5 into the relationship $Var[y] = E[(y - \bar{y})^2]$,

$$var[y] = E[(y - \bar{y})^2] = E\left[\left(f(\bar{x}) + \left.\frac{dy}{dx}\right|_{x=\bar{x}} (x - \bar{x}) - f(\bar{x}) \right)^2 \right] \tag{2.6}$$

$$= E\left[\left(\left.\frac{dy}{dx}\right|_{x=\bar{x}} (x - \bar{x}) \right)^2 \right] = \left(\left.\frac{dy}{dx}\right|_{x=\bar{x}} \right)^2 E(x - \bar{x})^2 = \left(\left.\frac{dy}{dx}\right|_{x=\bar{x}} \right)^2 var[x] \tag{2.7}$$

$$\therefore \sigma_y^2 = \left(\left.\frac{dy}{dx}\right|_{x=\bar{x}} \right)^2 \sigma_x^2 \tag{2.8}$$

The uncertainty (σ_y) of model output (Y) is associated with the uncertainty propagation rate ($\frac{dy}{dx}$), and uncertainty (σ_x) of independent variables (X) (Eq. 2.8).

2.4.Hornberger-Spear-Young (HSY) method

The HSY method is a type of global sensitivity analysis (GSA), and it was first used by Hornberger and Spear in appraising an environmental model for eutrophication and algal growth (1981). In the HSY method, model parameters are sampled from their prior PDFs, and are used in MC simulations of a particular model. The model's outputs are typically divided by binary classification into behavioral and non-behavioral dataset. In the HSY method, sensitivity is determined by comparing the cumulative distribution functions (CDF) of an individual parameter in each classification. For a parameter, the differences between the CDF in the behavioral and non-behavioral classes indicate the magnitude of sensitivity. In other words, when the individual parameter is less sensitive, the gap between the CDFs in two classes would be narrower. Furthermore, the quantitative measure of sensitivity can be expressed by the non-parametric Kolmogorov-Smirnov (KS) d statistic (Eq. 2.9). The KS test is performed under the null hypothesis that behavioral and non-behavioral classes have the same distribution.

$$H_0 : f(X_i \mid B) = f(X_i \mid \overline{B})$$
$$H_1 : f(X_i \mid B) \neq f(X_i \mid \overline{B})$$

$$d(X_i) = \sup\left\| F(X_i \mid B) - F(X_i \mid \overline{B}) \right\| \qquad (2.9)$$

where, X: parameter, i: the number of parameter, B: behavioral class, $\overline{B}$: non-behavioral class, and f: probability density function, and F: cumulative density function.

2.5. Generalized likelihood uncertainty estimation (GLUE)

The GLUE methodology, which is based on the Hornberger-Spear-Young global sensitivity analysis (Whitehead and Young, 1979; Hornberger and Spear, 1981; Young, 1983), involves forward Monte Carlo simulations using different parameter values sampled from distributions, usually with independent normal or uniform distributions for each parameter. The objective of the GLUE method is to identify a set of 'behavioral' or acceptable models within the possible model/parameter combination (Beven and Binley, 1992). Outputs from the all the simulations that are created by using the feasible parameter sets are weighted by likelihood measures, which is a function that describes how well the simulated model matches the observed data. Generally, likelihood measures based on Bayes equation (Eq. 2.10) can be estimated by several likelihood functions, such as inverse of sum of squared error, inverse of sum of absolute error, and Nash-Sutcliffe efficiency.

$$P(Z < z) = \sum \left(L\left[M\left(\Theta, I \right) \right] | \, Z < z \right) \tag{2.10}$$

where, P is posterior likelihood value and Z is the value of z simulated by the model. $L[M(\Theta, I)]$ is a likelihood measure of model prediction (M) for given parameter (Θ) and set of input data (I).

In flood modeling and mapping, a likelihood function can be defined by using the difference between observed and simulated water surface elevations (e.g., Kiczko et al., 2007; Aronica et al., 1998). The likelihood measure based on the difference between observed and simulated water levels is useful, but it cannot capture the spatial extent of

flood inundation area when observed flood maps are not available. Despite this limitation, the water level is a preferable variable to be used in likelihood measure in many practical situations because of the lack of observed flood inundation maps during flooding. Spatial uncertainties in flooding can be utilized when flood inundation maps are available. Spatial data related to flood inundation can also be extracted from satellite or air-borne remote sensing images (Horritt and Bates 2002). Likelihood function based on spatial extent of flooding is typically defined by F-statistic, which quantifies the discrepancy between two maps based on their intersection area (Horritt and Bates 2001; Aronica et al. 2002; Bates et al. 2004; Pappenberger et al. 2007). An F-statistic value of 100 means a perfect match between two maps (observed and predicted areas of inundation), and a lower *F* indicates discrepancy between the two.

A higher likelihood measure indicates better fit between the model output and the observed data, and vice versa. A cutoff threshold for likelihood measure then classifies the simulated outputs as behavioral (acceptable) or non-behavioral. The cut-off threshold can be defined in terms of either an absolute value (e.g., likelihood measure > 90), or a percentage of total simulations (e.g., top 75% of 1000 simulations). The likelihood measures of the behavioral models are then rescaled to obtain the cumulative density function (CDF) of the output prediction. The median of the rescaled CDF is generally taken as the deterministic model prediction (Blasone et al. 2008a and 2008b), and the uncertainty bound corresponding to this prediction is quantified by the 90% confidence interval chosen at 5% and 95% confidence levels.

As mentioned in the Introduction (chapter1), GLUE has been criticized in the literature for not being formally Bayesian and statistically coherent because of the subjectivity involved in defining the likelihood measure and the threshold for separating behavioral models from non-behavioral models. The debate on GLUE is still ongoing, and in the absence of any non-subjective solution to the current approach, it is necessary to investigate the roles of prior PDFs, posterior PDFs, likelihood measures and thresholds leading to the subjectivity in GLUE.

In the GLUE method, posterior PDFs are determined by prior PDFs, cut-off thresholds, and likelihood functions. Typically, prior PDFs in previously GLUE applications have been assumed to be normal or uniform for each model variable (Stedinger et al., 2008). When the model variables generated from different PDFs are combined, and if the posterior PDFs of each variable are robust, the posterior PDFs will be helpful in finding the combination dataset of the model variables for behavioral models. However, if the prior and posterior PDFs are similar to each other throughout the GLUE process, it will be difficult to obtain any information from the posterior PDFs for the behavioral models. A likelihood measure is a critical index to indicate good fitness with observations. In previous GLUE applications, likelihood measure was estimated by several likelihood functions. Generally, inverse of sum of squared error, inverse of sum of absolute error, and Nash-Sutcliffe efficiency were used as likelihood functions, but the uncertainty bounds are not consistent for likelihood functions. Therefore, a proper likelihood function can be selected for the purpose of a study. With the selection of a prior PDF and a likelihood function, a cut-off threshold is a subjective decision. A cut-off threshold

influences in the determination of behavioral models and the posterior PDF of model variable. For example, if all likelihood measures area selected as behavioral models in MC simulations for a certain threshold, the posterior PDF of model variables will be same to their prior PDFs for the range of model variable and distribution shapes. A tighter criterion can lead to posterior PDF different from the prior PDF because all parameter datasets are not selected as behavioral models. Therefore, a tighter threshold can lead to narrower ranges of model variables in their posterior PDF than a relaxed threshold (Kuczera and Parent, 1998; Jia and Culver, 2008).

CHAPTER 3. STUDY AREAS AND DATA

3.1.Description

This study used data from two river reaches, including a reach along the White River in Seymour, Indiana, and another along Strouds reach in Orange County, North Carolina (Fig. 3.1). Seymour reach is selected because of the availability of an observed flood inundation map for a historical flood in June 2008. The flooding of June 2008 was one of the worst in modern history, and led to evacuation of more than 100 homes in the area. Similarly, the area surrounding Strouds reach is designated as a high priority community by the U.S. Federal Emergency Management Agency (FEMA) because of the history of recurrence of floods in the area. An observed flood inundation map is necessary for using the GLUE technique to select behavioral models and to develop the uncertainty bound. Strouds reach is selected because of the availability of data and hydraulic model from a detailed flood inundation mapping study for FEMA. An observed flood inundation map for a storm event does not exist for Strouds reach, but the 100-yr flood inundation map from the FEMA study is treated as the base map in creating the uncertainty bound, thus enabling a sensitivity analysis of model output in response to variations in the input data. Both study areas have distinct physical (topographic and geomorphic) and climatic settings, thus providing good test beds for the study.

White River is one of the major rivers in Indiana, and is a tributary of the Wabash River which joins the Ohio River before draining to the Mississippi River. The Seymour reach selected in this study is 5.5 km long, and its floodplain is relatively flat with a U-shaped valley (Fig. 3.2.a). The geometric data for the Seymour reach contains 9 digitized cross-sections extracted from a 1.5 m resolution digital elevation model (DEM) developed by the Information Technology Services at Indiana University in Bloomington, IN. The DEM data for the Seymour Reach is generated from digital orthophotographs taken in 2006. The vertical accuracy of these data is 0.69 m for the study area, and is verified by comparing the DEM derived elevations with twelve bench mark points in the area. The average width of Seymour reach cross-sections is about 3.9 km with an average spacing of 700 m. The Strouds reach is a tributary of the Eno River, and is characterized by a relatively narrow floodplain with a V-shaped valley (Fig. 3.2.b). The available GIS data for Strouds reach, used in Map Mod and available from NCFMP, include 17 surveyed cross-sections and 6m horizontal resolution LIDAR DEM as shown in Fig. 3.1.b. The average width of these cross-sections is 142 m with an average spacing of 167 m. The LIDAR survey was conducted by the NCFPM in 2001-2002. NCFPM evaluated the accuracy of the LIDAR data by comparing the LIDAR-derived bare earth elevations with 100 check points in each county, and found the vertical accuracy to be in the range of ± 0.25 m for the Strouds reach (Sanders, 2007).

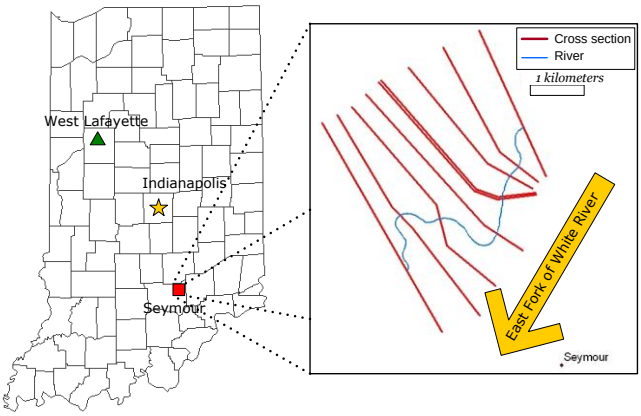

a) Seymour Reach, Indiana

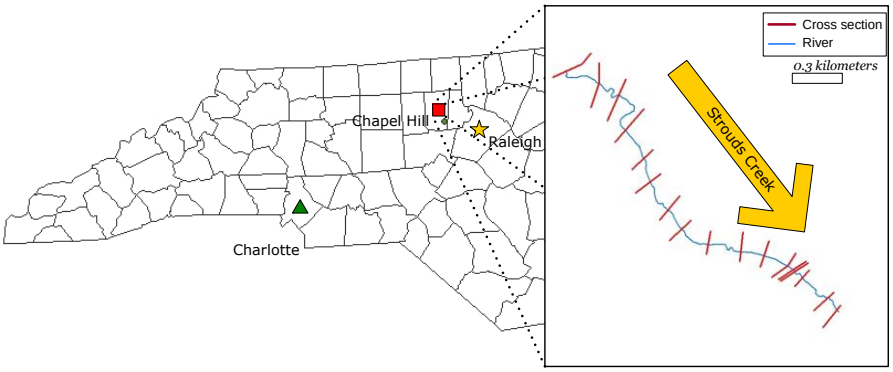

b) Strouds reach, North Carolina

Fig. 3.1: Study areas

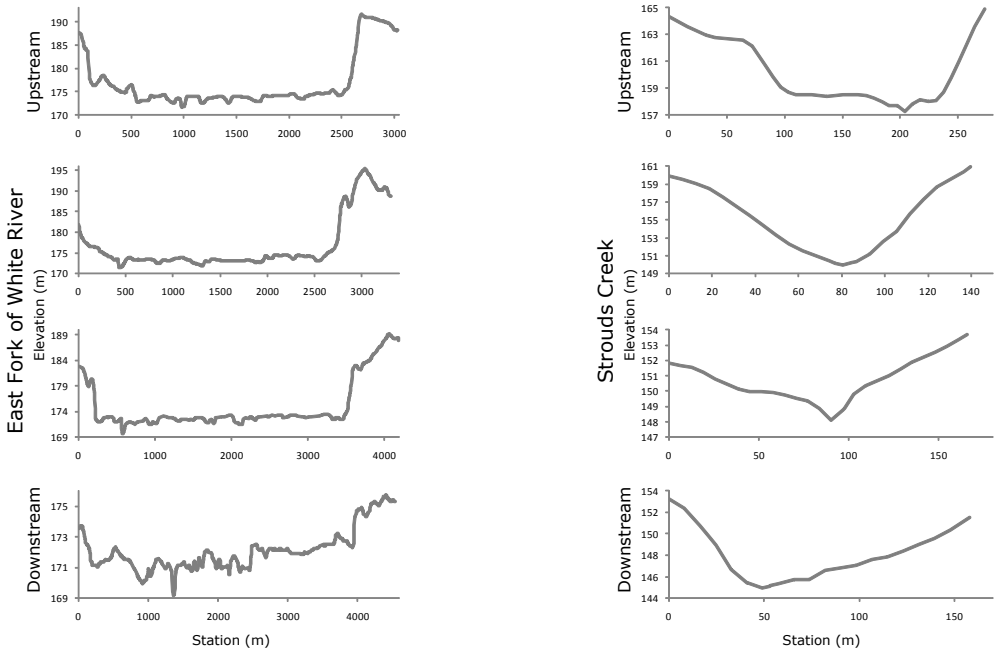

a) Seymour reach b) Strouds reach

Fig. 3.2: Cross-sections

Discharge data for the Seymour reach including the observed inundation extent for the June 2008 flood event were obtained from the United States Geological Survey (USGS) Water Science Center in Indianapolis. The flood inundation extent was prepared by USGS by using high water marks and 1.5m resolution DEM for the region. A total of 20 high water marks were collected by the Indiana Water Science Center and Indiana Department of Natural Resources staff for the Seymour reach. The reported vertical accuracy of these high water marks is less than 3 cm for most points (Morlock et al., 2008). The flow data used for hydraulic modeling of the Seymour reach include observed discharge of 2729.7 m^3/s for the June 2008 flood event with a reach boundary condition of downstream normal depth. The flow for the Seymour reach was estimated by the

USGS Water Science Center in Indiana by using a stage discharge rating curve. The Manning's n values for the Seymour reach hydraulic model are extracted from four land use conditions for the reach including cultivated & brush (n = 0.04), tree (n = 0.055), stream (n = 0.04), and urban (n = 0.12). The HEC-RAS model for Seymour Reach is manually calibrated for Manning's n. The design flow data including surface roughness (Manning's n) and boundary conditions for steady state flow simulation for Strouds reach are obtained from the hydraulic model input files from NCFMP. The Manning's n for Strouds reach main channel ranges from 0.04 – 0.05, and in the floodplain, it ranges from 0.1 - 0.2. The downstream boundary conditions for Seymour reach and Strouds reach are normal slopes of 0.016% and 0.58%, respectively. The design flow (100 year event) for Strouds reach, which is available from the FEMA study conducted by NCFMP, was estimated by using the USGS National Flood Frequency (NFF) computer program (Ries and Crouse, 2002). The NFF uses regression equations that relate design flow to watershed characteristics such as drainage area and impervious cover.

3.2. Accuracy of the model variables

3.2.1. Topography

As mentioned in the Study Area and Data section, cross-sections for the Seymour reach were extracted from a 1.5 m horizontal resolution DEM available from Indiana University. Cross-sections for the Strouds reach, which are available from NCFMP, are

created through a combination of manual surveying and by extracting elevations from LIDAR derived DEM. The reported accuracy for Strouds reach LDAR DEM is ± 0.25 m, and that for Seymour DEM is ± 0.69 m.

3.2.2. Discharge

The discharge data for the White River that are available from USGS for the 2008 flood event are included in this study. The USGS uses stage-discharge rating relationship to estimate discharge by measuring stages at their gauging stations. By using USGS field measurements of stage and discharge at the White River gauging station, a stage, H, (in meters) and discharge, Q, (in cubic meters per second) rating relationship (Eq. 3.1) is developed through regression.

$$Q = 10^{(1.58+1.44 \cdot \log H)} \qquad (3.1)$$

The stage corresponding to the observed flow of 2729.7 m^3/s is 19.67 m. The regression equation for the stage-discharge rating curve is developed assuming Student's t distribution. Using 95% confidence interval, a stage of 19.67 m gives a lower bound of 2257 m^3/s, and upper bound of 3301 m^3/s (Fig. 3.3).

Design discharge estimate for Strouds reach is derived through a regression equation (Eq. 3.2) that related the 100 year design discharge with drainage area using the USGS National Flood Frequency program.

$$Q_{100} = 745\ DA^{0.625}\ , \qquad (3.2)$$

Where Q_{100} is the 100-year flow in cubic feet per second and DA is the drainage area in square miles, with an applicable range of 0.1 – 41 square miles. The standard error of prediction, which is the square root of the summation of the mean square model error and the mean square sample error associated with logarithmic $Q_{100,}$ is reported to be in the range of – 19.4% to + 19.4% for the given range of drainage areas. For Strouds reach, with a drainage area of 9 sq. mi., Eq. 3.2 gives a Q_{100} of 83.3 m^3/s (2940 cfs) with an associated standard error range between 53.3 m^3/s (1,882 cfs) and 130.7 m^3/s (4616 cfs).

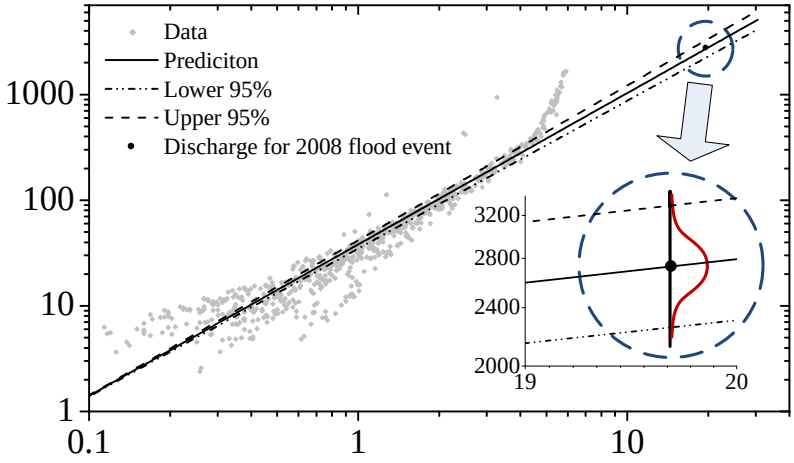

Fig. 3.3: Discharge distribution for Seymour reach. X axis shows stage height in meters and Y axis shows discharge in cubic meters per second.

3.2.3. Manning's n

Manning's roughness coefficient has been typically used as the only calibrating parameter in 1D hydraulic modeling. A flood inundation map using a 1D model is based

on the water surface elevations estimated at cross-sections associated with the right bank, main channel, and left bank. Therefore, there are at least three Manning's n values, and, moreover, the number of Manning's n values at a cross-section depends on the land use distribution in the floodplain. The Manning's n values at the Seymour reach are assigned by four types of land use (cultivated land, tree, urban area, and water). For Strouds reach, Manning's n is based on the land use map used in the previous FEMA study. For both reaches, a range of Manning's n is used based on values published in the literature (Chow, 1959) (Table 3.1).

Table 3.1: Roughness coefficients (Manning's n) for Seymour reach and Strouds reach. Model value represents the calibrated value of Manning's n

a) Seymour Reach

Land use	Model	Minimum	Maximum
Stream	0.04	0.025	0.055
Tree	0.055	0.034	0.076
Cultivated & Brush	0.04	0.025	0.055
Urban	0.12	0.075	0.165

b) Strouds Reach

Stream	0.04	0.025	0.062
Deciduous Forest	0.15	0.094	0.206
Pasture/Hay	0.1	0.063	0.138
Urban	0.2	0.125	0.275

CHAPTER 4. ESTIMATION OF UNCERTAINTY PROPAGATION IN FLOOD INUNDATION MAPPING

4.1.Introduction

The following two topics are described in this chapter: (i) propagation uncertainty rate estimation of key variables in flood inundation mapping by using the first order approximation (FOA) method; and (ii) evaluation of the relative sensitivity between the model variables utilizing the Hornberger-Spear-Young (HSY) method. Monte Carlo simulations using HEC-RAS and triangle-based interpolation are performed to investigate the uncertainty arising from discharge, topography, and Manning's n in the East Fork of the White River near Seymour, Indiana (Seymour reach) and in Strouds Creek in Orange County, North Carolina (Strouds reach).

4.2.Methodology

The methodology consists of the following steps: (i) choice of the probability distribution types and ranges for discharge, Manning's n, and topography; (ii) Monte Carlo simulations using a HEC-RAS model and a terrain analysis tool; (iii) estimation of the uncertainty propagation rates related to discharge, Manning's n, and topography using the

FOA method; and (iv) relative sensitivity analysis using HSY method. A brief description of each step is given below

4.2.1. Probability distribution for model variables

In Chapter 3.2, the ranges of model variables are determined, but there is no information on the probability distribution for model variables except for discharge in the Seymour reach. Generally, the probability distribution for a model variable is assumed to be uniform or normal in uncertainty analysis. In the case of Seymour reach, discharge data are obtained from a rating curve equation based on historical data, and the uncertainty in discharge is determined by Student's t-test with a 95% confidence interval. Therefore, a t-distribution is assumed for the discharge. However, topography and Manning's n are assumed to have a uniform distribution. For Strouds reach, it is assumed that all model variables (Manning's n, discharge, and topography) have uniform distribution.

Table 4.1: The conditions for random variables generated in a simulation

Study Area	Initial (variables)	Modeling Variables estimated by RV	Min	Max	Probability Type	No. of Chosen RV
Seymour	N_i Manning's n	$N = N_i (1+RV)$	-0.375	0.375	Uniform	1
Strouds		$N = N_i (1+RV)$	-0.375	0.375	Uniform	1
Seymour	F_i Discharge	$F = F_i * 10^{0.0286RV}$ [m^3/s]	-1.963	1.963	t-distribution	1
Strouds		$F = F_i * 10^{RV}$ [m^3/s]	-0.194	0.194	Uniform	1
Seymour	E_i Topography	$E = E_i + RV$ [m]	-0.69	0.69	Uniform	1
Strouds		$E = E_i + RV$ [m]	-0.25	0.25	Uniform	1

4.2.2. Monte Carlo simulations

Monte Carlo simulations are conducted to estimate the flood inundation areas by using random variables selected from their probability distribution in a 1D hydraulic model and a terrain analysis tool. The simulations are separately conducted for uncertainty propagation estimation with the FOA method and relative sensitivity analysis with the HSY method. For both methods, the same probability distribution and ranges in variable magnitudes (Manning's n, discharge, and topography) are used in the MC simulations. In addition, all target random variables are generated only once for each simulation. In the case of discharge, a t-distribution is used for the Seymour reach, and a uniform distribution is used for the Strouds reach. In the case of Manning's n, which is differently assigned at each cross-section, the selected random variable represents a percentage change that is applied to the entire cross-section. Similarly, a random number for topography represents an error in the selected range, and this error is applied to each elevation point within all cross-sections.

In estimating the uncertainty propagation rate of each variable, one variable (referred as target variable) among the three variables is randomly selected, and the two other variables (referred as conditional variables) are kept constant with minimum, mean, and maximum values in their feasible range. For example, Table 4.2 shows nine cases (Case 1 to 9) where topography and discharge (conditional variables) have minimum, mean, and maximum values to study the effect of Manning's n (target variable) on the flood inundation area. One thousand Monte Carlo simulations are conducted for each

condition. Therefore, a total of 9,000 simulations are performed for each target variable because of the nine conditions associated with the other two conditional variables.

Unlike the FOA method that uses one target variable and two conditional variables, Monte Carlo simulations for HSY sensitivity analysis use randomly selected two target variables, and one conditional variable, which is kept constant with minimum, mean, and maximum values. Two target variables are used to estimate their relative sensitivities on flood inundation area. Also, the relative sensitivities between two target variables are estimated for one conditional variable with minimum, mean, and maximum values, respectively. Table 4.3 shows three cases consisting of two target variables and one conditional variable for Seymour reach. Case H1 in Table 4.3 is for estimating relative sensitivities between two target variables (discharge and Manning's n) when one conditional variable is changed to minimum, mean, and maximum values. Fifteen thousand simulations are performed for each case (Case H1, H2, and H3), and thus a total of 45,000 simulations are conducted for each study reach.

Table 4.2: The conditions of topography and discharge for uncertainty propagation using the FOA method (A target variable: Manning's n; two conditional variables: topography and discharge)

	Topography	**Discharge**	**Iterations**
Case 1	Min	Min	1000
Case 2	Min	Mean	1000
Case 3	Min	Max	1000
Case 4	Mean	Min	1000
Case 5	Mean	Mean	1000
Case 6	Mean	Max	1000
Case 7	Max	Min	1000
Case 8	Max	Mean	1000
Case 9	Max	Max	1000

Table 4.3: The conditions for relative sensitivity of topography (E), discharge (F), and Manning's n (N) using the HSY method in Seymour reach

	Conditional variable	**Target variable 1**	**Target variable 2**	**Iteration**
Case H1	E_{Min}	F	N	5000
	E_{Mean}	F	N	5000
	E_{Max}	F	N	5000
Case H2	F_{Min}	E	N	5000
	F_{Mean}	E	N	5000
	F_{Max}	E	N	5000
Case H3	N_{Min}	E	F	5000
	N_{Mean}	E	F	5000
	N_{Max}	E	F	5000

4.2.3. Estimation of uncertainty propagation using FOA method

Estimation of uncertainty propagation using FOA is based on a function associated with multiple variables. Studying error propagation in flood inundation mapping is complex due to the difficulty of creating a mathematical equation that includes spatial extent of a flood inundation map. Instead of a function that includes all of the modeling variables, a regression equation between an individual variable and the inundation area can be developed. This approach is only feasible when the regression equation has a high coefficient of correlation. In this study, the minimum correlation coefficient between the simulated and regressed inundation area is 0.99. The effect of a single variable on a flood inundation area can be influenced by changes in the other variables. It is inefficient to consider simultaneous changes in all variables to study uncertainty propagation. Therefore, while studying the effect of one variable, the conditions of other variables are restricted to minimum, mean, and maximum values in the feasible range. As a result, one target variable has nine conditions associated with two other conditional variables, and in this study, a total of 27 conditions for each reach are used to quantitatively estimate uncertainty propagation. The FOA method is eventually applied to the regression equations based on the simulation results, and then the uncertainty propagation rate is estimated (Fig. 4.1). In the FOA method, the uncertainty propagation rate is the ratio of the flow inundation area to the modeling variable, which means the magnitude of uncertainty from the modeling variables is linearly transferred to the inundation area.

The FOA methodology for the uncertainty propagation includes: 1) creating the inundation area by randomly selecting one target variable by restricting the two

conditional variables to minimum, mean, and maximum values; 2) creating the regression equation based on the plot between a target variable and the simulated inundation area; and 3) evaluating the uncertainty propagation of the variable using the FOA method.

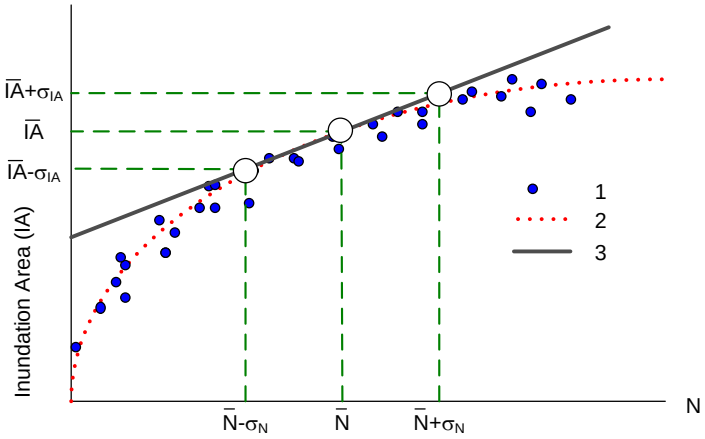

Fig. 4.1: Steps of FOA method for estimating uncertainty propagation: 1) plotting output; 2) adding regression equation; 3) making first order function, where X-axis indicates a variable, and Y-axis shows inundation area. IA indicates inundation areas, σ is standard error, and N means a parameter

4.2.4. HSY sensitivity analysis

When multiple variables are used in a model, all variables will have different effects on the model output. Therefore, it is important to understand how the multiple variables interact under various conditions. The HSY method, which is a global sensitivity analysis, is used to evaluate the relative influence among multiple model variables. In HSY sensitivity analysis, one variable is used as a conditional variable and two target variables are restricted to minimum, mean, and maximum values during the Monte Carlo simulations. In this study, the cut-off threshold is defined in terms of the top 70% of the ranked model outputs because there is no clear definition to distinguish the behavioral and non-behavioral classes (Hornberger et al. 1985). In addition, the cumulative density functions (CDF) of the two classes are estimated by a likelihood measure based on F-statistic (Eq. 4.1).

$$\text{F-statistic for the i}^{\text{th}}\text{ iteration, } F_i = \frac{1}{P_i} = \left(\frac{A_{op,i}}{A_o + A_{p,i} - A_{op,i}} \right) \times 100 \qquad (4.1)$$

where, A_o indicates the observed inundation area, A_p refers to the predicted flood inundation area, and A_{op} represents the intersection of both observed and predicted inundation areas.

The HSY methodology includes: 1) determining two target variables and one conditional variable; 2) fixing a conditional variable and randomly selecting two target variables in the feasible ranges; 3) estimating the water surface elevation by applying three variables to HEC-RAS; 4) estimating the flood inundation area by terrain analysis; 5) calculating

the F-statistic; 6) repeating Steps 1-5 5,000 times; 7) defining two classes of flood inundation areas for each target variable taking the top 70% and bottom 30% of the simulated flood inundation areas; 8) plotting CDFs for two classes separately; 9) calculating Kolmogorov-Smirnov (KS) d statistic; 10) comparing the estimated KS d statistics of two target variables.

4.3. Results

4.3.1. Monte Carlo simulations

For the uncertainty propagation estimation, Monte Carlo simulations were conducted for the individual variables, including Manning's n (N), topography (E), and discharge (F). Specifically, the uncertainty propagation from one target variable is estimated for the combined conditions of the other two conditional variables. In both study reaches, the differences between the maximum and minimum flood inundation areas are generally larger when the other two conditional variables are fixed at minimum values. In the case of the Seymour reach, Manning's n had the highest influence on the flood inundation area, and flow condition had the least influence. The differences between the simulated inundation areas are in the range of 0.07 to 4.49 km^2 (Table 4.4). In the case of Strouds reach, discharge shows the largest difference with 0.082 km^2, while the Manning's n variation yields the minimum inundation difference of 0.023 km^2 (Table 4.5). These simulated inundation areas are also used for estimating the regression model to overcome the difficulty of a mathematical equation for flood inundation modeling.

The results from the Monte Carlo simulations for HSY sensitivity analysis show the flood inundation area obtained by using two target variables with one fixed conditional variable in HEC-RAS. In the case of the Seymour reach, the combination datasets of two target variables among Manning's n, discharge, and topography involving uncertainty produced a flood inundation area in the range of 6.26 to 11.09 km^2 (Table 4.6). In the case of Strouds reach, the flood inundation area simulated by the combination dataset ranged from 0.127 to 0.259 km^2 (Table 4.7). Similar to the case of uncertainty propagation estimation, the deviations in flood inundation area increased when the conditional variable has minimum value for both study reaches.

Table 4.4: The deviations of flood inundation area under the given conditions for Seymour reach [km^2]

a. Target variable: Manning's n

	F_{Min}	F_{Mean}	F_{Max}
E_{Min}	3.47	3.07	2.68
E_{Mean}	0.99	0.88	0.73
E_{Max}	0.28	0.25	0.25

b. Target variable: discharge

	E_{Min}	E_{Mean}	E_{Max}
N_{Min}	1.38	0.41	0.11
N_{Mean}	0.91	0.23	0.07
N_{Max}	0.60	0.15	0.09

c. Target variable: topography

	N_{Min}	N_{Mean}	N_{max}
F_{Min}	4.49	2.26	1.31
F_{Mean}	3.86	1.75	1.05
F_{Max}	3.22	1.43	0.79

Table 4.5: The deviations of flood inundation area under the given conditions for Strouds reach [$0.1km^2$]

i. Target variable: Manning's n

	F_{Min}	F_{Mean}	F_{Max}
E_{Min}	0.48	0.42	0.37
E_{Mean}	0.45	0.35	0.34
E_{Max}	0.36	0.31	0.33

ii. Target variable: discharge

	E_{Min}	E_{Mean}	E_{Max}
N_{Min}	0.82	0.72	0.58
N_{Mean}	0.74	0.63	0.53
N_{Max}	0.69	0.62	0.55

iii. Target variable: topography

	N_{Min}	N_{Mean}	N_{max}
F_{Min}	0.43	0.40	0.32
F_{Mean}	0.37	0.29	0.26
F_{Max}	0.27	0.25	0.23

Table 4.6: Flood inundation area simulated by the combination two target random variables for Seymour reach [km^2]

a. Target variables: Manning's n and discharge

Area	E_{Min}	E_{Mean}	E_{Max}
Min	6.35	9.76	10.74
Max	10.25	10.88	11.09
Dev	3.90	1.12	0.35

b. Target variables: topography and Manning's n

Area	F_{Min}	F_{Mean}	F_{Max}
Min	6.26	6.97	7.67
Max	11.00	11.04	11.09
Dev	4.74	4.07	3.42

c. Target variables: discharge and topography

Area	N_{Min}	N_{Mean}	N_{max}
Min	6.31	8.75	9.73
Max	10.83	10.99	11.09
Dev	4.52	2.24	1.36

Table 4.7: Flood inundation area simulated by the combination two target random variables for Strouds reach [0.1 km^2]

i. Target variables: Manning's n and discharge

Area	E_{Min}	E_{Mean}	E_{Max}
Min	0.13	0.15	0.17
Max	0.24	0.25	0.26
Dev	0.11	0.10	0.09

ii. Target variables: topography and Manning's n

Area	F_{Min}	F_{Mean}	F_{Max}
Min	0.13	0.16	0.20
Max	0.25	0.23	0.26
Dev	0.12	0.07	0.06

iii. Target variables: discharge and topography

Area	N_{Min}	N_{Mean}	N_{max}
Min	0.13	0.15	0.18
Max	0.23	0.24	0.26
Dev	0.10	0.09	0.08

4.3.2. Uncertainty propagation estimation using the FOA method

All of the regression equations used in estimating the uncertainty propagation rate have high correlation coefficients of more than 0.99 with the flood inundation areas simulated from regression equation and MC simulations. Results from the FOA method show that error in a selected target variable (discharge, Manning's n, and topography) is differently transferred to the flood inundation area according to values of the two conditional variables. Tables 4.8 and 4.9 show the uncertainty propagation rates of each variable for both study reaches. The uncertainty propagation rate is the ratio of flood inundation area to the rate of change of the target variable. The uncertainty propagation rate of a target variable is maximized when the two conditional variables assume minimum values. The trend of uncertainty propagation rates using FOA method (Table 4.8 and 4.9) is very similar to the deviation of flood inundation areas in the MC simulations (Table 4.4 and 4.5). These results could have been influenced by the geometric features of both study reaches. Specifically, the Seymour reach has a wide U-shaped valley and the Strouds reach has a relatively small V-shaped valley. Typically, for these geometric features, a high conveyance which has large wet areas for a given flow condition leads to a wide top water surface. Therefore, although the same uncertainty in one individual variable is applied to flood inundation modeling, the uncertainty propagation could be lower in high conveyance channels, and higher in low conveyance channels.

In the case of the Seymour reach, 1% change in initial Manning's n values produced uncertainties from 0.27E-2 to 4.55E-2 km^2 in flood inundation area, 1% change in discharge produced uncertainties from 0.3E-2 to 5.36E-2 km^2, and 1 cm vertical error in

topography produced uncertainties between 0.4E-2 and 2.52E-2 km^2. In the case of Strouds reach, 1% change in Manning's n values produced uncertainties from 4.32E-4 km^2 to 6.62E-4 km^2, 1% change in logarithmic discharge produced uncertainties from 0.50E-4 to 0.70E-4 km^2, and 1 cm change in topography produced uncertainties from 4.98E-4 and 8.79E-4 km^2.

In Table 4.8 (a) the uncertainty propagation rate due to Manning's n is affected by topography and discharge, but its effect is drastically reduced with increasing topography values. Similarly, in Table 4.8 (b) the uncertainty propagation rate due to discharge gets affected more by increasing topography values than by increasing Manning's n values. As a result, topography is the main contributor to the uncertainty in flood inundation area for the Seymour reach, and the discharge is the main contributor of uncertainty for the Strouds reach. Assuming that the price to remove unit uncertainty in all model variables (Manning's n, discharge, and topography) is equal, in the case of the Seymour reach, discharge gets the highest priority in terms of uncertainty removal for more accurate flood inundation mapping for low conveyance channel, and topography for high conveyance channel. In the case of the Strouds reach, the uncertainty in topography should be removed first for accurate flood inundation mapping.

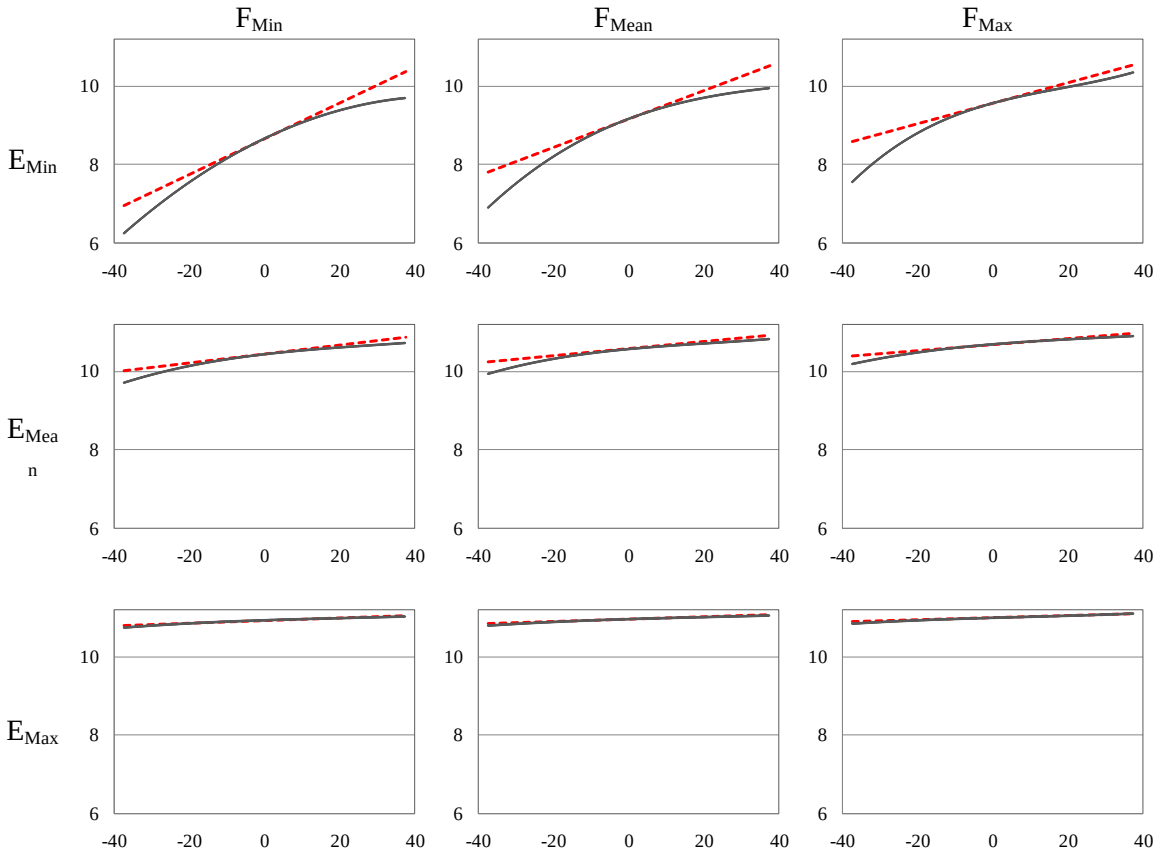

Fig. 4.2: Regression equations between Manning's n change rate and flood inundation of Seymour reach under the conditions of discharge and topography. x-axis indicates the relative change rate of Manning's n, and y-axis is flood inundation area ($0.1km^2$).

Table 4.8: The uncertainty propagation rates of target variables for Seymour reach

a. Target variable: Manning's n [0.01 km^2/%]

	F_{Min}	F_{Mean}	F_{Max}
E_{Min}	4.55	3.60	2.60
E_{Mean}	1.11	0.89	0.80
E_{Max}	0.31	0.28	0.27

b. Target variable: discharge [0.01 km^2/%]

	E_{Min}	E_{Mean}	E_{Max}
N_{Min}	5.36	1.59	0.44
N_{Mean}	3.74	0.89	0.30
N_{Max}	2.71	0.61	0.34

c. Target variable: topography [0.01 km^2/cm]

	N_{Min}	N_{Mean}	N_{max}
F_{Min}	2.52	1.28	0.68
F_{Mean}	2.06	1.07	0.52
F_{Max}	1.70	0.80	0.40

Table 4.9: The uncertainty propagation rates of target variables for Strouds reach

i. Target variable: Manning's n [10^{-4} km^2/%]

	F_{Min}	F_{Mean}	F_{Max}
E_{Min}	0.48	0.42	0.37
E_{Mean}	0.45	0.35	0.34
E_{Max}	0.36	0.31	0.33

ii. Target variable: discharge [10^{-4} km^2/% in logarithm]

	E_{Min}	E_{Mean}	E_{Max}
N_{Min}	0.82	0.72	0.58
N_{Mean}	0.74	0.63	0.53
N_{Max}	0.69	0.62	0.55

iii. Target variable: topography [10^{-4} km^2/cm]

	N_{Min}	N_{Mean}	N_{max}
F_{Min}	0.43	0.40	0.32
F_{Mean}	0.37	0.29	0.26
F_{Max}	0.27	0.25	0.23

4.3.3. Relative sensitivity analysis using the HSY method

The results from the HSY sensitivity analysis show the relative sensitivity when a pair of target variables generated from their prior probability distribution are analyzed in mapping the flood inundation area. Figs. 4.3 and 4.4 show CDFs of top 70% class and bottom 30% class for two target variables with one conditional variable restricted by minimum, mean, and maximum values. The difference between two CDFs in a target variable indicates sensitivity, and two target variables for a given condition have different sensitivities (relative sensitivity). In Table 4.10, cases H2 and H3 show that the topography is much more sensitive to the flood inundation area for the Seymour reach than the other variables; and case 1 shows that the D-statistic of Manning's n is higher than the discharge. These results indicate that topography is the most sensitive variable on the flood inundation area for the Seymour reach. For the Strouds reach, the discharge had a higher D-statistic than topography and Manning's n for H4 and H6 cases, which means that the discharge is most sensitive among the three variables. The results from the uncertainty propagation estimation, using FOA and HSY sensitivity analysis, show the same variables are most sensitive for each study reach.

Unlike the uncertainty propagation estimation corresponding to the simulated flood inundation area, the D-statistics calculated in this study are based on the F-statistic, which indicate the degree of fitness between the base maps and the simulated floodplains. For each case, the relative D-statistic values of the two target variables vary as a conditional variable is changed. Specifically, in the case of the Seymour reach, the relative sensitivities from the two target variables generally decreased with increasing value of a

conditional variable. However, in the case of the Strouds reach, Manning's n does not show any consistent trend with change in the conditional variable. Considering change in a conditional variable, the results for the Strouds reach are different for HSY method in comparison with the results from the FOA method. This is because the HSY method based is on F-Statistic that is related to the overlap between simulated and observed flood inundation; whereas the FOA method is based on just the change in the total inundation area (Table 4.8 and 4.10).

In Table 4.10, case H5 has two target variables (topography and Manning's n) and one conditional variable (discharge) for Strouds reach. This case shows that the topography has lower D-statistic than Manning's n for the minimum and mean discharge. However, when discharge is maximum, topography is more sensitive than Manning's n.

Table 4.10: D-statistics using the HSY method for Seymour and Strouds reaches

Cases	Conditional variable	Target variable1	Target variable2
Case H1 Seymour reach	topography	Manning's n	discharge
	E_{Min}	0.149	0.945
	E_{Mean}	0.099	0.941
	E_{Max}	0.153	0.926
Case H2 Seymour reach	discharge	topography	Manning's n
	F_{Min}	0.836	0.283
	F_{Mean}	0.789	0.266
	F_{Max}	0.735	0.262
Case H3 Seymour reach	Manning's n	Topography	discharge
	N_{Min}	0.987	0.049
	N_{Mean}	0.974	0.054
	N_{Max}	0.905	0.042
Case H4 Strouds reach	topography	Manning's n	discharge
	E_{Min}	0.601	0.316
	E_{Mean}	0.620	0.353
	E_{Max}	0.676	0.438
Case H5 Strouds reach	discharge	topography	Manning's n
	F_{Min}	0.237	0.472
	F_{Mean}	0.437	0.572
	F_{Max}	0.566	0.526
Case H6 Strouds reach	Manning's n	Topography	discharge
	N_{Min}	0.284	0.606
	N_{Mean}	0.326	0.681
	N_{Max}	0.403	0.757

a) Case H1 (Fixed variable: topography, Target variables: discharge and Manning's n)

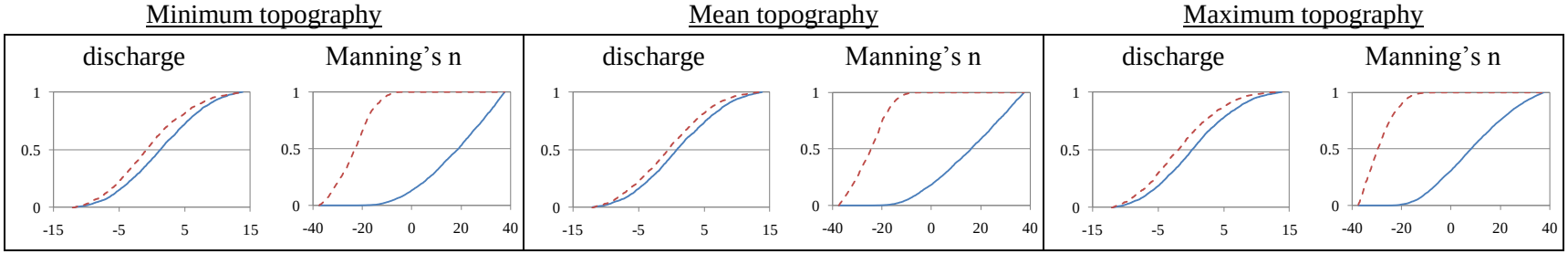

b) Case H2 (Fixed variable: discharge, Target variables: topography and Manning's n)

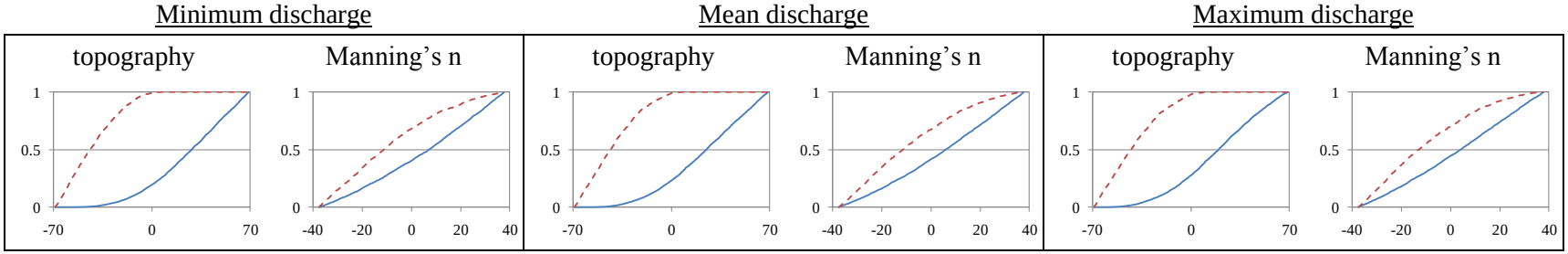

c) Case H3 (Fixed variable: Manning's n, Target variables: topography and discharge)

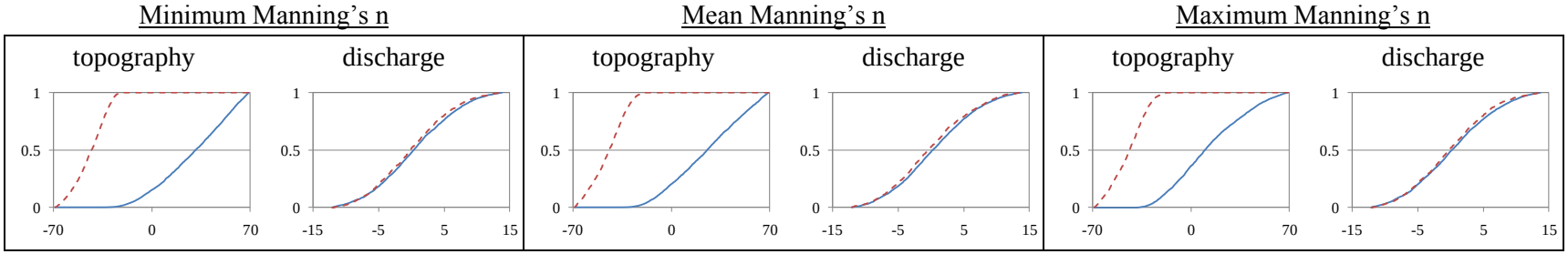

Fig. 4.3: CDFs of top 70% class and bottom 30% class for Seymour reach. Solid line indicates the top 70% class, and dashed line is bottom 30% class.

a) Case H4 (Fixed variable: topography, Target variables: discharge and Manning's n)

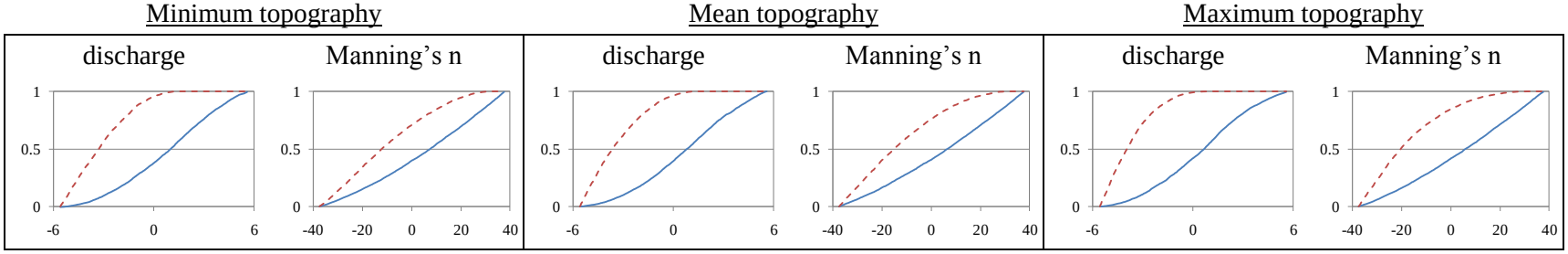

b) Case H5 (Fixed variable: discharge, Target variables: topography and Manning's n)

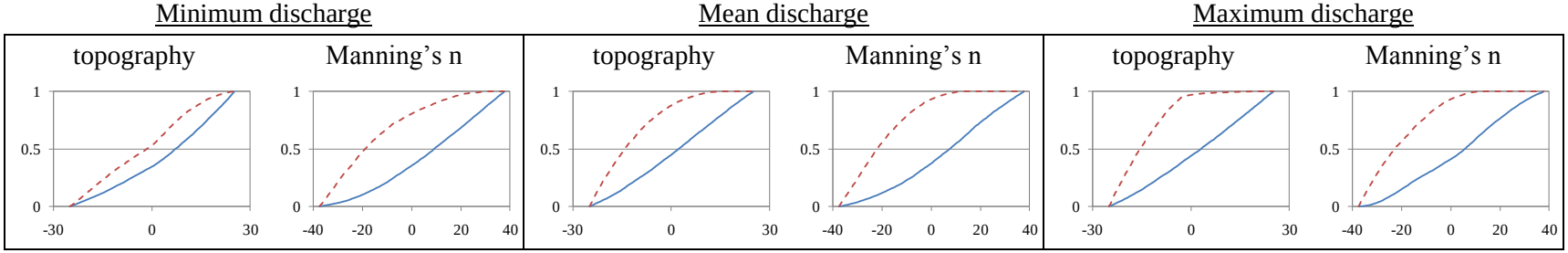

c) Case H6 (Fixed variable: Manning's n, Target variables: topography and discharge)

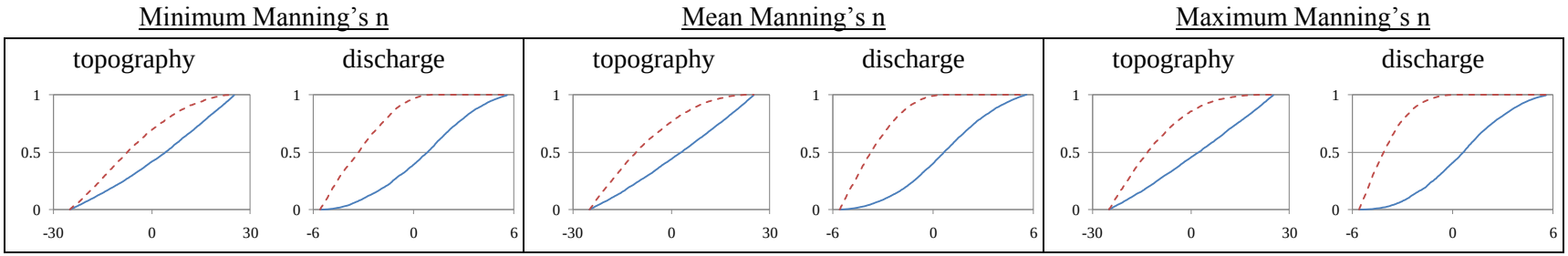

Fig. 4.4: CDFs of top 70% class and bottom 30% class for Strouds reach. Solid line indicates the top 70% class, and dashed line is bottom 30% class.

4.4.Conclusions

Accuracy in flood inundation prediction depends on the uncertainty of the variables involved in flood inundation modeling. Despite recognizing uncertainty in the input data and model parameters, several practical constraints make it difficult to completely remove the uncertainty. However, an improved understanding of uncertainty can lead toward finding ways for reducing the uncertainty. In reducing the uncertainty, the priority of the target variables that contribute to uncertainty should be considered for optimal flood risk management because the uncertainty from the input data and the model variables is differently propagated to flood inundation. This study addressed the issue of uncertainty propagation from combined variables through computation of the uncertainty propagation rates of individual variables using the FOA method and relative sensitivity between two target variables using the HSY sensitivity analysis.

The following conclusions are drawn from this study:

- Uncertainty analysis using the FOA and HSY methods show that topography is a major contributor of uncertainty for the Seymour reach, and discharge had the most impact for the Strouds reach.
- If the price to remove unit uncertainty in all model variables (Manning's n, discharge, and topography) is assumed to be equal, discharge gets the highest priority in terms of uncertainty removal for Seymour reach during low conveyance and topography during high conveyance. In the case of the Strouds

reach, the uncertainty in topography should be removed first for accurate flood inundation mapping.

- The uncertainty propagation rates estimated by using the FOA method shows that uncertainty in a target variable is differently propagated to a flood inundation area corresponding to values of two conditional variables. In addition, the results using the FOA method show that uncertainty in all model variables (Manning's n, discharge, and topography) is less propagated to flood inundation area for high conveyance channel with wide top water surface. Therefore, estimation of uncertainty propagation needs to consider the effect of physical geometry as well as uncertainty in model variables.
- The results from the HSY sensitivity analysis show that as a conditional variable gets higher values, the relative sensitivities between two target variables are lower for the Seymour reach, and higher for the Strouds reach. The HSY sensitivity analysis for Strouds reach produces inconsistent results with the results using the FOA method because HSY sensitivity analysis is based on F-statistic. From these results, it can be expected that discrepancy in the matches between simulations and observations is higher in high conveyance channel compared to low conveyance channel for the Strouds reach.
- For Strouds reach, the HSY sensitivity analysis shows that topography is more sensitive than Manning's n for high discharge, but Manning's n is more sensitive than topography for low discharge. Therefore, efficient flood risk management for Strouds reach needs to consider the magnitude of design flood in improving the quality of model variables.

CHAPTER 5. UNCERTAINTY QUANTIFICATION IN FLOOD INUNDATION MAPPING USING GENERALIZED UNCERTAINTY ESTIMATION (GLUE) AND SENSITIVITY ANALYSIS

5.1.Introduction

The process of creating flood inundation maps is affected by uncertainties in data, modeling approaches, parameters, and geo-processing tools. Generalized likelihood uncertainty estimation (GLUE) is one of the popular techniques used to represent uncertainty in model predictions through Monte Carlo analysis coupled with Bayesian estimation. The objectives of this study are to: (i) compare the uncertainty arising from multiple variables in flood inundation mapping using Monte Carlo simulations and GLUE; and (ii) investigate the role of subjective selection of the GLUE likelihood measure in quantifying uncertainty in flood inundation mapping. The roles of flow, topography and roughness coefficient are investigated on the output of one-dimensional HEC-RAS model and flood inundation map for an observed flood event on East Fork White River near Seymour, Indiana (Seymour reach) and Strouds reach in Orange County, North Carolina. Performance of GLUE is assessed by selecting three likelihood functions including the sum of absolute error (SAE) in water surface elevation and inundation width, sum of squared error (SSE) in water surface elevation and inundation width, and a statistic (F-statistic) based on the area of observed and simulated flood inundation map.

5.2.Methodology

The methodology involves: (i) creating probability distributions for discharge, Manning's n and topography; (ii) using the probability distributions to run Monte Carlo simulations using HEC-RAS model; and (iii) creating uncertainty bounds related to discharge, Manning's n and topography using the GLUE framework. A brief description of each step in the methodology is given below.

5.2.1. Probability distribution for model variables

In this chapter, probability types for model variables are same to those in chapter 4. All model variables, except discharge which has t-distribution in the Seymour reach, have uniform distributions. However, in the case of the Seymour reach, the number of uniform distributions to generate random numbers are 9 for either of Manning's n or topography because the model variables at each cross-section that has different effects on the output. Similarly, a total of 17 uniform distributions of Manning's n and topography values and one uniform distribution for discharge are required for the Strouds reach.

Table 5.1: The conditions for random variables generated in a simulation

Study Area	Initial (variables)	Modeling Variables estimated by RV	Min	Max	Probability Type	No. of Chosen RV
Seymour	N_i Manning's n	$N = N_i (1+RV)$	-0.375	0.375	Uniform	9
Strouds		$N = N_i (1+RV)$	-0.375	0.375	Uniform	17
Seymour	F_i Discharge	$F = F_i * 10^{0.0286RV}$ [m^3/s]	-1.963	1.963	T-distribution	1
Strouds		$F = F_i * 10^{RV}$ [m^3/s]	-0.194	0.194	Uniform	1
Seymour	E_i Topography	$E = E_i + RV$ [m]	-0.69	0.69	Uniform	9
Strouds		$E = E_i + RV$ [m]	-0.25	0.25	Uniform	17

5.2.2. Monte Carlo simulations

Monte Carlo simulations are conducted by using the HEC-RAS model with steady state flow conditions. A total of 1000 HEC-RAS simulations are performed for each variable (discharge, topography and channel roughness) by selecting a random number from their prior probability distributions. In the case of discharge, which is a single input to the model, only one random discharge value is generated to conduct one simulation. In the case of channel roughness, which is different for each cross-section, multiple random numbers (one for each cross-section) are generated for each simulation. As mentioned in the "Probability Distribution for Channel Roughness" sub-section, a random number actually represents a percentage, and this percentage is applied to each Manning's n within a cross-section. For example, if a cross-section has three Manning's n of 0.03 (left bank), 0.02 (main channel), and 0.04 (right bank), a random number of -10 (percent) will reduce these Manning's n to 0.027, 0.018 and 0.036 to represent a change of -10%.

Similarly, multiple random numbers are generated to conduct HEC-RAS simulations for topography. Similar to channel roughness, a random number for topography represents an error in the ± 0.25 m range, and this error is applied to each elevation point within a cross-section. The combination of uncertainty is performed by selecting all random variables for topography, flow, and roughness in a simulation. Therefore, the combination dataset include more uncertainty transferred to the flood inundation than uncertainty arising from a single variable.

5.2.3. Uncertainty bounds using GLUE

A description of GLUE is already presented in section 2.5. After Monte Carlo simulations, all outputs are evaluated by a likelihood measure to reflect how well the simulated model compares with the observed or baseline output. The selection of a likelihood measure is a subjective process, and the uncertainty bound obtained using GLUE is affected by the choice of the likelihood measure. To investigate the effect of the selection of likelihood measures on the uncertainty bound, xix likelihood measures are used in this study. These measures include: (W1) sum of absolute errors in inundation width (Eq. 5.1); (W2) sum of squared errors in inundation width (Eq. 5.2); (E1) sum of absolute errors in water surface elevation (Eq. 5.3); (E2) sum of squared errors in water surface elevation (Eq. 5.4); F-statistic (Eq. 5.5); and (U) uniform probability (Eq. 5.6) that describes the overall matching of the model flood inundation area with the model predicted area.

$$W1_i = \sum_{j=1}^{N} \left| W_{m,i} - W_o \right| \quad (5.1)$$

$$W2_i = \sum_{j=1}^{N} \left(W_{m,i} - W_o \right)^2 \quad (5.2)$$

where $W_{m,i}$ of ith iteration and W_o represent the model water surface width and observed water surface width, respectively for cross-section *j*.

$$E1_i = \sum_{j=1}^{N} \left| E_{m,i} - E_o \right| \quad (5.3)$$

$$E2_i = \sum_{j=1}^{N} \left(E_{m,i} - E_o \right)^2 \quad (5.4)$$

where $E_{m,i}$ of ith iteration and E_o represent the model water surface elevation and observed water surface elevation, respectively for cross-section *j*.

$$\text{F statistic of i}^{th}\text{ iteration, } F_i = \frac{1}{P_i} = \left(\frac{A_{op,i}}{A_o + A_{p,i} - A_{op,i}} \right) \times 100 \quad (5.5)$$

where A_o indicates the observed inundation area, A_p refers to the predicted flood inundation area, and A_{op} represents the intersection of both observed and predicted inundation areas.

$$U = \frac{1}{N} \quad (5.6)$$

A 1D model such as HEC-RAS provides water surface elevations along cross-sections only. To get inundation area from these discrete model output, the topography is

subtracted from the water surface area, which is derived by triangulated interpolation of water surface elevations at each cross-section. Likelihood measures W1 and W2 are related to inundation width, E1 and E2 are related to inundation elevation, and F is related to inundation area. Observed inundation width at each cross-section is extracted by intersecting the observed inundation area polygon with the cross-section, and the observed water surface elevation is extracted by reading the DEM elevation at the intersection point. It is assumed that the observed data do not have any errors, and this assumption will lead to a conservative analysis, thus yielding relatively narrower uncertainty bounds. In this study all simulation outputs are assumed as behavioral models to build the CDF for getting the uncertainty bound.

5.3. Results

5.3.1. Monte Carlo Simulations

Results from Monte Carlo simulations for each variable including roughness, topography and flow, and a combination of all variables are presented in Table 5.2 – 5.3, and Fig. 5.1 – 5.2. Results show that the combined parameters create the most deviation in the output compared to the base data. Because of the differences in size and topography of these two reaches, the effect of each variable on water surface elevation, extent and flood inundation area is different. In the case of Seymour reach, topography creates the most deviation in flood inundation area compared to the observed inundation map; whereas flow and topography are major factors in the case of Strouds reach. Considering that

there is a difference of 1044 m^3/s between the flow bounds, the narrowest uncertainty bound in the flow can be contributed to the wide U-shaped river valley along the Seymour reach.

The statistics presented in Tables 2 and 3 are computed by using the data from all Monte Carlo simulations for a particular variable or their combination. For example, a minimum WSE of 172.82 m from roughness (first row on Table 5.2) represents the minimum WSE among all cross-sections from all 1000 simulations. Similarly, the statistics for the combined column is computed using data from 5000 simulations. The WSE and extent bounds in Figs. 5.1- 5.4 are also computed by using the data at each cross-section from all Monte Carlo simulations for a specific variable, or the combination of all variables.

The observed minimum and maximum water surface elevations among all cross-sections for the Seymour reach are 173.27 m and 175.60 m, respectively. Combined uncertainty from all variables produces the largest deviation in minimum and maximum WSE by reducing the minimum WSE by 1.1 m, and increasing the maximum WSE by 0.88 m. Uncertainty in topography seems to contribute most variations in the WSE at the Seymour reach after the effect from all combined variables. Similarly, uncertainty in flow has the least effect on WSE variations at the Seymour reach. Changes in WSE affect the flood inundation extent and area. The combined effect of all variables produces the widest bound in the uncertainty in flood inundation area followed by topography, roughness and flow. The minimum and maximum inundation areas for the Seymour reach from MC simulations are shown in Fig. 5.3(a - c).

Table 5.2: MC simulation results for Seymour reach (WSE, extent and area)

a) Average WSE (m) from changes in

	Base	**Flow**	**Topography**	**Roughness**	**Combined**
Min	173.27	173.13	172.58	172.82	172.17
Max	175.60	175.73	176.28	175.88	176.48
Mean	174.34	174.34	174.38	174.32	174.37
St. Dev	0.76	0.76	0.77	0.75	0.77
(Max-Min)	2.33	2.60	3.70	3.06	4.31

b) Average extent (km) from changes in

	Base	**Flow**	**Topography**	**Roughness**	**Combined**
Min	3.02	3.02	2.79	3.01	2.78
Max	4.52	4.54	5.85	4.66	5.86
Mean	3.89	3.89	3.90	3.90	3.90
St. Dev	0.56	0.56	0.57	0.56	0.57
(Max-Min)	1.50	1.52	3.06	1.66	3.08

c) Area(km^2) from changes in

	Base	**Flow**	**Topography**	**Roughness**	**Combined**
Min	10.44	9.69	10.16	9.10	10.44
Max	10.67	10.89	10.77	10.95	10.67
Mean	10.56	10.54	10.54	10.51	10.56
St. Dev	0.05	0.21	0.11	0.28	0.05
(Max-Min)	0.23	1.20	0.61	1.85	0.23

Table 5.3: MC simulation results for Strouds reach (WSE, extent and area)

a) Average WSE (m) from changes in

	Base	**Flow**	**Topography**	**Roughness**	**Combined**
Min	146.66	146.30	146.41	146.60	145.75
Max	159.48	159.84	159.72	159.68	160.19
Mean	152.97	153.09	152.97	152.96	152.97
St. Dev	3.99	3.97	3.99	3.98	3.97
(Max-Min)	12.82	13.54	13.31	13.08	14.44

b) Average extent (km) from changes in

	Base	**Flow**	**Topography**	**Roughness**	**Combined**
Min	22.58	19.29	20.90	22.13	18.59
Max	299.82	321.44	316.00	315.69	370.06
Mean	188.13	190.05	187.85	187.77	189.61
St. Dev	64.00	61.22	63.54	63.18	61.49
(Max-Min)	277.24	302.16	295.11	293.56	351.48

c) Area (0.1 km^2) from changes in

	Base	**Flow**	**Topography**	**Roughness**	**Combined**
Min	1.75	1.95	1.93	1.64	1.75
Max	2.37	2.08	2.09	2.46	2.37
Mean	2.08	2.02	2.01	2.07	2.08
St. Dev	0.16	0.02	0.03	0.18	0.16
(Max-Min)	0.63	0.13	0.17	0.82	0.63

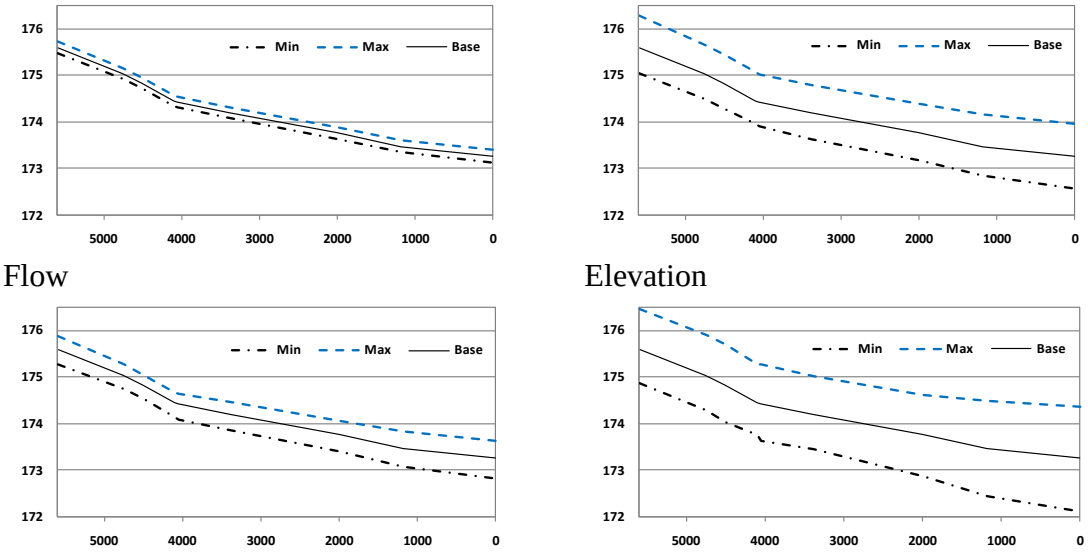

Fig. 5.1: WSE for Seymour reach. X axis shows stationing in meters and Y axis shows elevation in meters

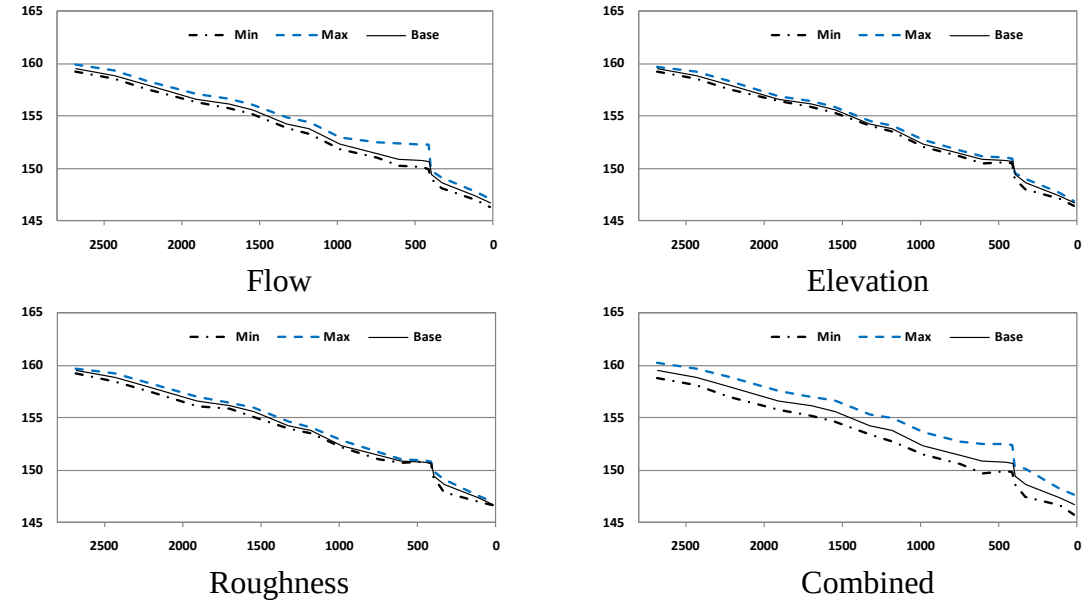

Fig. 5.2: WSE for Strouds reach. X axis shows stationing in meters and Y axis shows elevation in meters

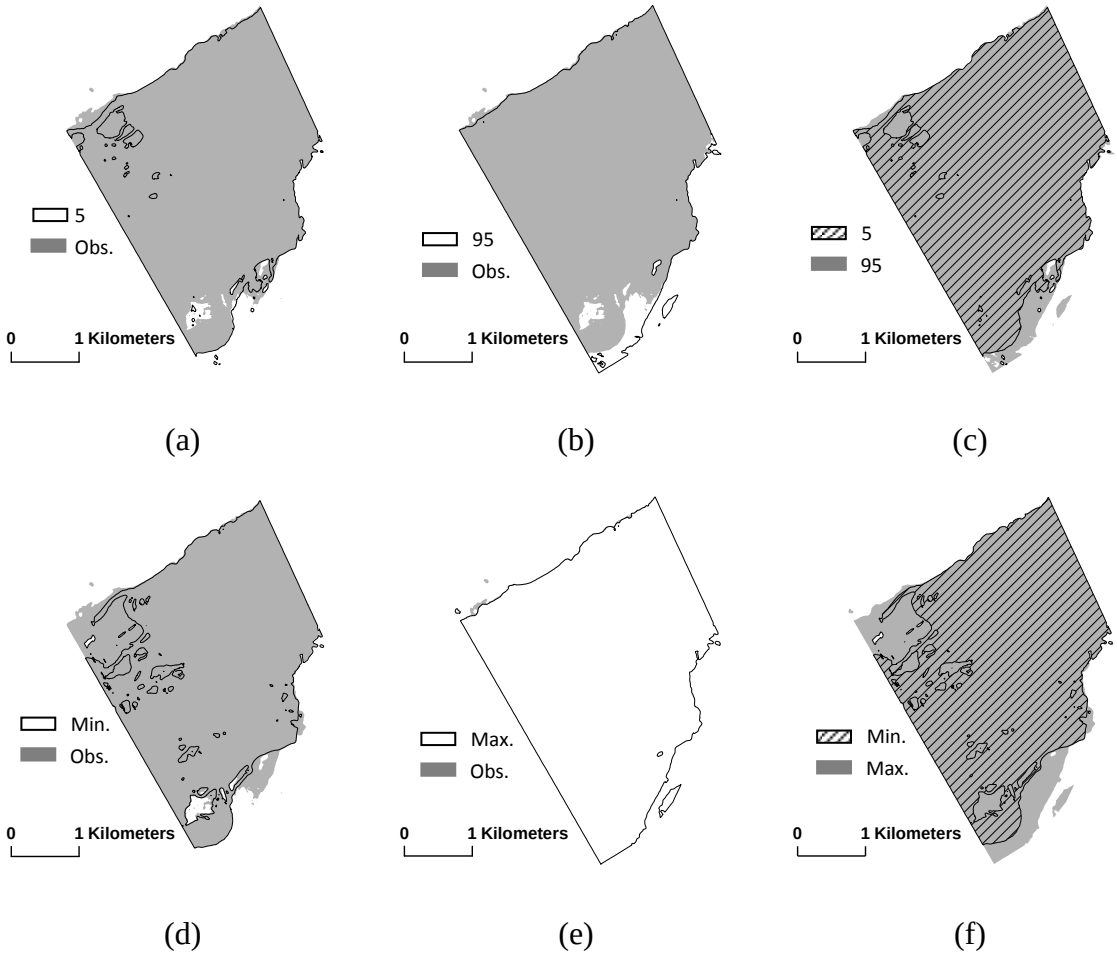

Fig. 5.3: Inundation areas for Seymour reach. 5 and 95 indicate the lower 5% and the higher 95% inundations areas, respectively. Min and max show the minimum and maximum inundation areas. Obs indicates the observed inundation area

In the case of Strouds reach, the observed minimum and maximum water surface elevations among all cross-sections are 146.66 m and 159.48 m, respectively. Similar to the Seymour reach, combined uncertainty from all variables produces the largest deviation in minimum and maximum WSE by reducing the minimum WSE by 0.91 m, and increasing the maximum WSE by 0.71 m. Unlike the Seymour reach, uncertainty in flow condition produces the largest variations in WSE at individual variable level

followed by uncertainty in topography and roughness. Except for the combined uncertainty from all variables, the uncertainty in flow conditions produces the widest bound in the flood inundation extent and area at Strouds reach, followed by topography and roughness. The minimum and maximum inundation areas for Strouds reach from MC simulations are shown in Fig. 5.4(a - c).

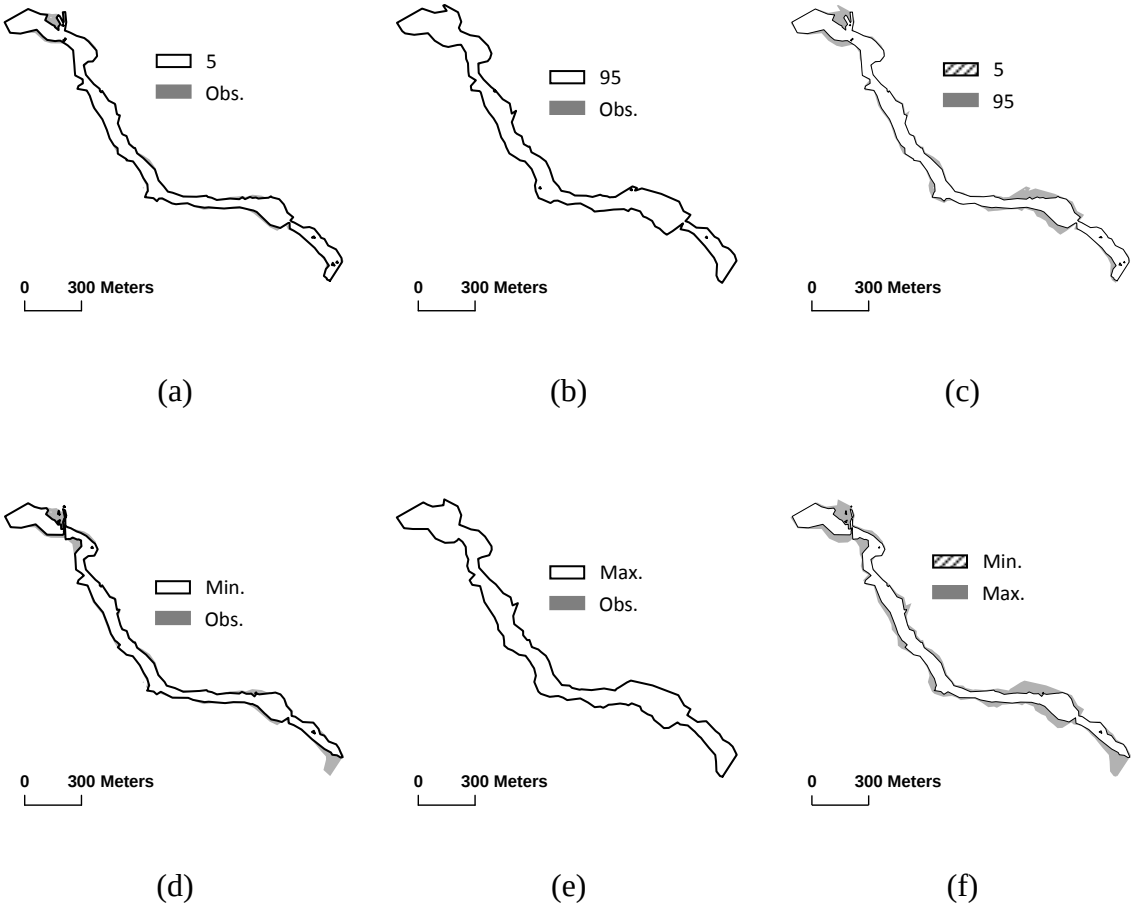

Fig. 5.4: Inundation areas for Strouds reach. 5 and 95 indicate the lower 5% and the higher 95% inundations areas, respectively. Min and max show the minimum and maximum inundation areas. Obs indicates the observed inundation area

5.3.2. GLUE and sensitivity analysis

Results from GLUE analysis at Seymour reach and sensitivity analysis at Strouds reach show the uncertainty bound in the flood inundation area from individual and combined effects of flow, topography and roughness for both study sites (Table 5.4 – 5.5 and Fig. 5.5 – 5.6). Table 5.4 and 5.5 show the 5 and 95% uncertainty bound using different likelihood measures. The uncertainty bound for the Seymour reach inundation area is in the range of 0.14 to 0.68 km^2 for individual variable, and is 0.53 to 0.88 km^2 for combined variables. Similar to Monte Carlo simulations, combination of all variables produce the widest uncertainty bound (0.88 km^2) followed by topography, roughness and flow. Considering the observed inundation area of 10.57 km^2 for the Seymour reach, the uncertainty bound for inundation area ranges from 1.3% to 8.3% of the base inundation area. Inundation areas for the Seymour reach corresponding to 5 and 95% confidence interval are shown in Fig. 5.3(d - f). The uncertainty bound for Strouds reach inundation area is in the range of 0.007 km^2 to 0.052 km^2 for individual variables, and is 0.058 km^2 for combined variables. At the individual variable level, flow data produce the widest uncertainty bound in the inundation area for Strouds reach. Considering the base inundation area of 0.2 km^2 for the Strouds reach, the uncertainty bound for the inundation area ranges from 4% to 29% of the base area. Inundation areas for Strouds reach corresponding to 5 and 95% confidence interval are shown in Fig. 5.4(d - f). The likelihood measure based on the E2 produces the narrowest uncertainty bound for the Seymour reach for each individual variable, as well as when the variables are combined.

Table 5.4: Uncertainty of inundation areas (in km^2) using GLUE for Seymour reach

Variable	Uncertainty Bound	Likelihood Measure					
		W1	W2	E1	E2	F	U
Flow	Lower 5%	10.50	10.51	10.47	10.52	10.52	10.47
	Upper 95%	10.65	10.66	10.66	10.66	10.67	10.64
	Bound	0.15	0.15	0.19	0.14	0.15	0.17
Elevation	Lower 5%	10.15	10.13	10.27	10.35	10.16	10.13
	Upper 95%	10.82	10.81	10.82	10.82	10.81	10.81
	Bound	0.67	0.68	0.55	0.47	0.65	0.68
Roughness	Lower 5%	10.37	10.37	10.36	10.43	10.43	10.35
	Upper 95%	10.71	10.70	10.67	10.72	10.72	10.71
	Bound	0.34	0.33	0.31	0.29	0.29	0.36
Combination	Lower 5%	9.99	9.97	10.20	10.30	10.03	9.96
	Upper 95%	10.84	10.83	10.84	10.83	10.84	10.84
	Bound	0.85	0.86	0.64	0.53	0.81	0.88

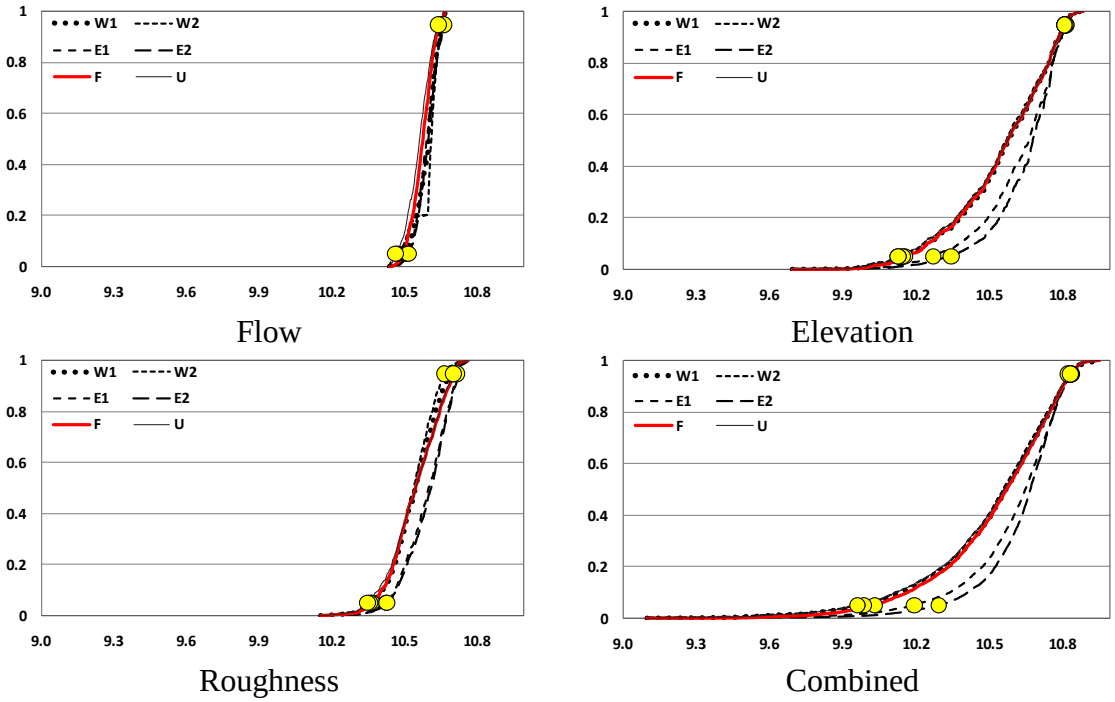

Fig. 5.5: GLUE for Seymour reach. X axis shows the inundation area and Y axis indicates CDF

Table 5.5: Uncertainty of inundation areas (0.1km^2) using GLUE for Strouds reach

Variable	Uncertainty Bound	Likelihood Measure					
		W1	W2	E1	E2	F	U
Flow	Lower 5%	1.79	1.77	1.78	1.78	1.77	1.78
	Upper 95%	2.28	2.28	2.27	2.27	2.26	2.30
	Bound	0.49	0.51	0.49	0.49	0.49	0.52
Elevation	Lower 5%	1.98	1.98	1.98	1.98	1.98	1.98
	Upper 95%	2.06	2.06	2.06	2.05	2.05	2.06
	Bound	0.08	0.08	0.08	0.07	0.07	0.08
Roughness	Lower 5%	1.96	1.96	1.97	1.97	1.96	1.96
	Upper 95%	2.05	2.05	2.06	2.06	2.04	2.06
	Bound	0.09	0.09	0.09	0.09	0.08	0.10
Combination	Lower 5%	1.78	1.76	1.77	1.76	1.75	1.77
	Upper 95%	2.30	2.30	2.28	2.26	2.28	2.35
	Bound	0.52	0.54	0.51	0.50	0.53	0.58

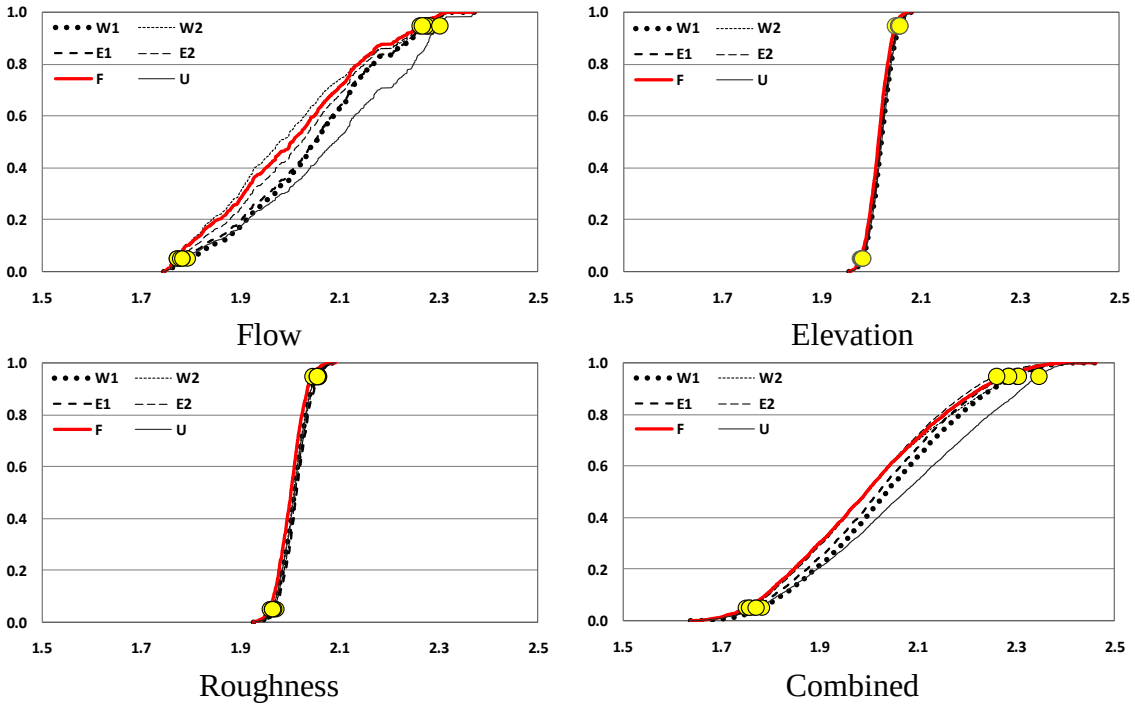

Fig. 5.6: GLUE for Strouds reach. X axis shows the inundation area and Y axis indicates CDF

The change in uncertainty bound from different likelihood measures is in the range of 0 to 2% for individual variable, and is in the range of 0 to 3.3% for combined variables. In the case of Strouds reach, all likelihood measures except U perform equally for all individual cases. The likelihood measure based on U produces the widest uncertainty bound for all individual and combined cases for the Strouds reach. The uncertainty bound from each variable does not add up to produce the combined uncertainty bound, thus demonstrating the non-linear nature of uncertainty propagation in the overall flood inundation mapping process.

5.4. Summary and Conclusions

Accurate communication of flood is critical for risk assessment in flood-prone areas, and to assist rescue and relief operations during floods. Accurate mapping and prediction of flood inundation is affected by uncertainty in input data and model parameters. Despite knowing the uncertainty in data and model parameters, it is still complex to understand and quantify the role of each uncertain variable in producing the final flood inundation map. Addressing this issue of uncertainty requires the knowledge of: (i) the extent to which the flood inundation map is affected by each variable; (ii) how the effect of any single variable changes from one area to another; and (iii) how the uncertainty from each variable propagates through the flood inundation process to contribute to the combined uncertainty in the flood inundation map. This study addresses the first issue of the impact of individual variables on the flood inundation extent through MC simulations. The second issue of the impact of uncertain variables in relation to different settings is

addressed to some extent, but this will require more than two study areas that are used in this study. In addition to looking at the uncertainty at each variable, this study also addresses the issue of quantifying and representing this uncertainty through the GLUE framework. The issue of subjective selection of a likelihood measure, and its effect on quantifying the uncertainty is investigated by using five different likelihood measures that are based on water surface elevation, extent and inundation area.

The following conclusions are drawn from this study:

- The overall flood inundation process is driven by the flow input, and it is logical to expect the uncertainty in flow to add the maximum uncertainty among all other variables (Prudhomme et al. 2003; Pappenberger et al. 2006c), but this may not hold true for all cases. In this study, it is found that a smaller "V" shaped cross-sectional reach (Strouds reach) is more affected by flow compared to a larger "U" shaped cross-sectional Seymour reach.
- Topography emerged as the top uncertain variable for Seymour Reach and ranked second after flow for Strouds reach. This finding can be attributed to the accuracy of topography data in flood inundation modeling and mapping. The vertical accuracy of Seymour DEM is 0.69 m, which is much lower than the vertical accuracy of the Strouds reach DEM. This conclusion is consistent with past studies that have found the accuracy of topography data to play a major role in flood inundation mapping (Wilson and Atkinson 2005; Merwade and Cook 2008b).
- The results from the Seymour reach show that the uncertainty from roughness coefficient is higher than the uncertainty from flow data, thus highlighting the

importance of this variable in the overall flood modeling process. This finding is related to the range of values and their corresponding distribution in applying the GLUE procedure, and the overall percentage changes in flow and Manning's n are in the range of 20 and 37.5% for Seymour reach, respectively. This result suggests that manipulating the roughness parameter during hydraulic model calibration without sound reasoning or physical basis will add more uncertainty in flood inundation mapping

- Results from GLUE for Seymour reach and sensitivity analysis for Strouds reach show that the difference in the uncertainty bound from all the likelihood measures produce less than 5% change in flood inundation for both study reaches. These results suggest that subjectivity involved in selecting the likelihood measure did not create significant impact on the overall quantification of the uncertainty in flood inundation mapping. It should be noted that the uncertainty bound depends on the nature of the flood event, the valley shape, model parameters, and assumptions made in the uncertainty analysis. Therefore, the generality of this finding in flood inundation mapping warrants investigation using data from more areas. In addition, it should be considered that as more variables are combined, the difference of uncertainty bounds between likelihood measures is larger.

5.5. Discussion

There are several aspects of this study that need more research to advance the treatment of uncertainty in flood inundation modeling and mapping. This study involved the use of only two datasets, and therefore similar studies must be conducted using more datasets with different topography, land use, hydrology, climatology and sizes. In addition, each variable must be investigated more thoroughly considering several aspects. For example, the topographic uncertainty in this study used only vertical accuracy as the source of uncertainty. Cook and Merwade (2009) found that other topographically derived model attributes such as geometry (cross-section spacing) can also have significant impact on the overall hydraulic model output including the subsequent mapping of flood inundation extent and area. Similarly, the flow data used in this study involved uncertainty arising from regression equations. When hydrologic modeling is used to get the design flow, uncertainties arising from input data and hydrologic model parameters should also be included.

The uncertainty arising from model choice and assumptions also needs additional work. This study used a simple 1D model, which only gives water surface elevations at individual cross-sections. The approach used to interpolate the water surface elevations at cross-sections to create a 2D water surface can also add uncertainty in creating the flood inundation polygon. While uncertainty in interpolation techniques used for creating water surface may be small in v-shaped valleys, but may be significant in flat floodplains.

In this study, the uncertainty in topography, roughness and flow information created an uncertainty bound in the inundation area that ranged from 1.4 to 6.5% of the base inundation area for the Seymour reach, and from 4 to 29% for Strouds reach. The question is: how significant is this uncertainty bound? Currently, there are no guidelines (e.g., less than 5% uncertainty bound is acceptable) in defining or quantifying the uncertainty that can be used for collecting data, executing models and eventually creating flood maps. The Federal Emergency Management Agency (FEMA) in the United States undertakes three levels of flood mapping projects called approximate, enhanced approximate and detailed. There are clear differences in the quality of data and level of modeling efforts in creating flood inundation maps for approximate and detailed FEMA studies, but it is unknown how the uncertainty bound changes using either approach, and how significant is this change in the uncertainty bound.

The importance of quantifying uncertainty in flood inundation mapping is illustrated in Fig. 5.7 that shows the base inundation map, minimum (L4) and maximum (L1) area inundation maps from MC simulations, and 5 (L3) and 95% (L2) confidence interval maps from GLUE for an area around Strouds reach overlaid on top of a Google earth image. Property P1 (which seems under construction at the cul-de-sac when this image was taken) is outside the 100-yr flood zone based on the base map, minimum area map and 5% confidence interval map, but is partially in the flood inundation zone based on 95% confidence interval and maximum area inundation map. Similarly, Property P2 (which does not look like a residential property) is partially in the 100-yr flood zone based on the base map, outside the flood zone based on minimum area map and 5%

confidence interval map, but is completely in the flood inundation zone based on 95% confidence interval and maximum area inundation maps. Fig. 5.7 illustrates the importance of uncertainty on real properties which can have implications on flood insurance and other decision making processes. Underlying the importance of quantifying uncertainty in flood inundation mapping is the complex nature of uncertainties from data and models that need more thorough research involving more datasets with wide array of issues associated with each uncertain variable in the overall process. The study presented in this chapter is just one step in this direction.

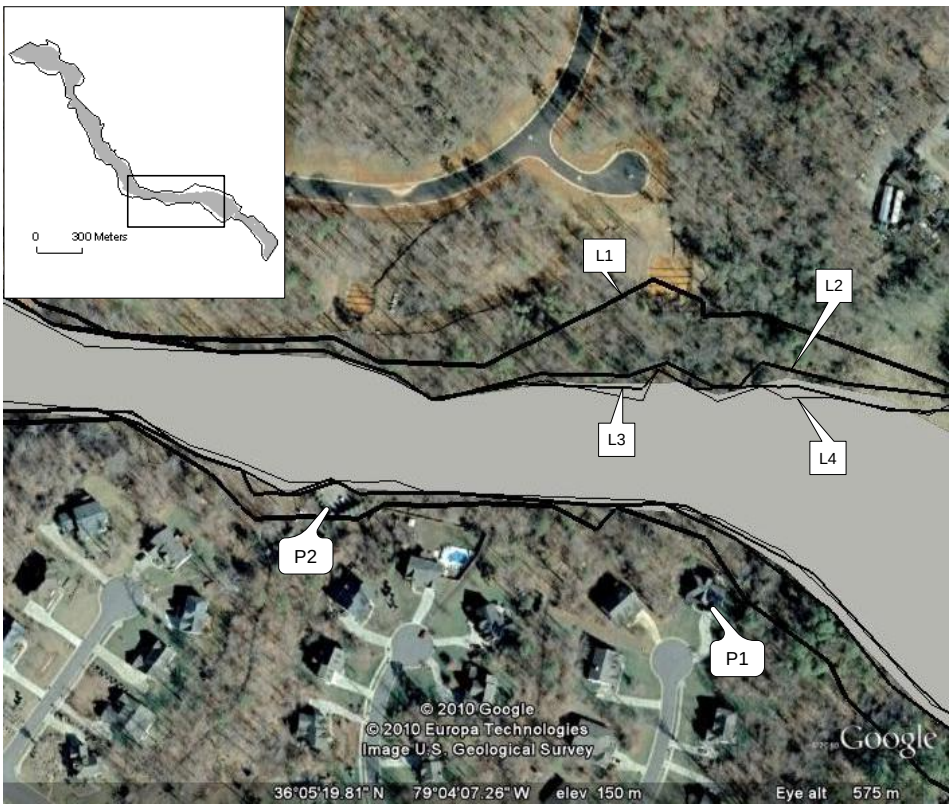

Fig. 5.7: Flood inundation extents applied to Google map (Strouds reach)

CHAPTER 6. ASSESSMENT OF THE ROLE OF PRIOR AND POSTERIOR PDFS IN THE GLUE METHODODLOGY

6.1. Introduction

The generalized likelihood uncertainty estimation (GLUE) methodology is commonly utilized for uncertainty estimation in flood inundation mapping, but the subjective decisions required for its implementation limit its use. Specifically, the selection of a likelihood measure can produce different uncertainty bounds for the flood inundation area. Prior and posterior PDFs of the model variables, however, can provide significant information to assist with making more appropriate selections. In this chapter, a specific range of the model variables which have more influence on the observed inundation is called as an “effective range”. The effective range can be determined by consistent posterior probability density function (PDF) types regardless of the prior PDF types for the model variables. Typically, uncertainty estimation using GLUE is based on the datasets defined as behavioral model. However, if the number of behavioral models for a cut-off threshold is too small, an uncertainty bound can be roughly estimated. Therefore, the objectives of this study involve the following: 1) finding a likelihood function to derive robust uncertainty estimation in flood inundation mapping among several likelihood functions over all combined datasets generated from a prior PDF assumed as normal or uniform; and (2) investigating effective variable ranges for several cut-off

thresholds. These objectives are accomplished by applying the GLUE methodology, including Monte Carlo simulations with hydraulic modeling and terrain analysis for a reach along the White River in Seymour, Indiana (Seymour reach). Among the many uncertainty sources, topography, discharge, and Manning's n are selected in this study. The likelihood measures used in this study are F-likelihood measure (F) based on F-statistic, W-likelihood measure (W) based on the spatial difference of flood extent between the simulations and observations, and E-likelihood measure (E) based on the difference in water surface elevations between the simulations and the observations.

6.2. Methodology

The methodology involves the following: 1) generation of random numbers from the assumed prior PDFs of the model variables (topography, discharge, and Manning's n); 2) Monte Carlo simulations with the combined model variables (Table 6.2) selected from their assumed prior PDFs; 3) estimation of the effective range of each model variable for cut-off thresholds; and 4) comparison of the uncertainty bounds based on the number of the selected acceptable datasets.

6.2.1. Random number generation for model variables

As mentioned previously in section 3.2, the range of uncertainty is determined by a RMSE of ± 0.69 m for topography, a 95% confidence interval of rating equation for discharge, and Chow's classification for Manning's n. In the Monte Carlo simulations, random values for topography are generated as the percentages change instead of absolute values from their prior PDFs. Each cross-section includes multiple Manning's n values, and the hydraulic modeling for Seymour reach is based on nine cross-sections. If individual Manning's n values along a cross-section are independently and randomly selected, investigating the effect of each Manning's n value on the flood inundation extent becomes necessary because each Manning's n can be considered as a separate model parameter. To overcome this problem, just one random percentage for Manning's n is selected, and then multiplied to the initial Manning's n values. For example, if all cross-sections have three Manning's n values of 0.04 (left bank), 0.06(main channel), and 0.05 (right bank), a random number of 20% would increase the Manning's n values to 0.048(left bank), 0.072(main channel), and 0.06 (right bank) at all cross-sections to represent the change in the initial values. Similarly, if a random value for topography indicates a vertical error in a DEM, it is added to the initial elevation. For example, if a random number of - 0.1 m is selected for topography, all elevations in the DEM are reduced by 0.1 m. For discharge, a generated random number is directly used as a flow condition used in HEC-RAS. For example, if a random number of 3000 m^3/s is generated, water surface elevations at all cross-sections are simulated for discharge of 3000 m^3/s.

Table 6.1: The conditions for random variables generated in a simulation

Initial (variables)	Modeling Variables estimated by Random variable (RV)	Min	Max	No. of Chosen RV	PDFs
N_i Manning's n	$N = N_i (1+RV)$	-0.375	0.375	1	Uniform, Normal
D_i Discharge	$D = RV\ [m^3/s]$	2257	3301	1	Uniform, Normal
T_i Topography	$T = T_i + RV\ [m]$	-0.69	0.69	1	Uniform, Normal

6.2.2. Monte Carlo simulations

In this study, the Monte Carlo simulations using HEC-RAS and triangular-based interpolations are conducted to find the effective ranges for the model variable in the GLUE methodology. HEC-RAS is a one-dimensional (1D) hydraulic model based on an energy equation and Manning's equation; and HEC-RAS can simulate the basic profile and the total conveyance for steady and unsteady flow conditions in river channels, including floodplains. Some of the literature (Cook and Merwade, 2009) illustrated that a 2D hydraulic model catches better flood inundation than a 1D hydraulic model. However, the use of a 1D model in this study is justified because the main channel and the floodplain are treated as a single channel for the observed flow condition for all simulations.

The data for the HEC-RAS model involves the geometric data, flow data, Manning's n, and boundary conditions. Generally, geometric data in HEC-RAS model is obtained by

HEC-GeoRAS, which is an ArcGIS tool that allows extraction of cross- sections by reading information from a DEM and a land use map, and exporting this information to HEC-RAS. In the HEC-RAS model used for this study, a downstream condition of normal depth is used as the boundary condition, and steady flow conditions are assumed for a flood event. Water surface elevations from HEC-RAS are then interpolated by using a triangle-based linear interpolation (Matlab function "griddata") (Watson and Philip, 1984) to get a water surface. A flood inundation map is created by subtracting the topography from the water surface. In this study, Monte Carlo simulations are performed with random variables selected from a combination of prior PDFs for each variable. A total of 5000 simulations are conducted for each combination. Table 6.1 shows the conditions of the random variables generated in a simulation for each model variable.

6.2.3. The effect of prior PDFs in the GLUE methodology

In the GLUE methodology, the role of a prior PDF is significant in assessing the robustness of distribution for model variables with a posterior PDF based on the likelihood measures calculated by model outputs and the observations. However, it is difficult to obtain information about the distribution of input data as well as the model parameters. Therefore, many applications in flood inundation modeling assume the prior PDFs model variables simply to be uniform. This simple assumption for model variables might be necessary when conducting very large computations in order to obtain behavioral variables. In this study, the model variables are randomly selected from

uniform and normal PDFs and then combined for input dataset in the GLUE methodology (Table 6.2).

Table 6.2: The combinations of prior PDFs for model variables

Case	1	2	3	4	5	6	7	8
Combination	$T_ND_NN_N$	$T_ND_NN_U$	$T_ND_UN_N$	$T_ND_UN_U$	$T_UD_NN_N$	$T_UD_NN_U$	$T_UD_UN_N$	$T_UD_UN_U$

Model variable is denoted by A_B: A indicates a model variable such as topography (T), discharge (D), and Manning's n (N); B means a prior PDF type of normal (N) and uniform (U).

A likelihood measure is a key factor in the GLUE methodology because the uncertainty bounds can be narrowed or widened by the choice of a particular likelihood measure. Among the several likelihood functions proposed in the literatures, inverse error variance and Nash and Sutcliffe efficiency are representative likelihood functions, but these functions are difficult to apply to non temporal data. Therefore, F-statistic, which considers spatial distribution of flood extent, has been used as a likelihood measure in flood inundation mapping. An observed flood inundation map can provide the vertical water surface elevations (WSE) and spatial flood extent with a DEM. In this study, three different likelihood measures are used in the GLUE procedure. These measures include: (W) the sum of the absolute errors in inundation width. (Eq. 6.1); (E) the sum of absolute errors in the water surface elevation (Eq. 6.2); and a F-statistic that describes the overall matching of the model's flood inundation area with the model's predicted area (Eq. 6.3).

$$W_i = \sum_{j=1}^{N} \left| W_{m,i} - W_o \right| \qquad (6.1)$$

where, $W_{m,i}$ and W_o represent the i^{th} iteration of the modeled water surface width and observed water surface width, respectively for the j^{th} cross-section.

$$E_i = \sum_{j=1}^{N} \left| E_{m,i} - E_o \right| \qquad (6.2)$$

where, $E_{m,i}$ and E_o represent the i^{th} iteration of the modeled water surface elevation and the observed water surface elevation, respectively for the j^{th} cross-section.

$$\text{F-statistic of i}^{\text{th}}\text{ iteration, } F_i = \frac{1}{P_i} = \left(\frac{A_{op,i}}{A_o + A_{p,i} - A_{op,i}} \right) \times 100 \qquad (6.3)$$

where A_o indicates the observed inundation area, A_p refers to the predicted flood inundation area, and A_{op} represents the intersection of both the observed and the predicted inundation areas. In this study, the assumption that the observed data did not contain any errors allowed a conservative analysis.

6.2.4. Posterior PDFs and effective range of model variables for cut-off thresholds

With a likelihood measure, a cut-off threshold to accept behavioral parameters has an impact on deciding the uncertainty bounds. In previous applications using GLUE, a cut-off threshold is used in finding sets of behavioral variables, but there is no clear definition for behavioral models. The term, “behavioral” might not be appropriate without the comparison of the prior and posterior PDFs for model variables because the consistency

of behavioral models can be validated by robustness of posterior PDF corresponding to the prior PDF types.

Typically, a tight cut-off threshold leads to a small number of acceptable datasets, while a relaxed cut-off threshold produces the large number of acceptable datasets. Therefore, GLUE needs a systematic procedure to find a proper likelihood measure and threshold in defining behavioral models. In this study, the behavioral models are defined by appraisal of prior and posterior PDF for model variables. The defined acceptable dataset associated with multiple variables involves the ranges for each variable, and these ranges are considered as effective ranges for model variables in this study. However, all datasets generated in the effective ranges of model variables are not defined as behavioral models because uncertainty estimation using GLUE is based on the combination dataset of model variables. Conversely, datasets generated outside the effective range can produce the behavioral models through MC simulations. For a certain cut-off threshold the number of the dataset can affect the uncertainty bound of flood inundation area because the uncertainty quantification in GLUE is based on the cumulative density function rescaled from estimates of marginal probability for the acceptable dataset. A small number of dataset defined as behavioral models can lead to the rough uncertainty bounds, and need massive computations.

For a certain cut-off threshold, the effective range suggested in this study can lead to replenishment of deficient acceptable dataset by providing the specific range which has more impact on the observations than other ranges. For example, if only 10 datasets from 1000 simulations are selected as behavioral models for a certain cut-off threshold, the

uncertainty bounds using the 10 datasets can be roughly estimated because a small number of datasets are selected. Because the effective range estimated from the 1000 simulations has higher chance to generate behavioral models, more acceptable dataset generated from the effective range can supplement the roughly estimated uncertainty bounds using those 10 datasets. However, it should be noted that the GLUE methodology based on only datasets generated in the effective range can produce an overestimated or underestimated uncertainty bound.

In this study, the effective ranges are estimated by the use of prior and posterior PDFs for several cut-off thresholds. The effective range does not exist for all cut-off thresholds. For example, if all datasets used in GLUE are defined as behavioral models, there are no effective ranges for each variable because the prior and the posterior PDFs of model variables are same. In addition, the effective range is not constant for all cut-off thresholds, and can be changed for a certain cut-off threshold.

Eventually, effective range for each model variable in the GLUE methodology is determined by comparing a posterior PDF with the prior PDF for several cut-off thresholds. For example, if a posterior PDF is normal for a prior PDF of normal distribution, and uniform for a prior PDF of uniform distribution, it will be difficult to determine the effective ranges from the posterior PDFs of model variables. However, if posterior PDFs are normal for prior PDF of normal or uniform distribution, an effective range will be determined by ranges of model variables from robust posterior PDFs regardless of the prior PDF types. In this study, the effective range is estimated by taking the average for the range of the posterior PDFs obtained from 8 combinations of prior PDFs.

6.2.5. Uncertainty quantification

For Each simulation output, W, E, and F likelihood measures are calculated by using Eqs. 6.1, 6.2, and 6.3, respectively. Uncertainty bounds of flood inundation areas are quantified for 100% of W, E, and F likelihood measures. These uncertainty bounds are then compared with the results for top 3.5% of E-likelihood measure. In addition, the effect of selection of the number of behavioral models on uncertainty quantification for top 3.5% of E-likelihood measures (supplemented with dataset from effective range) is investigated.

6.3.Results

6.3.1. Monte Carlo simulations

The results from the Monte Carlo simulations show different scatters corresponding to the likelihood measures in the dot plots for the Seymour reach (Fig. 6.1). The dot plots generated from uniform prior PDFs are have more scatter compared to that from normal prior PDFs (Table 6.2). The scatters of the F-likelihood measure, considering the water surface elevation and spatial distribution of flood extents are concentrated in the top for all model variables (topography, discharge, and Manning's n) (F in Fig. 6.1). F-likelihood measures have more scatter for negative uncertainties in for topography and Manning's n, but the scatter is symmetric for discharge. In particular, the scatter of F-likelihood measure for topography is more concentrated at high values for positive

uncertainty, but widely spread for negative uncertainty. Concentrated scatter at high values for a likelihood measure indicates that the simulations generally match well with the observations.

The dot plots for W-likelihood measure (W) considering only flood widths at nine cross-sections show layered scatters for all model variables (W in Fig. 6.1). The horizontal parallel layers in the scatters of W-likelihood measure are created by the irregular shape of the cross-sections. Specifically, when shape of a cross-section is drastically wide or steep at a certain point, a layer will be created. For example, if the shapes of all cross-sections are perfectly rectangular, W-likelihood measure will be constant in the given range of model variables because of no change in the simulated flood extents at cross-sections.

E-likelihood measure (E), which is based on only vertical difference between simulated and observed water surface elevations, shows different scatter for neative and positive uncertainty only for topography (E in Fig. 6.1). The scatters of E-likelihood measure for discharge and Manning's n are relatively symmetric in comparison with the scatter for topography. It is also possible from the scatter plot to guess the prior PDF based on the symmetry of the scatter. For example, for a normal prior PDF, the scatter in the dot plot is symmetric along a vertical line, with more concentration in the center. On the other hand, the scatter plot for a variable with uniform PDF is evenly symmetric. Similarly, a symmetric scatter plot indicates relatively less uncertain variable compared to a variable that has an asymmetric plot (e.g. topography and Manning's n in Fig. 6.1)

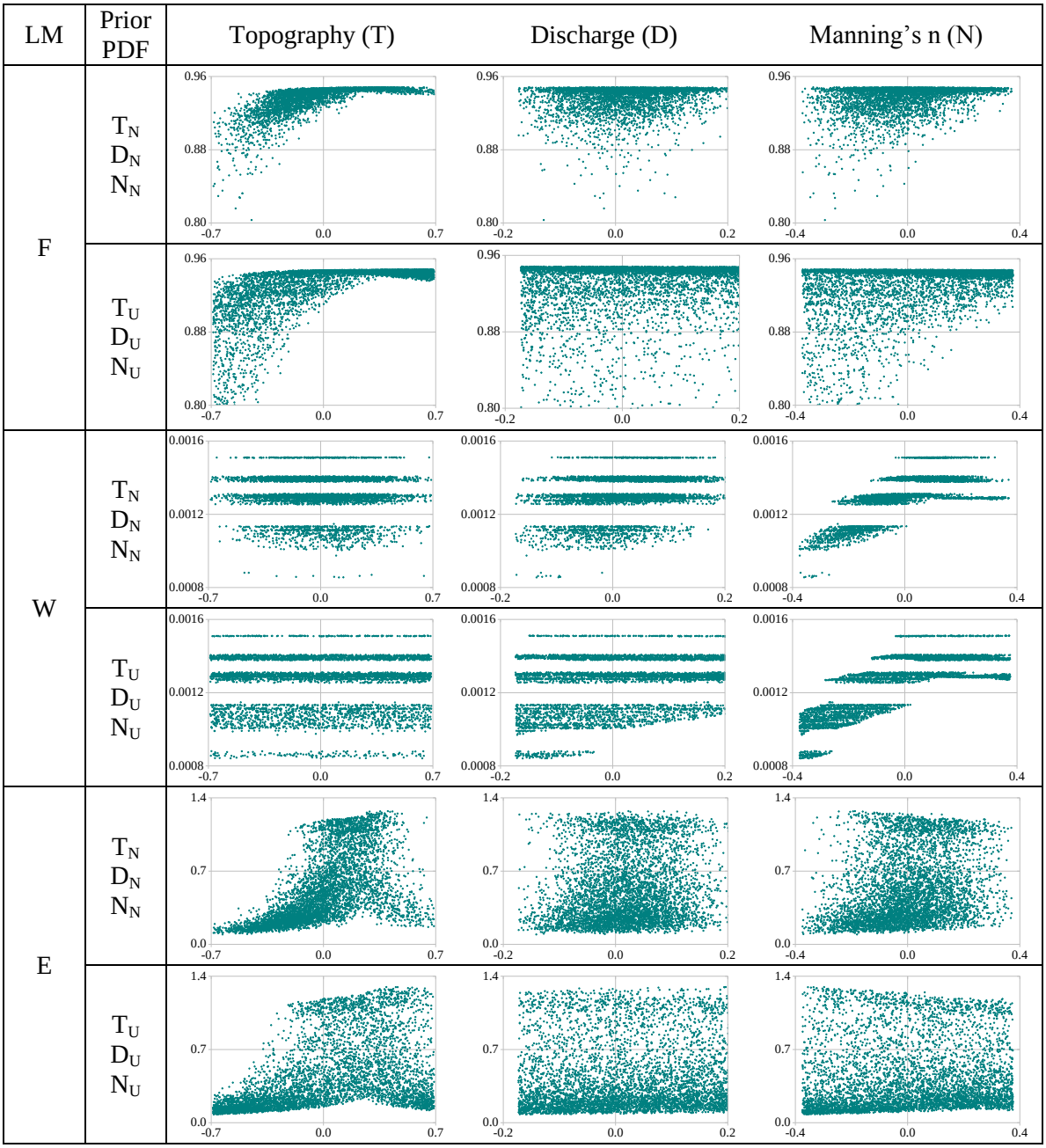

LM indicates likelihood measure.

Fig. 6.1: Dot plots of model variables (T, D, and N) based on different likelihood measures and the combination of the prior PDFs (case 1($T_N D_N N_N$) and 8($T_U D_U N_U$)). X-axis indicates change of uncertainty in model variables, and Y-axis shows the likelihood measures.

Table 6.3: Uncertainty bounds based on likelihood measure [unit: km^2]

LM	Case / UB*	1	2	3	4	5	6	7	8	AVG	MD*
F	Lower 5%	9.83	9.72	9.82	9.66	9.46	9.36	9.45	9.29	9.57	0.21
	Upper 95%	10.89	10.92	10.90	10.92	10.95	10.98	10.96	10.98	10.94	0.04
	Bound	1.06	1.20	1.08	1.26	1.49	1.62	1.52	1.69	1.36	0.25
W	Lower 5%	9.83	9.80	9.82	9.78	9.43	9.38	9.42	9.38	9.61	0.22
	Upper 95%	10.90	10.92	10.90	10.92	10.95	10.98	10.97	10.99	10.94	0.03
	Bound	1.07	1.12	1.08	1.14	1.53	1.61	1.55	1.61	1.34	0.25
E	Lower 5%	10.32	10.27	10.31	10.25	10.16	10.14	10.14	10.13	10.21	0.08
	Upper 95%	10.87	10.88	10.87	10.89	10.92	10.92	10.92	10.92	10.90	0.02
	Bound	0.55	0.61	0.56	0.64	0.76	0.78	0.78	0.79	0.68	0.10

UB* means uncertainty bounds
MD* shows the maximum difference in uncertainty bounds for each likelihood measure

6.3.2. The effect of prior PDFs

The results from GLUE show the uncertainty bounds of flood inundation area based on W, E, and F likelihood measures for each case (Table 6.3). The flood inundation areas with a 90% uncertainty bound (lower 5% and upper 95%) for the Seymour reach are in the range of 9.29 to 10.98 km^2 for the F-likelihood measure, 9.83 to 10.99 km^2 for the W-likelihood measure, and 10.13 to 10.92 km^2 for the E-likelihood measure. Also, it is shown that when all model variables are randomly selected from uniform distribution, wider uncertainty bounds are obtained with all the likelihood measures. As a result, the E-likelihood measure produced the smallest uncertainty bound with an averaged value of 0.68 km^2 and the standard deviation of 0.1 km^2. This means that the E-likelihood measure produced the robust uncertainty bounds regardless of the prior PDF types of model variables. Overall, the 90% uncertainty bounds considering prior PDF with several

likelihood measures range from 0.55 to 1.69 km^2. The maximum difference in uncertainty bounds is about 11% of the base area (10.57 km^2). This difference in uncertainty bounds is two times larger than the difference found in Chapter 5. From these results, the effect of the prior PDF type, including its subjectivity on uncertainty quantification is illustrated.

6.3.3. Posterior PDFs of model variables

With likelihood measures, a cut-off threshold plays a critical role in determining posterior PDFs. Fig. 6.2 and 6.3 shows the posterior PDFs of the model variables for the top 3.5% and 100% of W, E, and F likelihood measures (X-axis is change of uncertainty in model variable, and Y-axis indicates likelihood measure values). The posterior PDFs of each model variable have different distribution for different cut-off thresholds. Regardless of prior PDF combinations, consistent shapes of the posterior PDFs is shown in topography for the top 3.5% of F and E likelihood measures, and in Manning's n for the top 3.5% of W-likelihood measure. However, for top 100% of F, W and E likelihood measures, posterior PDFs for 3 model variables are similar to their prior PDFs. Posterior PDFs of model variables for 1, 2, 3, 4, 5, 10, 20, and 50% cut-off thresholds is included in Appendix.

Fig. 6.4 shows the ranges of model variables from posterior PDFs based on each likelihood measure corresponding to 1, 2, 3, 4, 5, 10, 20, 50, and 100% cut-off thresholds. The ranges of all model variables are widened by a relaxed cut-off threshold to include

more datasets. Also, the ranges of all model variables based on the F and E likelihood measures showed a similar trend with changes in the cut-off threshold. For a cut-off threshold tighter than the top 3.5% of the F and E likelihood measures, the range of the topography is biased towards positive values. However, the range of topography for the W-likelihood measure is symmetric and is close to its initial range, which means that the range of topography for the W-likelihood measure is not affected by a cut-off threshold. For all likelihood measures (W, E, and F), the thresholds produce very small changes for the range of discharge. In the case of Manning's n, the range is largely affected by thresholds higher than the top 5% of the F and E likelihood measures. However, Manning's n shows positive bias for thresholds tighter than the top 1% of the W-likelihood measures.

Prior PDFs	F			W			E		
	Topography	Discharge	Manning's n	Topography	Discharge	Manning's n	Topography	Discharge	Manning's n
Case 1	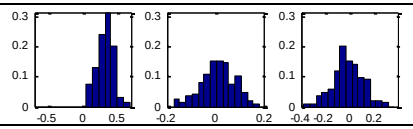			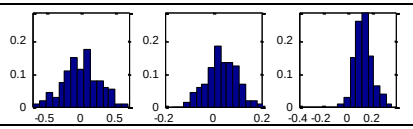			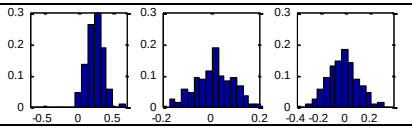		
Case 2	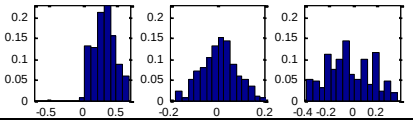			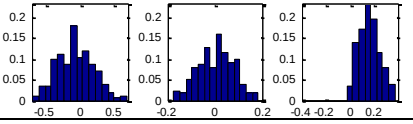			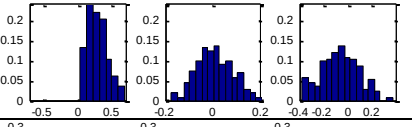		
Case 3	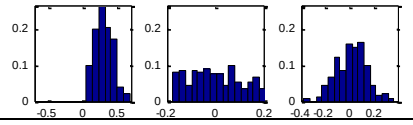			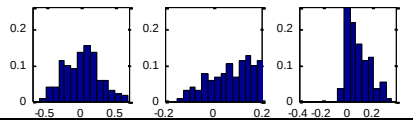			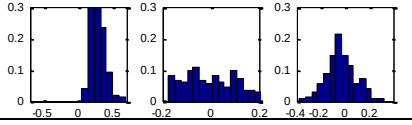		
Case 4	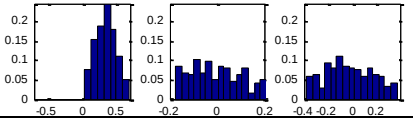			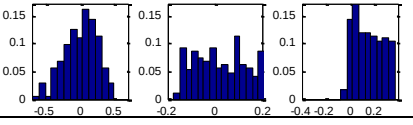			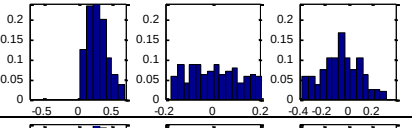		
Case 5	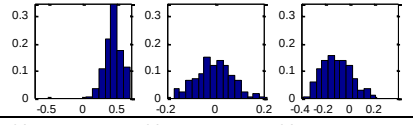			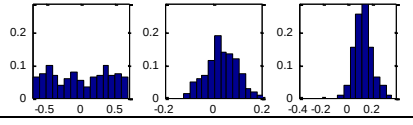			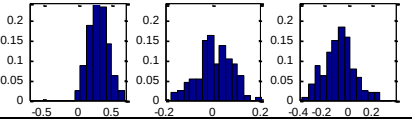		
Case 6	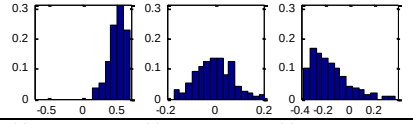			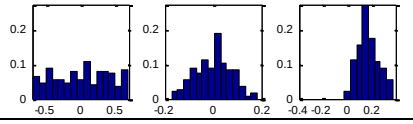			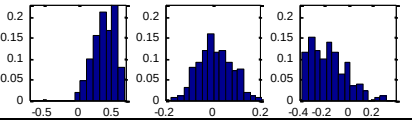		
Case 7	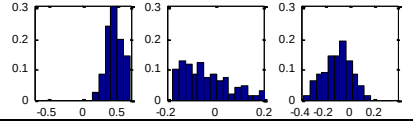			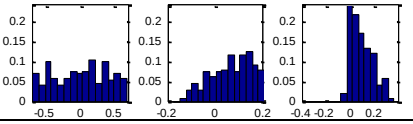			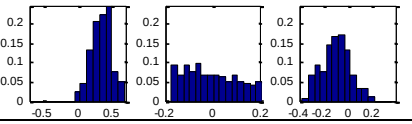		
Case 8	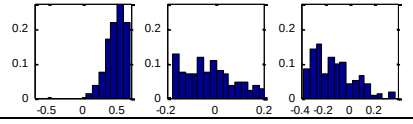			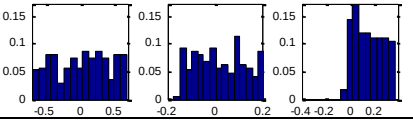			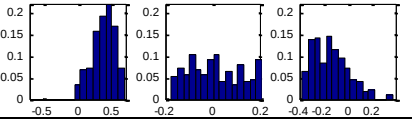		

Fig 6.2: The posterior PDFs of model variables for top 3.5% of W, E, and F likelihood measures.

Prior PDFs	F			W			E		
	Topography	Discharge	Manning's n	Topography	Discharge	Manning's n	Topography	Discharge	Manning's n
Case 1	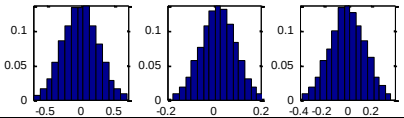			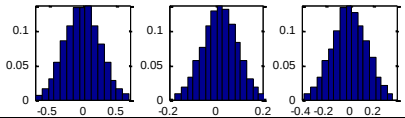			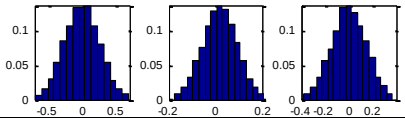		
Case 2	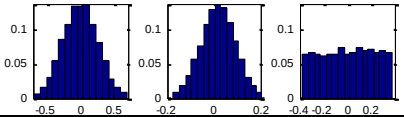			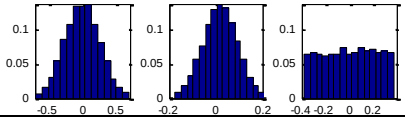			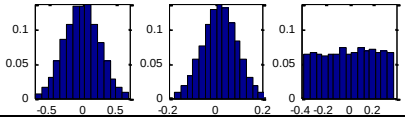		
Case 3	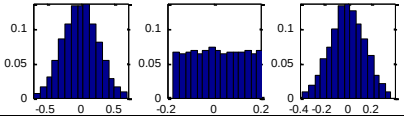			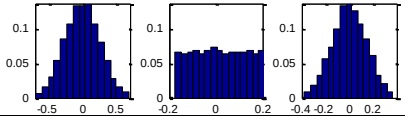			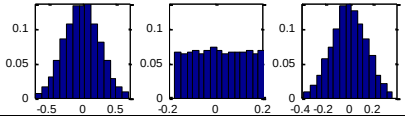		
Case 4	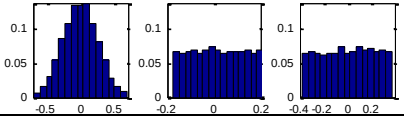			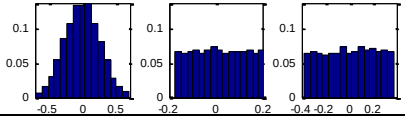			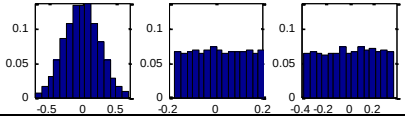		
Case 5	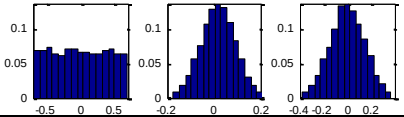			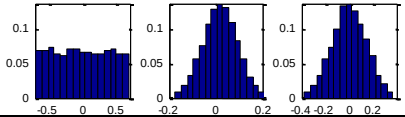			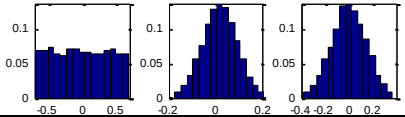		
Case 6	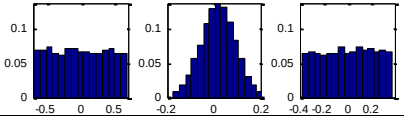			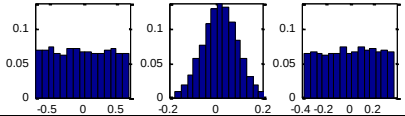			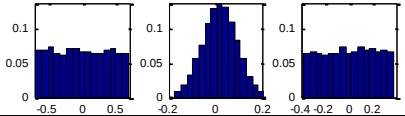		
Case 7	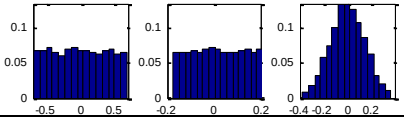			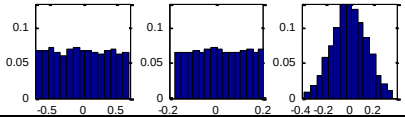			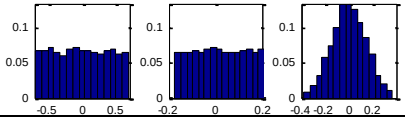		
Case 8	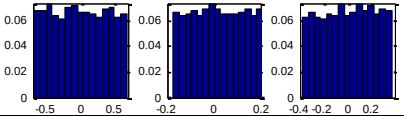			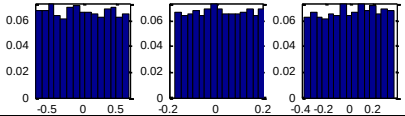			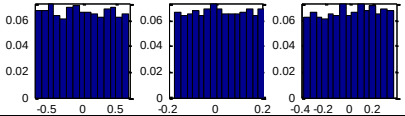		

Fig 6.3: The posterior PDFs of model variables for top 100% of W, E, and F likelihood measures.

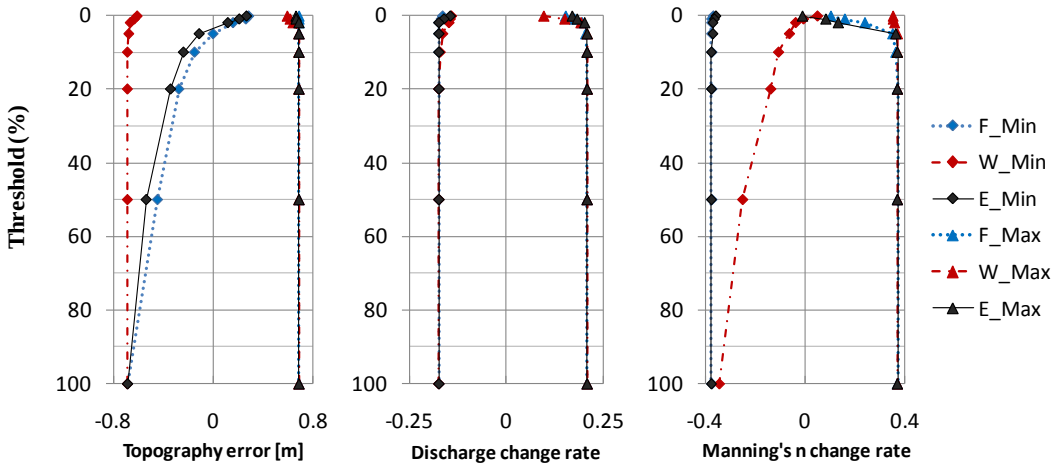

Fig. 6.4: The ranges of model variables based on likelihood measures corresponding to 1, 2, 3, 4, 5, 10, 20, 50, and 100% cut-off thresholds

6.3.4. Effective range of model variables

Based on the posterior PDFs, effective ranges for each model variable are determined by considering consistency in the shape of posterior PDFs. As an example for estimating effective range, Fig. 6.5 shows eight posterior PDFs of each model variable by taking the top 3.5% of the E-likelihood measures for eight prior PDF combinations (Table 6.2). The top 3.5% of E-likelihood measure is selected as a criterion because E-likelihood measure produces the smallest difference in uncertainty bounds (Table 6.3), and initial values (median value) of model variables in the posterior PDFs are included by top 3.5% of E-likelihood measure. Eight posterior PDFs for topography is consistently normal for all prior PDF combinations. However, in the case of discharge, the posterior PDFs are clearly distinguished by the prior PDFs of discharge. The prior and posterior PDFs for discharge commonly have normal distributions in cases 1, 2, 5, and 6, and uniform

distributions in cases 3, 4 ,7, and 8. Based on this result, it is difficult to obtain any information about the distribution of error in discharge from the posterior PDFs because posterior PDFs are identical to their prior PDFs. Therefore, the effective range for discharge is same to the initial range.

In the case of Manning's n, although there is little difference in shapes of the posterior PDFs over all cases, the shapes of all posterior PDFs are close to a normal distribution. Table 6.4 shows the effective ranges of model variables for top 3.5% of E-likelihood measure. Effective ranges of model variables for top 1, 2, 3, 4, 5, 10, 20, 50, and 100% of W, E, and F likelihood measures determined by the same method are shown in Table 6.5. With a tighter cut-off threshold, the effective ranges of topography for F and E likelihood measures are more clearly determined because topography has the most impact on the flood inundation area, and the number of the selected datasets defined as behavioral models for a tight threshold are small.

Table 6.4: The effective range of model variables by taking 3.5% of E-likelihood measures for the Seymour reach

	Topography [m]		Discharge [m^3/s]		Manning's [%]	
	lower	upper	lower	upper	lower	upper
Initial Range	-0.69	0.69	2257	3301	-37.5	37.5
Effective range	-0.011	0.69	2257	3301	-36.8	31.6

Table 6.5: The effective ranges of model variables for thresholds of W, E, and F likelihood measures

Threshold	Range	F			W			E		
		T	D	N	T	D	N	T	D	N
1%	lower	0.265	2257	-37.5	-0.690	2257	-0.1	0.207	2257	-36.2
	upper	0.689	3301	16.1	0.690	3301	35.4	0.666	3301	8.6
2%	lower	0.173	2257	-37.5	-0.690	2257	-4.5	0.116	2257	-36.9
	upper	0.689	3301	37.5	0.690	3301	36.6	0.689	3301	14.8
3%	lower	0.093	2257	-37.5	-0.690	2257	-7.0	0.024	2257	-36.9
	upper	0.689	3301	37.5	0.690	3301	36.6	0.689	3301	30.4
4%	lower	0.047	2257	-37.5	-0.690	2257	-7.0	-0.011	2257	-36.9
	upper	0.689	3301	37.5	0.690	3301	37.2	0.689	3301	34.7
5%	lower	0.001	2257	-37.5	-0.690	2257	-7.0	-0.114	2257	-37.5
	upper	0.689	3301	37.5	0.690	3301	37.2	0.689	3301	37.5
10%	lower	-0.160	2257	-37.5	-0.690	2257	-10.7	-0.240	2257	-37.5
	upper	0.689	3301	37.5	0.690	3301	37.2	0.689	3301	37.5
20%	lower	-0.286	2257	-37.5	-0.690	2257	-14.5	-0.343	2257	-37.5
	upper	0.689	3301	37.5	0.690	3301	37.2	0.689	3301	37.5
50%	lower	-0.447	2257	-37.5	-0.690	2257	-24.4	-0.550	2257	-37.5
	upper	0.689	3301	37.5	0.690	3301	37.2	0.689	3301	37.5
100%	lower	-0.690	2257	-37.5	-0.690	2257	-37.5	-0.690	2257	-37.5
	upper	0.690	3301	37.5	0.690	3301	37.5	0.690	3301	37.5

indicates that the effective range has a normal PDF.

Indicates that the effective range has a normal or uniform PDF.

where, T is topography in meters, D is discharge in cubic meters per second, and N is a relative change (%) of Manning's n.

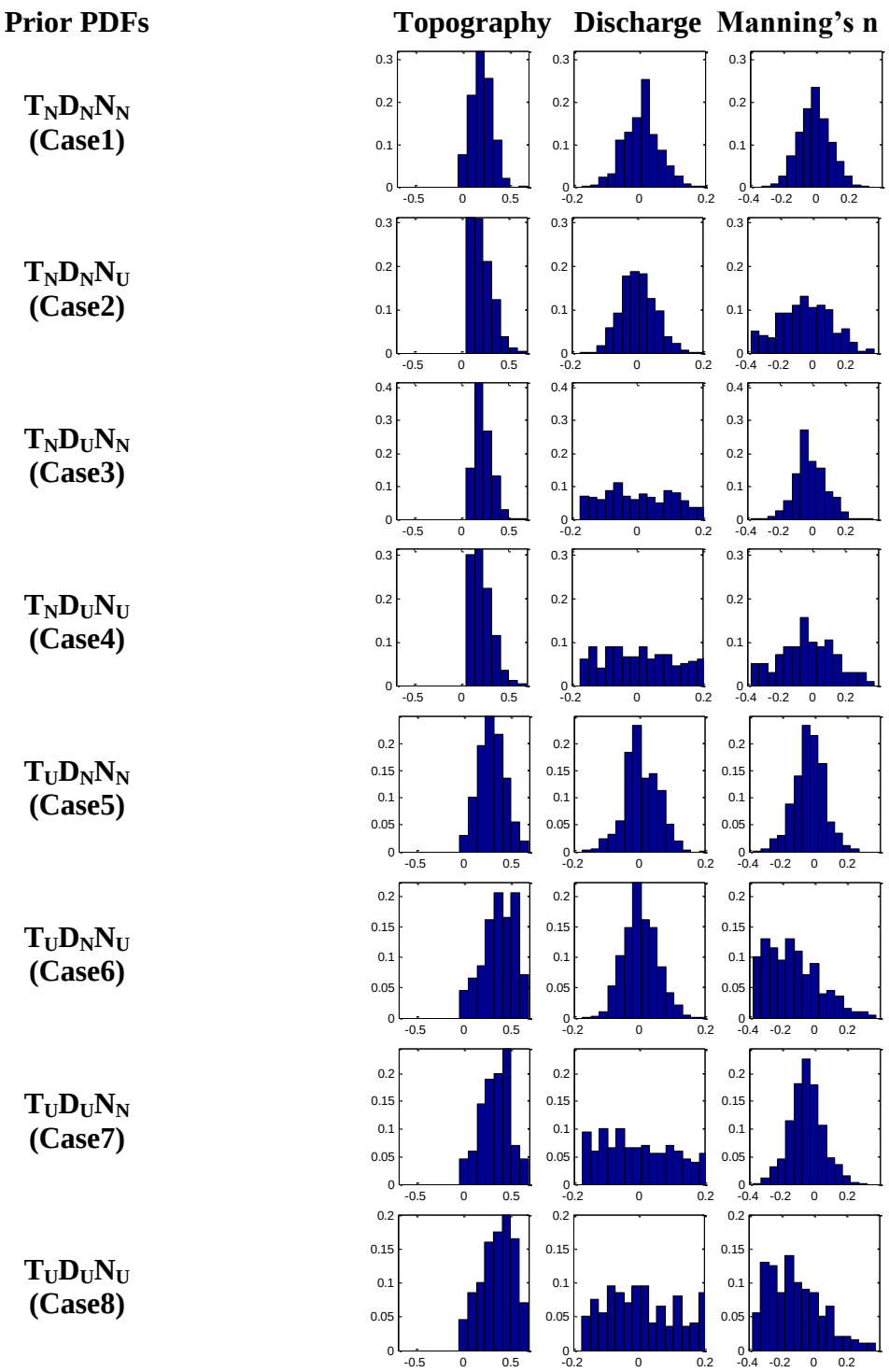

Fig. 6.5: The posterior PDFs of model variables by taking top 3.5% of E-likelihood measures. Left one is topography, middle on is discharge, and right one is Manning's n for each likelihood measure. X-axis indicates the range for each variable, and Y-axis shows the probability density.

6.3.5. Uncertainty quantification

Table 6.5 shows the uncertainty bound in the flood inundation area for the top 1, 2, 3.5, 5, 10, 20, 50, and 100% of E-likelihood measure. As the cut-off threshold is relaxed with a low E-likelihood measure, the uncertainty bound of inundation area is wider (Fig. 6.6). In particular, change in lower bounds is greater than the change in upper bounds. For top 3.5% of E-likelihood measure, the threshold value is 1.173 km^{-1}, and 175 datasets are selected as behavioral models. Also, the uncertainty bound for top 3.5% of E-likelihood measure is 0.037 km^2, which is about 0.35% of the observed area. This uncertainty bound is approximate because it is based on only 175 datasets from a total of 5000 datasets. Therefore, it is better to supplement 175 datasets with the dataset from effective range to get a more realistic uncertainty bound.

The uncertainty bound supplemented by using the effective range is compared with the uncertainty bounds that are estimated by using 5000 datasets for each of W, E, and F likelihood measure for initial ranges with no criteria, and using 175 datasets selected by the top 3.5% of E-likelihood measures for initial ranges (Fig. 6.7 and Table 6.7). For the effective ranges, the updated prior PDFs are normal for topography and Manning's n because the posterior PDFs for topography and Manning's n are normal. However, the posterior PDF for discharge is normal or uniform corresponding to its prior PDF types. In this study, a uniform prior PDF for discharge is selected by considering all possible uncertainties because when a prior PDF is uniform the uncertainty bounds are generally wider. Uncertainty bound based on 175 dataset from initial ranges is supplemented by 4305 datasets from the effective ranges (e in Table 6.7). In other words, a total of 4480

datasets among a total of 10000 simulations (5000 for finding effective range and 5000 for supplementing datasets) are defined as behavioral models for E-likelihood measure of 1.172 km^{-1}. The comparison of the flood inundation areas is graphically shown in Fig. 6.7. The uncertainty bounds produced by GLUE using initial range and no criteria are 0.56 km^2 for E-likelihood measure and 1.08 km^2 for both F and W likelihood measures. Uncertainty bound using initial range and top 3.5% of E-likelihood measure is 0.04 km^2.

In addition, when the datasets are supplemented by the effective range for E-likelihood measure greater than 1.172 km^{-1}, GLUE produces an uncertainty bound of 0.21 km^2. From the above result, it is clear that the number of dataset used in GLUE affect the uncertainty quantification. In addition, the uncertainty bound estimated by using only initial ranges is five times smaller than the one estimated by datasets supplemented by effective ranges. When considering the base inundation area of 10.57 km^2 for the Seymour reach, the uncertainty bound for the inundation area ranged from 0.4% to 10% of the base area (Fig. 6.8).

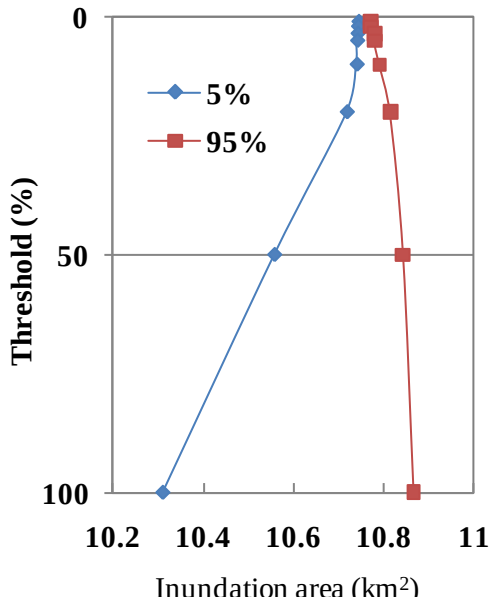

Fig.6.6: Uncertainty bounds according to the thresholds based on E-likelihood measure

Table 6.6: E-likelihood measure values, the number of dataset, and uncertainty bounds corresponding to the thresholds

Threshold (%)	E-likelihood (km^{-1})	The number of dataset	Lower 5% (km^2)	Upper 95% (km^2)	Bound (km^2)
1	1.215	50	10.745	10.771	0.026
2	1.196	100	10.744	10.773	0.029
3.5	1.173	175	10.743	10.78	0.037
5	1.156	250	10.742	10.78	0.038
10	1.095	500	10.741	10.792	0.051
20	0.879	1000	10.719	10.815	0.096
50	0.41	2500	10.558	10.844	0.286
100	0.093	5000	10.31	10.867	0.557

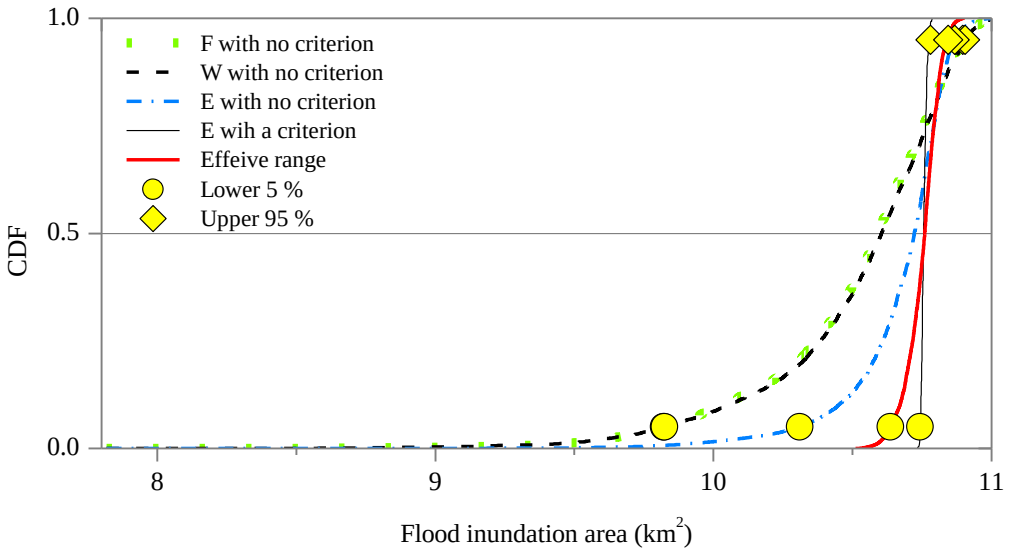

Fig. 6.7: Comparison of the GLUE results from initial and efficient ranges. X-axis indicates the inundation area in squared kilometer and Y-axis show the CDF.

Table 6.7: Uncertainty bounds using initial range and effective range [unit: km^2]

	Initial Range and no criterion			d) Initial range and ($E \geq 1.173\ km^{-1}$)	e) Effective range and ($E \geq 1.173\ km^{-1}$)
	a) F	b) W	c) E		
Lower 5%	9.82	9.82	10.31	10.74	10.64
Upper 95%	10.90	10.90	10.87	10.78	10.85
Bound	1.08	1.08	0.56	0.04	0.21
Selected dataset*	5000	5000	5000	175	4480
Total dataset	5000	5000	5000	5000	10000

The selected dataset* indicates the number of dataset satisfied with a criterion

Fig. 6.8: Inundation areas for Seymour reach. 5 and 95 indicate the lower 5% and the higher 95% inundations areas, respectively. Min and max show the minimum and maximum inundation areas. Obs indicates the observed inundation area. a) - c) are inundations areas for each likelihood measure using initial ranges. d) - f) are inundation areas based on top 3.5% of E-likelihood measure. g) - i) show the inundation area simulated by datasets supplemented from effective range.

6.4.Conclusions

- The subjectivity in selecting a likelihood measure is illustrated from the dot plots. The model variables selected from the normal prior PDF produce more concentrated plot than the uniform prior PDF. Therefore, when model variables are randomly selected from the normal prior PDF, narrower uncertainty bounds are produced.

- The uncertainty bounds of the flood inundation area are affected by the prior PDF types of the model variables and the type of likelihood measure (W, E, and F). However, this study shows that the E-likelihood measure is less affected by the combination of prior PDFs for the Seymour reach. Also, this study shows that the selection of the prior PDF and the type of likelihood measure both adds uncertainty in flood inundation modeling.

- As more likelihood measures are defined as behavioral models for a relaxed threshold, the ranges of model variables in the posterior PDFs are wider. The subjectivity of thresholds is illustrated by the range of model variables in their posterior PDFs and the distribution shape.

- With the selection of likelihood measure and threshold, it is illustrated that the size of the acceptable datasets to define behavioral models affects the uncertainty quantification using the GLUE methodology. A tighter threshold may need massive computations to collect sufficient acceptable datasets, and smaller number of datasets can lead to a very narrow uncertainty bound. This study shows that the effective

range provides a reasonable number of datasets to quantify the uncertainty in flood inundation mapping.

CHAPTER 7. SYNTHESIS

7.1.Flood risk management

The main goal of flood risk management is to reduce risk from flood. Basic components of flood risk consist of hazard, exposure, and vulnerability. Flood hazard means the probability of occurrence based on flood frequency at a certain level of magnitude. Flood mapping graphically describes the information on the flood hazard including the spatial variation and extent of the flood (Noson, 2002). Flood exposure represents the extent of properties and activities of humans geographically involved in flood-prone areas (Barroca et al. 2006; McEwen et al. 2002). Exposure relates the distance between floodplain and a place where there are properties and human activities. Flood vulnerability indicates the lack of resistance to flood damaging energy. Therefore, vulnerability is proportional to the exposure because if nothing is exposed in flooding, no damage will be done. Flood risk can be mathematically estimated as the product of hazard, exposure and vulnerability.

Flood inundation mapping is a basic source in providing information in making a decision for flood risk management. The accuracy of the flood inundation map directly affects a decision in risk management. In addition, even if the accuracy is reached for a certain target level, inaccurate uncertainty analysis for flood inundation map can cause

severe consequences resulting from a natural disaster. Decision making in flood risk management involves both safety and monetary concerns. Accordingly, decision makers need to find an optimal solution that provided maximum safety with minimal cost. In this study, safety is related to the accuracy in flood inundation mapping and robust uncertainty analysis, and cost is related to reduction of error in data including topography, discharge, and Manning's n. Therefore, this study for efficient flood risk management focuses on: 1) estimation of the uncertainty propagation rate; 2) the uncertainty quantification in flood inundation mapping; and 3) assessment of the roles of the prior and posterior PDFs in the uncertainty analysis method.

7.2. Estimation of the uncertainty propagation rate

One finding presented in Chapter 4 is that the errors in a model variable can be differently propagated into uncertainty in a flood inundation map based on the conditions of other variables. It is illustrated that a low flooding condition leads to high uncertainty propagation from a single model variable into flood inundation maps, while a high flooding condition brings low propagation of error from a model variable through FOA sensitivity analysis. These results show that geometric shape of river cross-sections affects uncertainty propagations because the magnitude of flood has a close relationship with top water surface width and elevation from the shape of valley. However, relative sensitivity between two model variables through HSY sensitivity analysis is dependent on the fitness between observation and simulation rather than conveyance. Main

contributors to uncertainty in flood inundation mapping are topography for the Seymour reach, and discharge for Strouds reach.

7.3. Uncertainty quantification in flood inundation mapping

The application of GLUE methodology in this study (chapter 5) shows that the uncertainty bound from each variable is non-linearly accumulated to the combined uncertainty bound. Unlike expectation that errors in discharge add the most uncertainty, in this study, the first ranked uncertain variables are topography for large U shaped cross sectional Seymour reach, and discharge for small V shaped cross-sectional Strouds reach. The shape of valley can affect flood inundation modeling because it is related to the conveyance dependent to top surface width and elevation. However, discharge is still one of the major uncertain variables, which is estimated by a stage-discharge rating equation including hysteresis with errors in measurement. Accordingly, the uncertainty quantification depends on the degree of the difficulty to overcome errors in model variables.

The subjectivity in selecting likelihood measure has small influence in quantifying uncertainty bounds for Seymour reach and Strouds reach. Considering base map areas for each reach, the difference between uncertainty bounds based on all the likelihood measure is less than 5% for both reaches. However, these results cannot be generalized for other study reaches because likelihood measures are affected by the nature of the flood event, the cross-section shape, the observations, and model variables. In addition,

the difference between uncertainty bounds from all likelihood measures for a single variable is less than for the combined model variables.

7.4. The role of posterior PDFs on the uncertainty analysis method

The GLUE methodology used in this study is simple and flexible, but involves subjective decisions on a likelihood measure and a cut-off threshold. This study (chapter 6) shows that the prior PDF types of model variables with the likelihood measures affects uncertainty bounds using the GLUE methodology. In addition, a relaxed threshold brings ambiguous information between the prior and posterior PDFs, while a very tight threshold makes it difficult to estimate uncertainty bounds due to a small number of the acceptable dataset. Also, this study shows that when the prior PDF has a uniform distribution uncertainty bound of flood inundation areas is wider than when a normal distribution.

One of the findings from this study is that even though subjectivity cannot be completely removed from the GLUE methodology, the prior and posterior PDFs for model variables can be useful in finding a likelihood measure to derive robust uncertainty bounds, and the effective ranges of model variables which have higher chance defined as behavioral models in the procedures of the GLUE methodology. Specifically, the combination of prior PDFs for model variables is used to find a likelihood measure to obtain the most robust one among uncertainty bounds using GLUE. The effective range leads to the robust posterior PDFs of model variables for the prior PDF combinations. In this study, it

is illustrated that a number of the acceptable dataset affects uncertainty quantification using the GLUE methodology. The effective range for a cut-off threshold can be used to supplement acceptable datasets in uncertainty quantification based on a small number of dataset. Further investigation on this issue will need applications for other sites with physically and climatically different characteristics and for other elements arising uncertainty in flood inundation mapping.

LIST OF REFERENCES

LIST OF REFERENCES

Aronica, G., Hankin, B. G., and Beven, K. J. (1998) Uncertainty and equifinality in calibrating distributed roughness coefficients in a flood propagation model with limited data. Adv. Water Resour., 22(4), 349-365.

Aronica, G., Bates, P.D., and Horritt, M.S. (2002) Assessing the uncertainty in distributed model predictions using observed binary pattern information within GLUE. Hydrological Processes, 16, 2001-2016.

Bahremand, A. and De Smedt F. (2008) Distributed hydrological modeling and sensitivity analysis in Torysa watershed, Slovakia, Water Resour Manag 22, 393–408.

Bales, J.D. and Wagner, C.R. (2009) Sources of uncertainty in flood inundation maps, J Flood Risk Management, 2, 139–147.

Barroca, B., Bernardara, P., Mouchel, J.M. and Hubert, G. (2006) Indicators for identification of urban flood vulnerability. Natural Hazards and Earth System Sciences, 6, 553–561.

Bates, B.C. and Towntey, L.R. (1988) Nonlinear, discrete flood event models, 1. Bayesian estimation of parameters, J. Hydrol., 99, 61-76.

Bates, P. D., Horritt, M. S., Aronica, G., and Beven, K. J. (2004) Bayesian updating of flood inundation likelihoods conditioned on flood extent data Hydrol. Process. 18, 3347–3370.

Bates, P. D., Marks, K. J., and Horritt, M. S. (2003) Optimal use of high-resolution topographic data in flood inundation models. Hydrolog. Process., 17(3), 537–557.

Beck, M. B. (1987) Water quality modeling: A review of the analysis of uncertainty, Water Resour. Res., 23(5), 1393–1441.

Benjamin, J.R. and Cornell, C.A. (1970) Probability, Statistics and Decision Making for Civil Engineers. McGraw-Hill, New York, N.Y.

Beven, K. J. (2009) Environmental Modelling: An uncertain future?, Routledge

Beven, K. J., and Binley, A. M. (1992) The future of distributed models: model calibration and uncertainty prediction. Hydrol. Process., 6, 279-298.

Blasone, R. S., J. A. Vrugt, H. Madsen, D. Rosbjerg, B. A. Robinson, and G. A. Zyvoloski (2008a), Generalized likelihood uncertainty estimation (GLUE) using adaptive Markov chain Monte Carlo sampling, Adv. Water Resour., 31, 630–648.

Blasone, R. S., Madsen, H., and Rosbjerg, D. (2008b), Uncertainty assessment of integrated distributed hydrological models using GLUE with Markov chain Monte Carlo sampling, J. Hydrol., 353, 18–32.

Blazkova, S. and Beven, K. (2009) A limits of acceptability approach to model evaluation and uncertainty estimation in flood frequency estimation by continuous simulation: Skalka catchment, Czech Republic, Water Resour. Res., 45, W00B16, doi:10.1029/2007WR006726.

Blumberg, A.F. and Georgas, N. (2008). Quantifying uncertainty in estuarine and coastal ocean circulation modeling, J. Hydr. Eng., 134(4), 403-415.

Chow, V.T. (1959) Open-channel hydraulics, New York, McGraw- Hill Book Co.

Clarke, R. T. (1999) Uncertainty in the estimation of mean annual flood due to rating curve indefinition. J. Hydrol. 222, 185–190.

Clarke, R. T., Mendiondo, E. M., and Brusa, L. C. (2000) Uncertainties in mean discharges from two large South American rivers due to rating curve variability, Hydrological Sciences Journal, Vol. 45(2), 221-236.

Cook, Aaron and Merwade, V. (2009) Effect of topographic data, geometric configuration and modeling approach on flood inundation mapping. Journal of Hydrology, Vol. 377, 131-142.

Collins, M. J. (2009), Evidence for Changing Flood Risk in New England Since the Late 20th Century. JAWRA Journal of the American Water Resources Association, 45, 279–290.

Di Baldassarre, G. and Montanari, A. (2009) Uncertainty in river discharge measurements: a quantitative analysis, Hydrol. Earth Syst. Sci., 13, 913–921.

Freeman, G. E., Copeland, R. R., and Cowan, M. A. (1996) Uncertainty in stage-discharge relationships. Stochastic Hydraulics, '96 Proc. 7th IAHR on Stochastic Hydraulics, IAHR, 601–608.

Garen, D. C., and Burges, S. J. (1981) Approximate error bounds for simulated hydrographs, J. Hydraul. Div., Am. Soc. Civ. Eng., 107(11), 1519–1534.

Heidari, A., Saghafian B., and R. Maknoon, R. (2006) Assessment of flood forecasting lead time based on generalized likelihood uncertainty estimation approach, Stochastic Environmental Research and Risk Assessment, 20(5), 363-380.

Herschey, R. W. (2002) The uncertainty in a current meter measurement. Flow Measur Instru., 13, 281–4.

Hornberger, G. M. and Spear, R. C. (1981) An approach to the preliminary analysis of environmental systems, J. Environmental Management, 12, 7-18.

Hornberger, G. M. and Cosby, B. J. (1985) Selection of parameter values in environmental models using sparse data: a case study. Applied Math. and Comp.,17, 335-355.

Horritt, M. S. (2005) Parameterisation, validation and uncertainty analysis of CFD models of fluvial and flood hydraulics in the natural environment, in: Computational Fluid Dynamics Applications in Environmental Hydraulics, edited by: Bates, P. D., Lane, S. N., and Ferguson, R. I., John Wiley and Sons Ltd, 193–213.

Horritt, M.S. and Bates, P.D. (2001) Predicting floodplain inundation: raster-based modelling versus the finite element approach. Hydrological Processes, 15, 825-842.

Horritt, M.S. and Bates, P.D. (2002) Evaluation of 1D and 2D numerical models for predicting river flood inundation, Journal of Hydrology, Volume 268, Issues 1-4, 1, 87-99.

Hossain, F., Anagnostou, E. N., Dinku, T., and Borga, M. (2004) Hydrological model sensitivity to parameter and radar rainfall estimation uncertainty. Hydrol. Process., 18, 3277–3291.

Hunter, N. M. (2005) Utility of different data types for calibrating flood inundation models within a GLUE framework, Hydrol. Earth Syst. Sci., 9, 412–430.

Hurkmans, R. T. W. L., Terink, W., Uijlenhoet, R., Moors, E. J., Troch, P. A., Verburg, P. H. (2009), Effects of land use changes on streamflow generation in the Rhine basin. Water Resour. Res., 45, 6.

Jia, Y. B., and Culver, T. B. (2008) Uncertainty analysis for watershed modeling using generalized likelihood uncertainty estimation with multiple calibration measures, J. Water Resour. Plann. Manage, 134(2).

Johnson, P. A., and Rinaldi, M. (1998) Uncertainty in stream channel restoration. Uncertainty modeling and analysis in civil engineering, B. M. Ayyub, ed., CRC Press, Boca Raton, Fla., 425–437.

Kiczko, Pappenberger, F. and Romanowicz, R.J. (2007) Flood Risk Analysis Of The Warsaw Reach Of The Vistula River. In Proceedings of 11th Conference of the ERB Luxembourg.

Koivumäki, L., Alho, P., Lotsari, E., Käyhkö, J., Saari, A. and Hyyppä, H. (2010) Uncertainties in flood risk mapping: a case study on estimating building damages for a river flood in Finland. J Flood Risk Management, 3, 166–183

Krzysztofowicz, R. (1999) Bayesian theory of probabilistic forecasting via deterministic hydrologic model. Water Resources Research, 35(9), 2739-2750.

Krzysztofowicz, R. (2002) Probabilistic flood forecast: bounds and approximations. Journal of Hydrology 268 (1-4), 41-55.

Kuczera, G., and Parent, E. (1998) Monte Carlo assessment of parameter uncertainty in conceptual catchment models: The Metropolis algorithm, J. Hydrol., 211, 69–85.

Lara, Oscar G. (1987) Method for estimating the magnitude and frequency of floods at ungaged sites on unregulated rural streams in Iowa. U.S. Geological Survey, Water resources investigation report G87-4A132.

Lee, H. L., and Mays, L. W. (1986) Hydraulic uncertainties in flood levee capacity, J. Hydraul. Eng., 112(10), 928–934.

Lei J, Schilling W. (1994). Parameter uncertainty propagation analysis for urban rainfall runoff modeling. Water Science and Technology 29(1–2): 145–154.

Linton, O. (1995). Second order approximations in a partially linear regression model. Econometrica, 63, 1079-1113.

Liu, J., Tian, F., and Huang, Q. (2001) A risk analyzing method for reservoir flood control. Hydrology, 21(3), 1-3.

Liu, Y.B., Batelaan, O., De Smedt, F., Poórová, J., Velcická, L. (2005) Automated calibration applied to a GIS based flood simulation model using PEST. In: van Alphen J, van Beek E, Taal M (eds) Floods, from defense to management. Taylor-Francis, London, 317–326.

Marks, K. and Bates, P. (2000) Integration of high-resolution topographic models with floodplain flow models. Hydrological Processes, 14, 2109-2122.

Maskey, S., Guinot, V. and Price, R.K. (2004). Treatment of precipitation uncertainty in rainfall-runoff modelling: a fuzzy set approach. Advances in Water Resources, 27 (9), 889-898.

McEwen, L., Hall, T., Hunt, J., Dempsey, M. and Harrison, M. (2002) Flood warning, warning response and planning control issues associated with caravan parks: the April 1998 floods on the lower Avon floodplain, Midlands region, UK. Applied Geography, 22, 271–305.

Melching, C.S. (1992) An improved first-order reliability approach for assessing uncertainties in hydrologic modeling, Journal of Hydrology, 132, 157-177.

Merwade, V.M., Olivera, F., Arabi, M., and Edleman, S. (2008a) Uncertainty in flood inundation mapping – current issues and future directions. ASCE Journal of Hydrologic Engineering, 13 (7), 608–620

Merwade, V., Cook A., Coonrod, J. (2008b) GIS techniques for creating river terrain models for hydrodynamic modeling and flood inundation mapping, Environmental Modelling & Software, Vol. 23, 10-11, 1300-1311.

Morlock, S.E., Menke, C.D., Arvin, D.V., and Kim, M.H., (2008) Flood of June 7–9, 2008, in central and southern Indiana: U.S. Geological Survey Open File Report 2008–1322, 15.

Nicholas, A. P. (2005) Roughness parameterization in CFD modelling of gravel-bed rivers, in: Computational Fluid Dynamics Applications in Environmental Hydraulics, edited by: Bates, P. D., Lane, S. N., and Ferguson, R. I., John Wiley and Sons Ltd, 329–355.

Noson, L. (2002) Hazard mapping and risk assessment, Regional Workshop on Best Practices in Disaster Mitigation, Bali, Indonesia; 24–26

Omer, C. R., Nelson, E. J., and Zundel, A. K. (2003) Impact of varied data resolution on hydraulic modeling and floodplain delineation. J. Am. Water Resour. Assoc., 39(2), 467–475.

Pappenberger F., Beven K.J., Hunter N., Gouweleeuw B., Bates P., de Roo A., Thielen J.(2005a) Cascading model uncertainty from medium range weather forecasts (10 days) through a rainfall-runoff model to flood inundation predictions within the European Flood Forecasting System (EFFS). Hydrol. Earth Syst. Sci. 9: 381–393.

Pappenberger, F., Beven K., et al. (2005b) Uncertainty in the calibration of effective roughness parameters in HEC-RAS using inundation and downstream level observations. Journal of Hydrology, 302(1-4), 46-69.

Pappenberger F., Beven K.J., Frodsham K., Romanovicz R., Matgen P. (2006a) Grasping the unavoidable subjectivity in calibration of flood inundation models: a vulnerability weighted approach. J. Hydrol., 333, 275–287.

Pappenberger, F., Frodsham, K., Beven, K. J. , Romanowicz, R., and Matgen, P. (2007) Fuzzy set approach to calibrating distributed flood inundation models using remote sensing observation. Hydrology & Earth System Science, 10, 1-14.

Pappenberger, F., Matgen P., et al. (2006b) Influence of uncertain boundary conditions and model structure on flood inundation predictions. Advances in Water Resources, 29(10), 1430-1449

Pappenberger, F., Matgen, P., Beven, K., Henry, J., Pfister, L., and Fraipont de, P. (2006c) Influence of uncertain boundary conditions and model structure on flood inundation predictions. Advances in Water Resources, Vol. 29, 10, 1430-1449

Parodi, U., and Ferraris, L. (2004) Influence of stage discharge relationships on the annual maximum discharge statistics. Natural Hazards, 31, 603–611.

Prudhomme,C., Jakob D., and Svensson, C. (2003) Uncertainty and climate change impact on the flood regime of small UK catchments. Journal of Hydrology, 277(1-2), 1-23.

Purvis, M., Bates, P.D. and Hayes, C.M. (2008) A probabilistic methodology to estimate future coastal flood risk due to sea level rise. Coastal Eng., 55, 1062–1073.

Ries, K.G., III, and Crouse, M.Y. (2002) The National Flood Frequency Program, Version 3: A computer program for estimating magnitude and frequency of floods for ungaged sites, U.S. Geological Survey Water-Resources Investigations Report 02-4168

Romanowicz, R. and Beven, K.J. (1998) Dynamic real-time prediction of flood inundation probabilities. Hydrol. Sci. J., 43, 181–196

Sanders, B. (2007) Evaluation of on-line DEMs for flood inundation modeling, Advances in Water Resources, Vol. 30, 8, 1831-1843.

Schmidt, A. R. (2002) Analysis of stage-discharge relations for openchannel flows and their associated uncertainties. Ph.D. thesis, Univ. of Illinois at Urbana-Champaign, Champaign, Ill.

Sitar, N., Cawfield, J.D., and Der Kiureghian, A. (1987) First-order reliability approach to stochastic analysis of subsurface flow and contaminant transport. Water Resour. Res., 23, 794-804.

Stedinger, J. R. and V. W. Griffis (2008) Flood frequency analysis in the United States: Time to Update. Journal of Hydrologic Engineering, 13(4), 199-204

Tang, W. H., Mays, L. W., and Yen, B. C. (1975) Optimal risk-based design of storm sewer networks. J. Environ. Eng., 101(3), 381–398.

Tate, E. C., Olivera, F., and Maidment, D. R. (2002) Creating a terrain model for floodplain mapping. J. Hydrol. Eng., 7(2), 100–108.

USACE (2006a) HEC-RAS hydraulic reference manual. Hydrologic Engineering Center, Davis California. (www.hec.usace.army.mil/software/hec-ras/hec-georas.html).

USACE (2006b) HEC-GeoRAS user's manual. Hydrologic Engineering Center, Davis California. (http://www.hec.usace.army.mil/software/hec-ras/hecras-document.html)

USACE (2006c) HEC-RAS user's manual. Hydrologic Engineering Center, Davis California.(http://www.hec.usace.army.mil/software/hec-ras/hecras-document.html)

Vazquez, R. F., Feyen, L., Feyen, J., and Refsgaard, J. C. (2002) Effect of grid size on effective parameters and model performance of the MIKE-SHE code. Hydrolog. Process., 16(2), 355–372.

Vrugt, J. A., Diks, C. G. H., Gupta, H. V., Bouten, W., and Verstraten, J. M. (2005) Improved treatment of uncertainty in hydrologic modeling: Combining the strengths of global optimization and data assimilation. Water Resour. Res., 41, W01017, doi:10.1029/2004WR003059.

Wang, Y., and Zheng, T. (2005) Comparison of digital elevation models and understanding of their impact on the flood extent mapping on a coastal floodplain of North Carolina. Nat. Hazards Rev., 6(1), 34–40.

Watson, D.F. and Phillip, G.M. (1984) Triangle based interpolation. Mathematical Geology, 8(16), 779–795.

Weichel, T., Pappenberger, F., and Schulz, K. (2007) Sensitivity and uncertainty in flood inundation modelling – concept of an analysis framework. Adv. Geosci., 11, 31–36.

Werner, M. J. F. (2001) Impact of grid size in GIS based flood extent mapping using a 1D flow model. Phys. Chem. Earth, Part B, 26(7–8), 517–522.

Whitehead, P. G. and Young, P. C. (1979) Water quality in river systems: Monte-Carlo analysis. Water Resources Research, 15, 451-459.

Wilson, M.D. and Atkinson, P.M. (2005) Prediction uncertainty in elevation and its effect on flood inundation modelling. In: Atkinson PM, Foody GM, Darby S, Wu F, editors. GeoDynamics. John Wiley and Sons Ltd.

Xu, Y., Xu, C., Gao X., and Luo, Y. (2009) Projected changes in temperature and precipitation extremes over the Yangtze River Basin of China in the 21st century, Quaternary International, Volume 208, Issues 1-2

Yatheendradas, S., T. Wagener, V. Gupta, K. Unkrich, D. Goodrich, M. Schaeffer, and A. Stewart (2008), Understanding uncertainty in distributed flash-flood forecasting for semi-arid regions, Water Resour. Res., 44, W05S19, doi:10.1029/2007WR005940.

Yen, B.C. (1989) Engineering approaches to risk and reliability analysis. In: Y. Haimes and E.Z. Stakhiv (Editors), Risk Analysis and Management of Natural and Man-Made Hazards. Am. Soc. Civ. Eng., New York, 22-49.

Young, P. C. (1983) The validity and credibility of models for badly-defined systems. In M B Beck and G van Straten (Eds.) Uncertainty and Forecasting of Water Quality. Springer-Verlag: Berlin, 69-98.

Zhang, H. X., and Yu, S. L. (2004) Applying the first-order analysis in determining the margin of safety for total maximum daily load computations. J. Environ. Eng., 130(6), 664–673.

Zhao, X., Shen, Z., Xiong, M., and Qi, J. (2011). Key uncertainty sources analysis of water quality model using the first order error method. Int. J. Environ. Sci. Tech., 8 (1), 137-148.

APPENDIX

APPENDIX

Prior PDFs	F			W			E		
	Topography	Discharge	Manning's n	Topography	Discharge	Manning's n	Topography	Discharge	Manning's n
Case 1	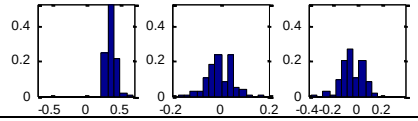			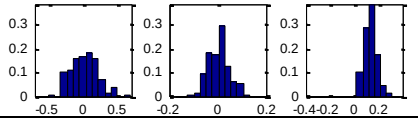			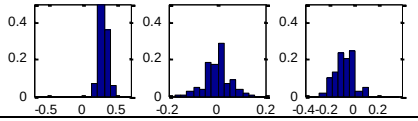		
Case 2	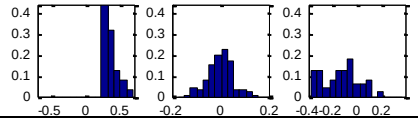			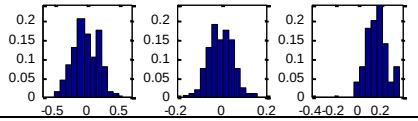			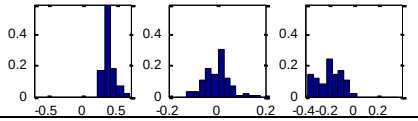		
Case 3	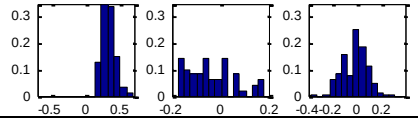			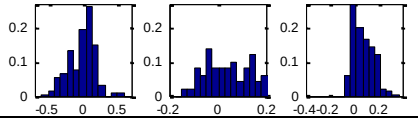			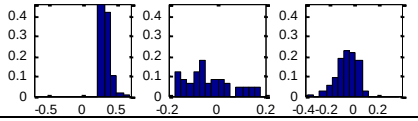		
Case 4	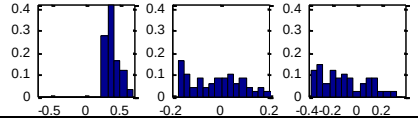			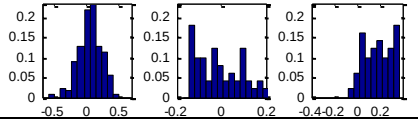			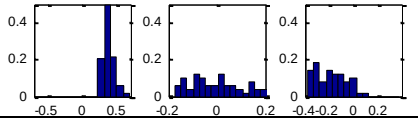		
Case 5	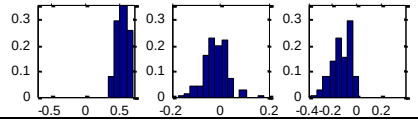			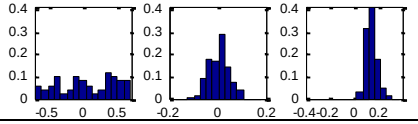			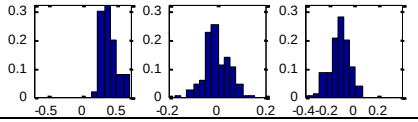		
Case 6	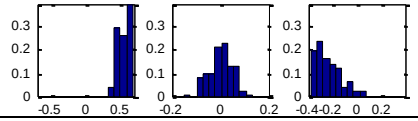			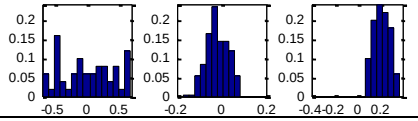			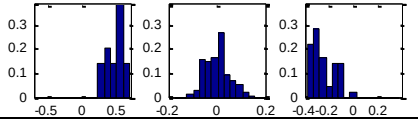		
Case 7	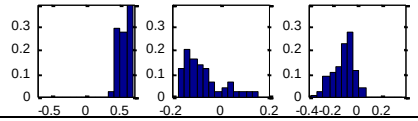			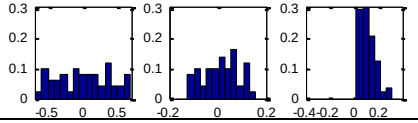			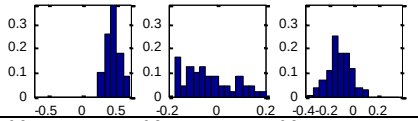		
Case 8	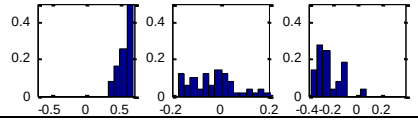			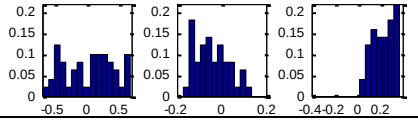			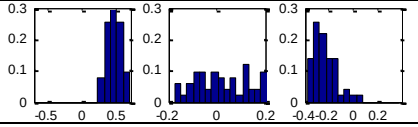		

Fig. A.1: The posterior PDFs of model variables for top 1% of W, E, and F likelihood measures.

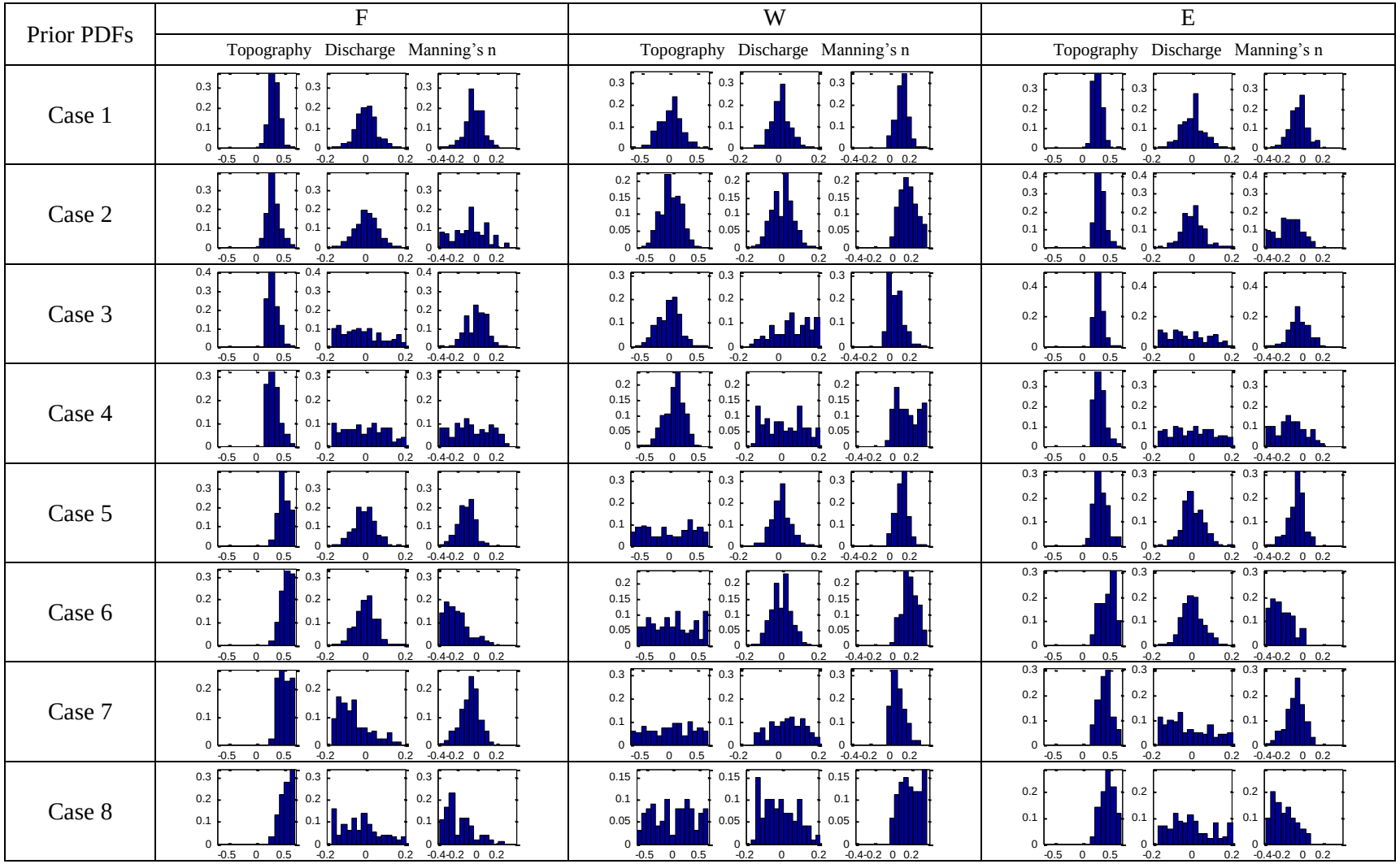

Fig. A.2: The posterior PDFs of model variables for top 2% of W, E, and F likelihood measures.

Prior PDFs	F			W			E		
	Topography	Discharge	Manning's n	Topography	Discharge	Manning's n	Topography	Discharge	Manning's n
Case 1	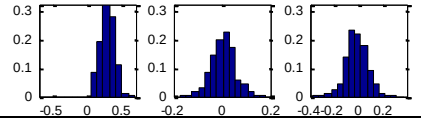			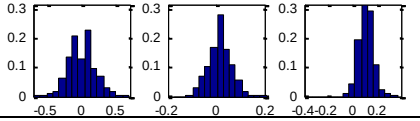			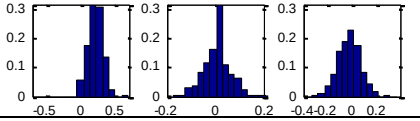		
Case 2	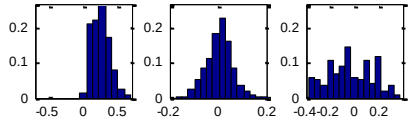			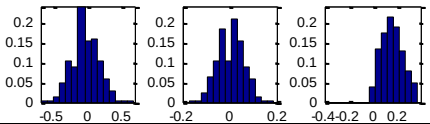			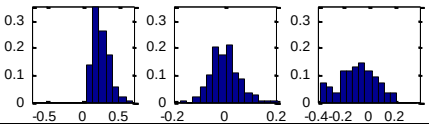		
Case 3	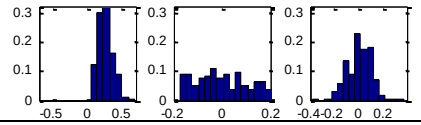			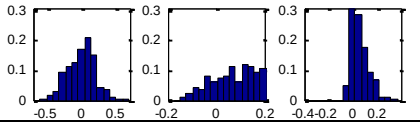			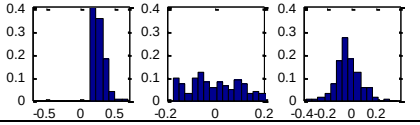		
Case 4	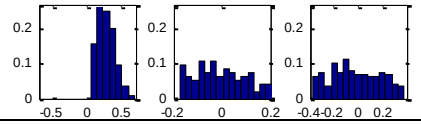			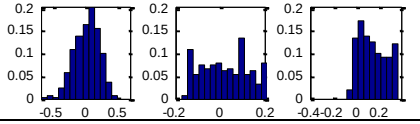			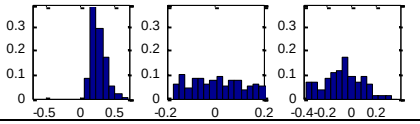		
Case 5	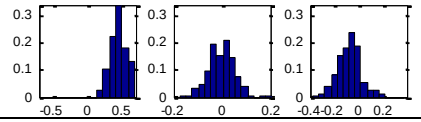			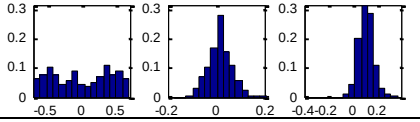			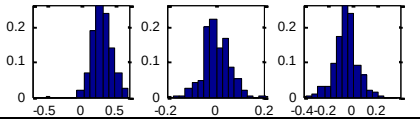		
Case 6	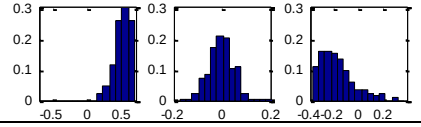			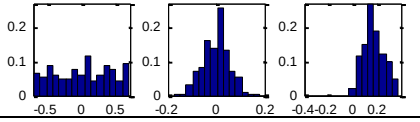			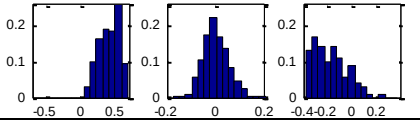		
Case 7	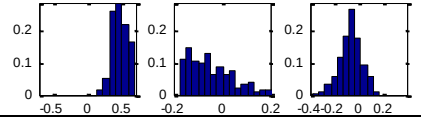			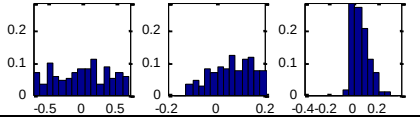			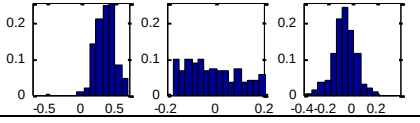		
Case 8	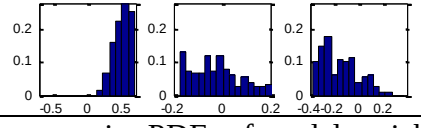			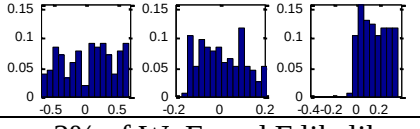			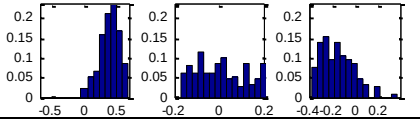		

Fig. A.3: The posterior PDFs of model variables for top 3% of W, E, and F likelihood measures.

Prior PDFs	F			W			E		
	Topography	Discharge	Manning's n	Topography	Discharge	Manning's n	Topography	Discharge	Manning's n
Case 1	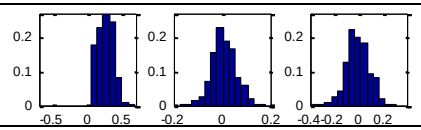			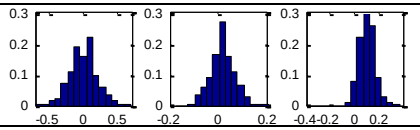			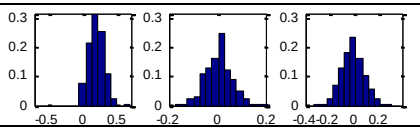		
Case 2	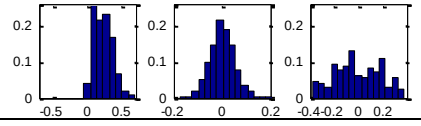			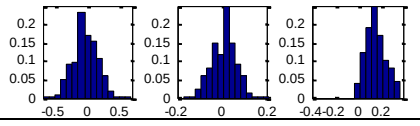			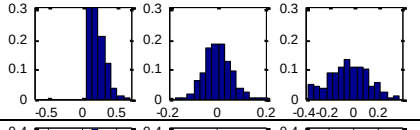		
Case 3	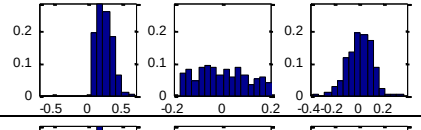			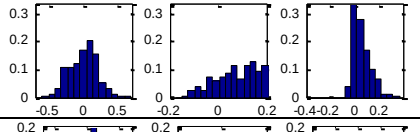			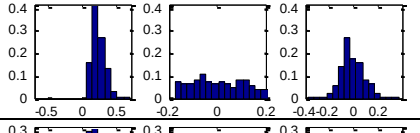		
Case 4	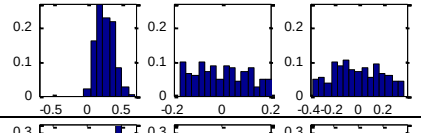			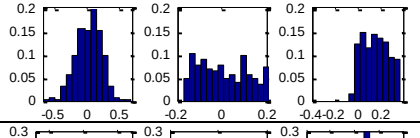			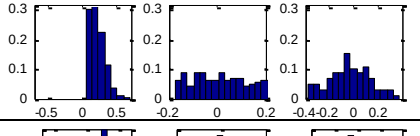		
Case 5	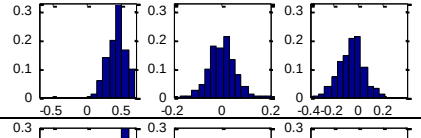			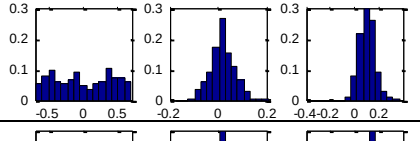			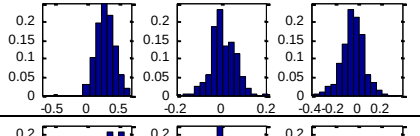		
Case 6	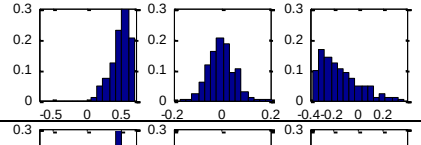			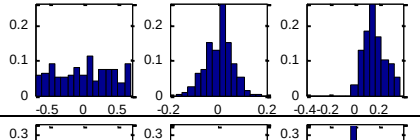			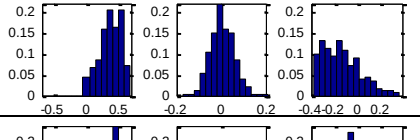		
Case 7	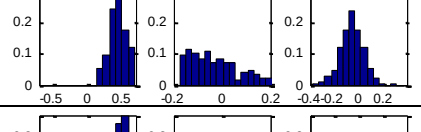			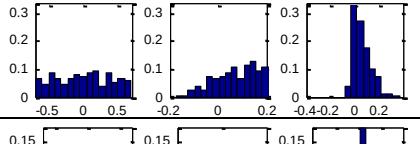			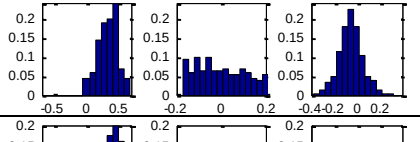		
Case 8	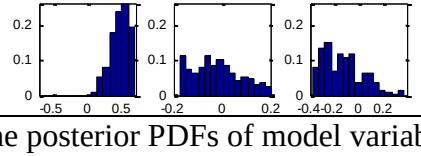			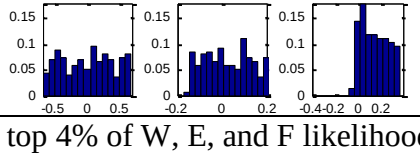			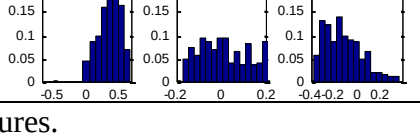		

Fig. A.4: The posterior PDFs of model variables for top 4% of W, E, and F likelihood measures.

Prior PDFs	F			W			E		
	Topography	Discharge	Manning's n	Topography	Discharge	Manning's n	Topography	Discharge	Manning's n
Case 1	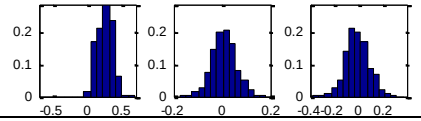			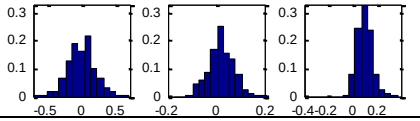			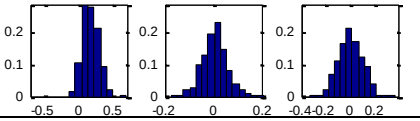		
Case 2	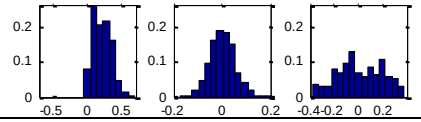			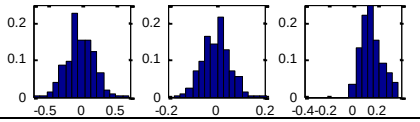			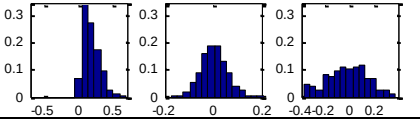		
Case 3	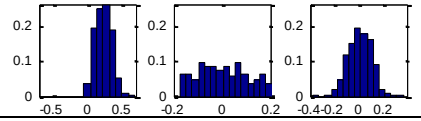			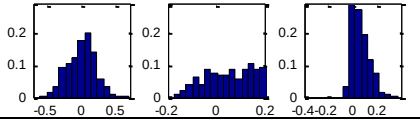			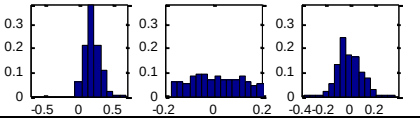		
Case 4	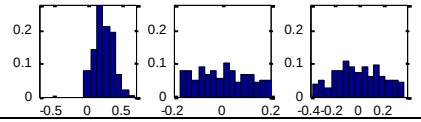			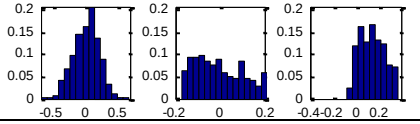			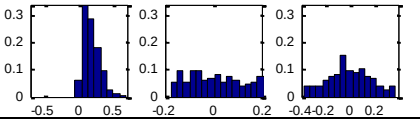		
Case 5	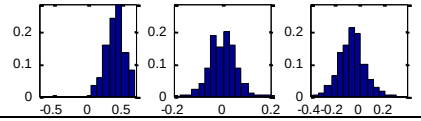			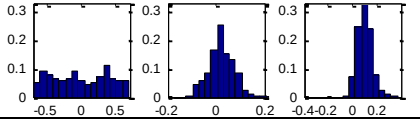			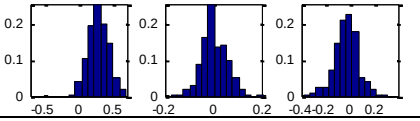		
Case 6	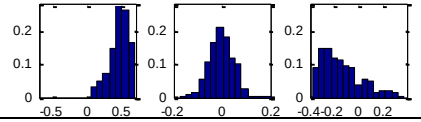			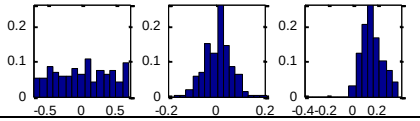			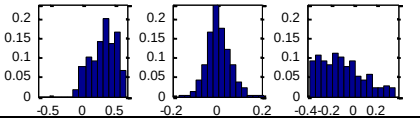		
Case 7	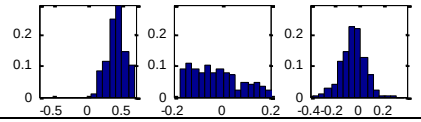			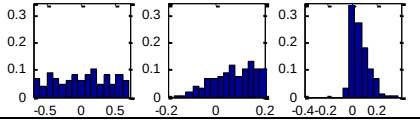			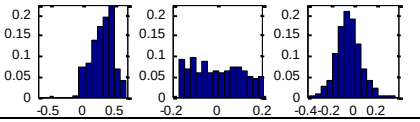		
Case 8	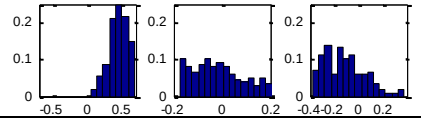			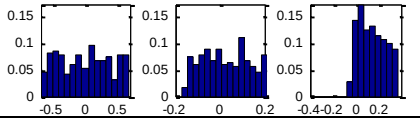			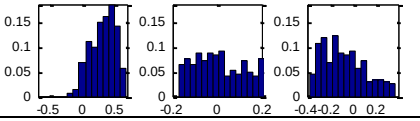		

Fig. A.5: The posterior PDFs of model variables for top 5% of W, E, and F likelihood measures.

Prior PDFs	F			W			E		
	Topography	Discharge	Manning's n	Topography	Discharge	Manning's n	Topography	Discharge	Manning's n
Case 1	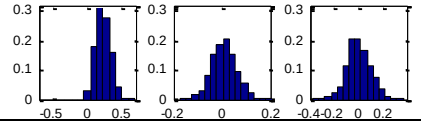			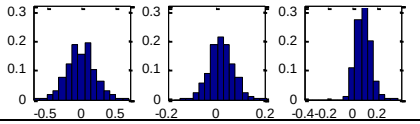			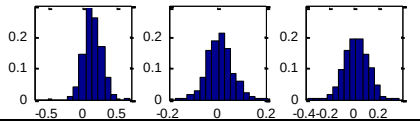		
Case 2	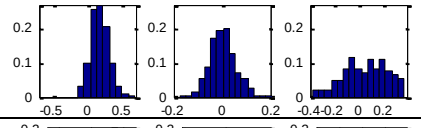			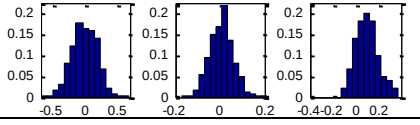			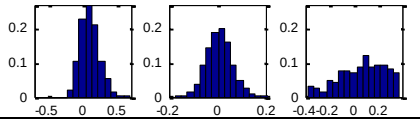		
Case 3	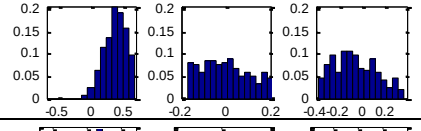			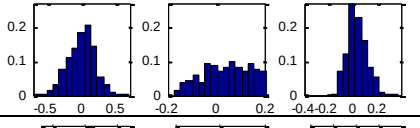			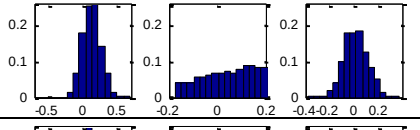		
Case 4	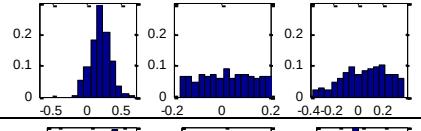			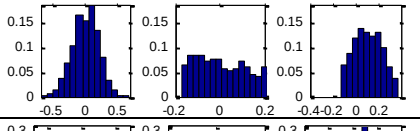			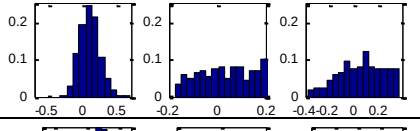		
Case 5	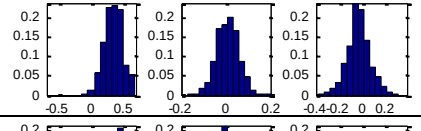			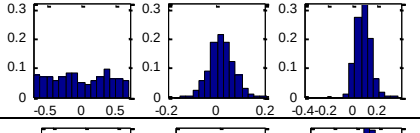			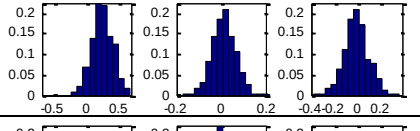		
Case 6	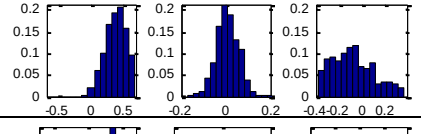			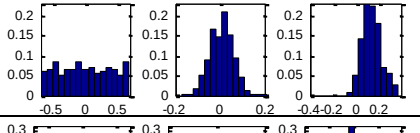			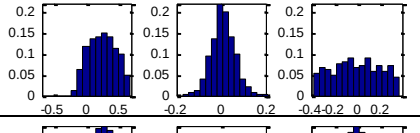		
Case 7	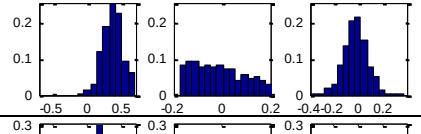			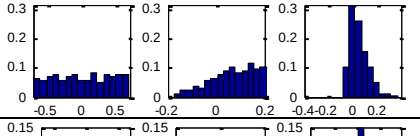			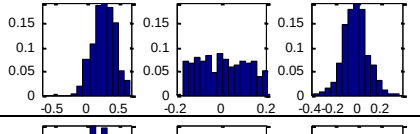		
Case 8	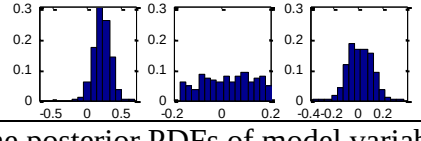			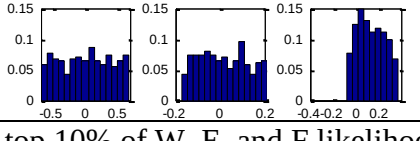			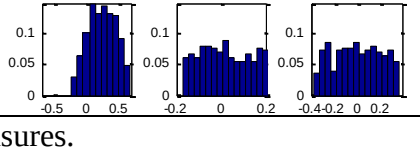		

Fig. A.6: The posterior PDFs of model variables for top 10% of W, E, and F likelihood measures.

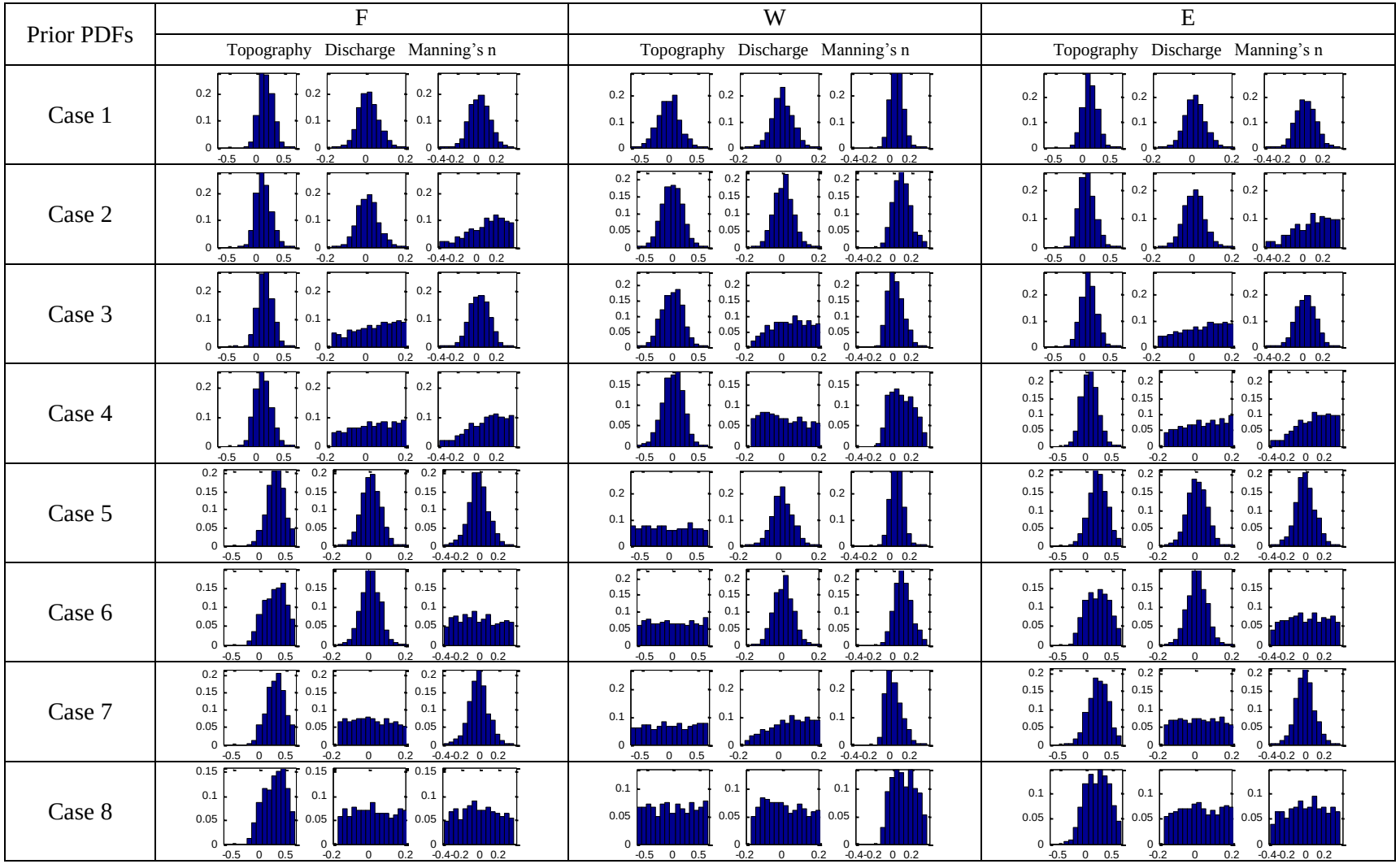

Fig. A.7: The posterior PDFs of model variables for top 20% of W, E, and F likelihood measures.

Prior PDFs	F			W			E		
	Topography	Discharge	Manning's n	Topography	Discharge	Manning's n	Topography	Discharge	Manning's n
Case 1	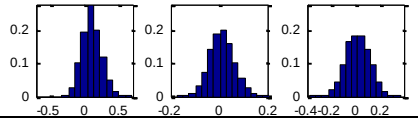			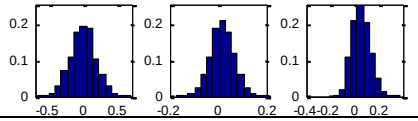			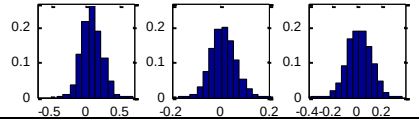		
Case 2	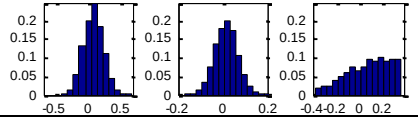			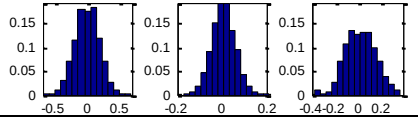			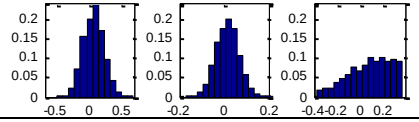		
Case 3	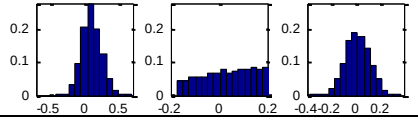			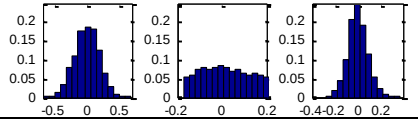			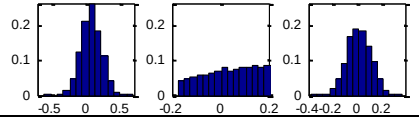		
Case 4	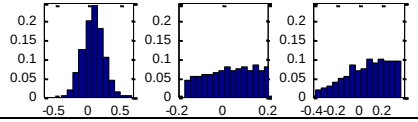			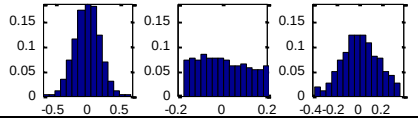			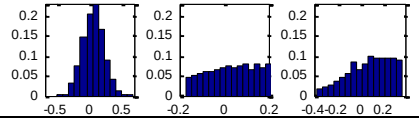		
Case 5	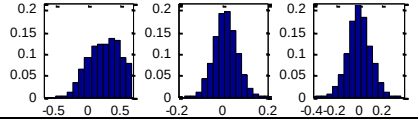			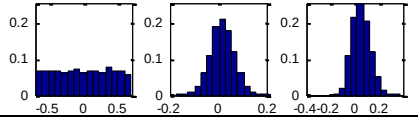			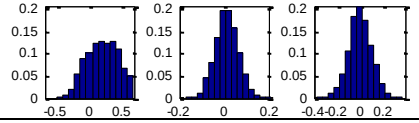		
Case 6	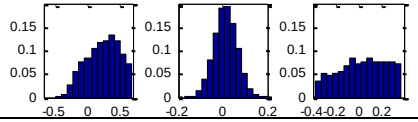			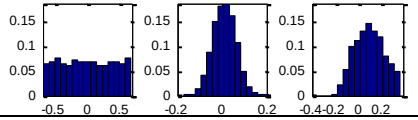			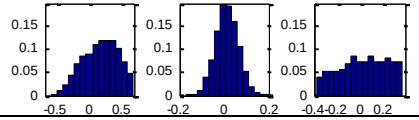		
Case 7	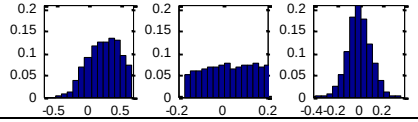			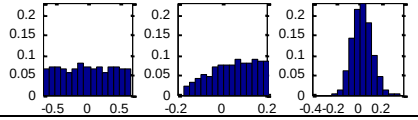			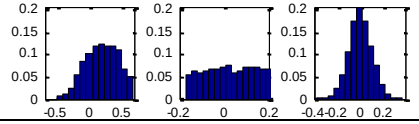		
Case 8	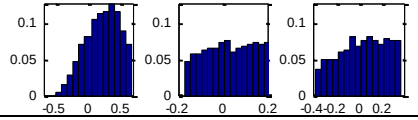			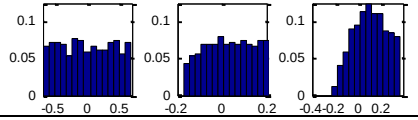			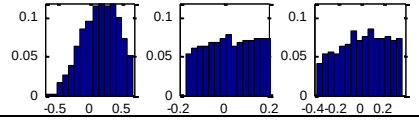		

Fig. A.8: The posterior PDFs of model variables for top 50% of W, E, and F likelihood measures.

VITA

VITA

Younghun Jung was born in Okcheon, South Korea. He received his Bachelor and Master of Engineering Degrees in Civil Engineering from Inha University, Incheon, South Korea in 2002 and 2004, respectively. He received his Master of Science degree in Civil and Environmental Engineering from Georgia Institute of Technology, Atlanta, United States in 2007. He joined the Ph.D. program of Purdue University in January 2008.